



N62-7484
N63-12975
code-1

TECHNICAL MEMORANDUM

X-24

AERODYNAMIC CHARACTERISTICS OF A 0.0667-SCALE
MODEL OF THE NORTH AMERICAN X-15 RESEARCH
AIRPLANE AT TRANSONIC SPEEDS

By Robert S. Osborne

Langley Research Center
Langley Field, Va.

Declassified September 1, 1961

NATIONAL AERONAUTICS AND SPACE ADMINISTRATION
WASHINGTON

September 1959

1
copy
vce 1

NATIONAL AERONAUTICS AND SPACE ADMINISTRATION

TECHNICAL MEMORANDUM X-24

AERODYNAMIC CHARACTERISTICS OF A 0.0667-SCALE

MODEL OF THE NORTH AMERICAN X-15 RESEARCH

AIRPLANE AT TRANSONIC SPEEDS

By Robert S. Osborne

SUMMARY

In order to determine its aerodynamic characteristics at transonic speeds, a 0.0667-scale force model of configuration 1 of the North American X-15 research airplane has been tested in the Langley 8-foot transonic pressure tunnel at Mach numbers from 0.60 to 1.43, angles of attack up to 20° , and angles of sideslip from 0° to 5.1° .

The drag of the configuration was relatively high; the maximum lift-drag ratios decreased from 6.7 to approximately 4.5 with increases in Mach number from 0.60 to 1.43. Positive longitudinal stability was indicated for the model except at Mach numbers near 0.95 where neutral stability occurred at approximately zero lift. The configuration was stable directionally and had positive effective dihedral for the ranges investigated. The horizontal tail provided satisfactory longitudinal and lateral control power. Differentially deflecting the horizontal tail for lateral control produced large favorable yawing moments at low angles of attack but had little effect on longitudinal stability and control. Opening the speed brakes 45° at a Mach number of 1.43 increased zero-lift drag by a factor of 5, produced large longitudinal trim changes, increased directional stability by 30 percent, and doubled effective dihedral at the lower angles of attack.

INTRODUCTION

As part of the wind-tunnel program required to determine a satisfactory configuration for the North American X-15 research airplane, a 0.0667-scale force model of the original, or configuration 1, of the

X-15 has been tested in the Langley 8-foot transonic pressure tunnel in order to obtain its aerodynamic characteristics at transonic speeds. It should be noted that configuration 1 was not the final version of the airplane and that subsequent configuration changes have been made in order to alleviate certain stability and flutter problems. Low-speed characteristics of configuration 1 are available in reference 1.

The X-15 is a rocket-powered research airplane designed for hypersonic speeds at very high altitudes. It employs a 5-percent-thick low-aspect-ratio trapezoidal wing mounted in the midposition on a fuselage consisting of a body of revolution with large side fairings. The 45°-swept horizontal tail is all-movable for pitch control and may be deflected differentially for roll control. The upper vertical tail is all-movable for directional control, whereas a fixed lower vertical tail is provided for increased directional stability at high angles of attack and Mach numbers.

L
3
7
6

The model was tested at angles of attack up to 20° for angles of sideslip from 0° to 5.1° and Mach numbers from 0.60 to 1.43. Drag, static longitudinal stability, and static lateral directional stability characteristics were determined; the effectiveness of the horizontal tail as a pitch and roll control was measured, and the effects of opening the speed brakes on drag and stability were determined. The results are presented herein.

SYMBOLS

b	wing span, in.
C_D	drag coefficient, D/qS
C_{D_0}	drag coefficient at zero lift
C_L	lift coefficient, L/qS
$C_{L,(L/D)_{\max}}$	lift coefficient for maximum lift-drag ratio
C_{L_t}	trim lift coefficient
$\frac{\partial C_{L_t}}{\partial \delta_e}$	trim lift effectiveness parameter per degree
C_{L_α}	lift-curve slope per degree
C_l	rolling-moment coefficient, M_{X_S}/qSb

$C_{l\beta}$	effective dihedral parameter $\frac{\partial C_l}{\partial \beta}$ per degree
$C_{l\delta_a}$	rolling moment due to differential tail deflection $\frac{\partial C_l}{\partial \delta_a}$ per degree
C_m	pitching-moment coefficient, $M_Y/qS\bar{c}$
C_{mC_L}	static longitudinal stability parameter, $\frac{\partial C_m}{\partial C_L}$
$C_{m\delta_e}$	pitch effectiveness parameter at constant lift coefficient $\frac{\partial C_m}{\partial \delta_e}$ per degree
C_n	yawing-moment coefficient, M_{Zs}/qSb
$C_{n\beta}$	static directional stability parameter $\frac{\partial C_n}{\partial \beta}$ per degree
$C_{n\delta_a}$	yawing moment due to differential tail deflection $\frac{\partial C_n}{\partial \delta_a}$ per degree
$C_{p,b}$	base pressure coefficient, $\frac{P_b - P}{q}$
C_Y	lateral-force coefficient, Y/qS
\bar{c}	wing mean aerodynamic chord, in.
D	force along X_S -axis, positive rearward, lb
L	lift, lb
$(L/D)_{\max}$	maximum lift-drag ratio
M	free-stream Mach number
M_{Xs}	moment about X_S -axis, in-lb
M_Y	moment about Y-axis, in-lb

M_{Z_S}	moment about Z_S -axis, in-lb	
P_b	static pressure at model base, lb/sq ft	
p	free-stream static pressure, lb/sq ft	
q	free-stream dynamic pressure, lb/sq ft	
R	Reynolds number	
S	total wing area, sq ft	L
Y	lateral force, lb	3
α	angle of attack of fuselage center line, deg	7
β	angle of sideslip, deg	6
δ_a	differential deflection of horizontal tail when used as roll control, positive when left-hand surface has more positive (trailing edge down) deflection, deg	
δ_e	deflection of horizontal tail when used as pitch control (taken as the average of the left- and right-hand surface deflections and positive when the trailing edge is down), deg	
X_S, Y, Z_S	stability coordinates	

APPARATUS AND TESTS

Model

The 0.0667-scale model of the North American X-15 research airplane used in this investigation was supplied by the contractor. It was constructed of steel, aluminum, and plastic. Photographs of the model are presented in figure 1, and dimensional details are shown in figure 2 and table I.

The model represents configuration 1 of the X-15. Distinguishing features of this original configuration include fuselage side fairings which originate well forward of the canopy, exposed (when retracted) landing skids located in the side fairings beneath the wing, double-wedge vertical-tail airfoil sections, and a total vertical-tail exposed area distributed 73 percent above the fuselage and 27 percent below.

Speed-brake deflections on the full-scale airplane were designed to be obtained by spreading apart the convergent portions of the upper and lower vertical tails about hinge lines along the line of maximum thickness of each surface. A speed-brake deflection of 45° was simulated on the present model by attaching wedge-shaped blocks to the convergent sections of the tails.

Tunnel and Model Support

The tests were conducted in the Langley 8-foot transonic pressure tunnel which is a single-return, rectangular, slotted-throat wind tunnel having controls that allow for the independent variation of Mach number, stagnation pressure, temperature, and humidity. For test Mach numbers to 1.20, the tunnel was operated in the conventional manner. In order to obtain a Mach number of 1.43, the variable Mach number transonic nozzle was changed to a fixed Mach number supersonic nozzle by enclosing the slots with fairings. (See ref. 2.)

The model was attached to a sting support through an electrical strain-gage balance located inside the fuselage. The sting support was cylindrical for 2.5 base diameters downstream of the model base and had a diameter of 0.55 base diameters. At its downstream end, the sting was attached to an arc-shaped support strut which spanned the tunnel from top to bottom. This support strut was rotated to obtain changes in angle of attack, the center of rotation of the system being near the model in order to minimize overall vertical motion of the model.

Measurements and Accuracy

Model forces and moments were measured by a six-component internal strain-gage balance and converted by automatic electrical computing equipment to lift, drag, pitching moment, lateral force, yawing moment, and rolling moment about stability axes (see fig. 3) for a center-of-gravity location of 25 percent of the mean aerodynamic chord based on the total wing area. Accuracies of the coefficients are estimated at a Mach number of 1.0 and a dynamic pressure of 784 pounds per square foot to be:

C_L	± 0.01
C_D	± 0.002
C_m	± 0.002
C_l	± 0.0005
C_n	± 0.0005
C_y	± 0.005

The angle of attack was set to within $\pm 0.1^\circ$ by means of a pendulum-type attitude indicator located in the nose of the model. The angle of sideslip was determined to within $\pm 0.2^\circ$ by means of a calibration of sting and balance deflection with respect to model load. Control deflections are estimated to be accurate within $\pm 0.2^\circ$.

The Mach number was determined within ± 0.003 from a calibration with respect to the pressure in the chamber surrounding the slotted test section. Base pressure coefficients were obtained from an orifice located inside the model forward of the base and are estimated to be accurate within ± 0.005 .

L
3
7
6

Tests

The complete model was tested with horizontal-tail deflections for pitch and roll and with a speed brake deflection of 45° . The model was also tested with the horizontal tail, vertical tail, and fuselage side fairings removed. The detailed test program, including a listing of the figures presenting the basic data, is shown in table II.

The test range included Mach numbers from 0.60 to 1.43, angles of attack from -2° to approximately 20° , and angles of sideslip of 0° , 2° , and 5.1° . The average test Reynolds number based on the mean aerodynamic chord of the total wing varied from 2.2×10^6 to 2.9×10^6 over the Mach number range. (See fig. 4.) The model was tested in a smooth condition with natural boundary-layer transition.

Corrections

Subsonic tunnel boundary interference is minimized by the slotted test section, and no corrections for this interference have been applied. No corrections are necessary for the effects of supersonic boundary-reflected disturbances since they are negligible for Mach numbers to 1.03 (ref. 3), and the reflected disturbances pass well downstream of the base of the model at Mach numbers of 1.18, 1.20, and 1.43.

With the measured base pressure coefficients (presented for three of the configurations tested in figure 5), the data have been adjusted to an assumed condition of free-stream static pressure acting over the base of the fuselage. No sting-interference corrections have been applied.

PRESENTATION OF RESULTS

The basic data adjusted to represent free-stream static pressure at the fuselage base are presented as functions of lift coefficient or angle of attack at constant Mach number in figures 6 to 16 as indicated in table II. Included in these figures are a comparison of the basic longitudinal data for the complete model with various horizontal-tail deflections in pitch and with the horizontal tail off (fig. 6) and a comparison of the basic lateral-directional data for the complete model with and without horizontal-tail deflections for roll control. (See fig. 9.)

The longitudinal stability and control characteristics are summarized as a function of Mach number in figures 17 to 19; the drag characteristics, in figure 20; and the lateral-directional stability and control characteristics, in figures 21 to 23.

DISCUSSION

Longitudinal Characteristics

Lift-curve slopes.- The lift curves for the complete model with various horizontal-tail deflections were generally similar and indicated small increases in slope at an angle of attack of about 2° , which were followed by approximate linearity up to the highest angles tested. (See fig. 6.) The lift-curve slopes for the complete model with a horizontal-tail deflection of 0° are summarized for angles of attack of 0° and 10° in figure 17. At a Mach number of 1.43, opening the speed brakes decreased the lift-curve slope of the complete model approximately 6 percent.

As indicated in figure 17, effects of the horizontal tail on lift-curve slope were large, especially at the higher angles of attack; the removal of the tail reduced the lift-curve slope of the complete model on the order of 20 percent over the Mach number range at an angle of attack of 10° . This was the expected result of the large ratio of tail area to wing area (0.55) for this configuration. It is of interest to note that the lift effectiveness of the tail was severely reduced at angles of attack near 0° for Mach numbers from 0.90 to 1.03. It is possible that this reduction was due to a wake effect of the wing, or, as has been indicated by unpublished data obtained with the wing off, to an effect of the body flow field.

The fuselage side fairings contribute significantly to the total lifting surface of this configuration and, as a result, produced a sizable portion of the total lift, especially at the higher angles of attack. (See fig. 17.)

Longitudinal stability.- Positive longitudinal stability was indicated for the complete model with various horizontal-tail settings for all conditions tested except at Mach numbers of 0.925 and 0.95, where approximately neutral stability occurred at lift coefficients near and slightly below zero. (See fig. 6.) Even at these Mach numbers, however, positive stability was regained with increases in lift coefficient above zero. The loss in stability was probably caused by the loss of horizontal-tail lift effectiveness in this same region. As indicated in figure 6, differential deflection of the horizontal tail had little effect on the pitch curves.

At zero lift, the static margin of the complete model with a horizontal-tail deflection of 0° was 5 percent of the wing mean aerodynamic chord at subsonic speeds, decreased to zero at Mach numbers near 0.95, and increased to 33 percent at a Mach number of 1.43 (fig. 18). With increases in lift coefficient above zero, the static margin generally increased. Deflecting the speed brakes increased the static margin of the complete model only 2 percent of the mean aerodynamic chord at a Mach number of 1.43. (See fig. 18.) However, the change in pitching moment at a given lift due to opening the speed brakes was large (compare figs. 6 and 10) and would require about a 4° horizontal-tail deflection to trim out.

With the horizontal tail off, the model was stable at low lift coefficients for Mach numbers above 1.03; however, at lift coefficients above 0.60, it was unstable over the speed range tested. (See figs. 6 and 18.) The increased stability contribution of the horizontal tail at the higher lift coefficients as compared with the lower lift coefficients (fig. 18) was a result of the increased lift effectiveness of the horizontal tail at the higher angles of attack noted previously.

The data for a Mach number of 1.43 indicated that the fuselage side fairings had a pronounced destabilizing effect on the model. (See fig. 18.) This effect was caused by the relatively large portion of side-fairing plan-form area ahead of the wing and in the vicinity of the canopy.

Longitudinal control.- The ability of the horizontal tail to produce changes in pitching moment at a given Mach number was approximately constant over the angle-of-attack range tested (fig. 6). There was some loss in control power at Mach numbers from 0.95 to 1.00 with increases in lift coefficient from 0 to 0.8 (fig. 19); however, at higher lift coefficients, no further loss was indicated. The variation of the control effectiveness parameter with Mach number (fig. 19) indicated the usual increase up to a Mach number of 0.90 followed by a decrease of approximately 40 percent with an increase in Mach number to 1.43. As indicated in figure 6 deflecting the horizontal tail differentially for roll control had little effect on longitudinal control power.

The ability of the horizontal tail to produce increments in trim lift coefficient decreased steadily with increases in Mach number above 0.90 (fig. 19). This was a combined result of the increase in static margin and decrease in control power previously noted.

Drag and lift-drag ratio.- As would be expected from a study of the configuration, the drag of the model was comparatively high at transonic speeds. (See figs. 6 and 20.) It should be noted, however, that drag with the speed brakes closed is of minor importance to design performance of the airplane.

The speed brakes were very effective. When the brakes were deflected 45° , they increased the zero-lift drag by a factor of 5 at a Mach number of 1.43. (See fig. 20.) The drag increment due to speed brakes obtained at zero lift remained approximately constant up to a lift coefficient of at least 1.2. (Compare figs. 6 and 10.)

The maximum lift-drag ratio for the model with horizontal tail and speed brakes undeflected decreased from 6.7 at a Mach number of 0.60 to approximately 4.5 at Mach numbers above 1.00. (See fig. 20.) Opening the speed brakes decreased the maximum lift-drag ratio to 2 at a Mach number of 1.43.

Lateral Directional Characteristics

Directional stability.- The complete model was directionally stable (positive values of $C_{n\beta}$) over the Mach number, angle-of-attack, and angle-of-sideslip ranges of these tests. (See figs. 8 and 21.) The degree of stability remained approximately constant for angles of attack up to 12° , the lower vertical tail apparently becoming more effective as the angle of attack increased and the upper tail moved into the wake of the wing and fuselage. At higher angles of attack, directional stability decreased slightly. As indicated in figure 21, Mach number effects on $C_{n\beta}$ were small for the range tested.

Opening the speed brakes had a large favorable effect on directional stability, increasing $C_{n\beta}$ approximately 30 percent over the angle-of-attack range at a Mach number of 1.43. (See figs. 10 and 21.)

With the vertical tail off, the model was directionally unstable over the Mach number and angle-of-attack range, the instability increasing slightly with increasing angle of attack. (See figs. 14 and 21.)

Effective dihedral.- The complete model with the horizontal tail and speed brakes undeflected had positive effective dihedral ($-C_{l\beta}$) for the

Mach number, angle-of-attack, and angle-of-sideslip ranges investigated. (See figs. 8 and 22.) Generally, small increases in dihedral effect were indicated with increasing angle of attack and Mach number.

Some idea of the relative contribution of the various configuration components to the effective dihedral of the complete model may be obtained from figure 22, which presents $C_{l\beta}$ as a function of Mach number for angles of attack of 0° and 12° . At an angle of attack of 0° , the horizontal tail, because of its negative dihedral, had a small destabilizing effect. The lower vertical tail also contributed a destabilizing effect. However, the upper vertical tail had an area approximately 2.7 times that of the lower tail and contributed enough positive dihedral to more than balance the destabilizing moments and result in a stable complete configuration. At an angle of attack of 12° , the wing and horizontal tail contributed large positive dihedral effects. The net effect of the vertical tail, however, was destabilizing, the contribution of the upper vertical tail to positive effective dihedral having decreased while that of the lower tail to instability increased. As a result, the effective dihedral of the complete model at an angle of attack of 12° was only slightly higher than it was at 0° .

L
3
7
6

Opening the speed brakes at a Mach number of 1.43 almost doubled the effective dihedral of the complete model at an angle of attack of 0° and had little effect at an angle of attack of 12° . (See figs. 10 and 22.) These effects were due to the asymmetry of the brakes at low angles of attack and the change in relative effectiveness of the upper and lower brakes at the higher angles of attack.

Lateral control.- The differentially deflected horizontal tail was effective as a roll control for all Mach numbers and angles of attack tested. (See figs. 9(a) and 23.) Mach number and angle-of-attack effects on lateral control were relatively small except for a Mach number of 1.43 where control power decreased steadily with increases in angle of attack above 8° . However, at an angle of attack of 19° , the highest attained, the tail as a roll control was still 60 percent as effective as it was at the lower angles.

Large favorable yawing moments were produced when the horizontal tail was differentially deflected for roll control at the lower angles of attack. (See fig. 9(b).) These yawing moments were caused by a combination of loads induced on the vertical tail by the deflected horizontal tail, high drag on the deflected side of the horizontal tail, and side force resulting from the negative dihedral of the deflected horizontal tail. The resulting large values of the ratio of yawing effectiveness to rolling effectiveness (fig. 23) are generally considered undesirably excessive from a flying qualities standpoint. With increasing angle of attack, the favorable yaw decreased and finally became adverse above angles of attack varying from above 20° at a Mach number of 0.60 to 14°

at a Mach number of 1.43. (See figs. 9(b) and 23.) This effect was the result of a shift in relative loading between the left- and right-hand horizontal tails as the angle of attack increased.

CONCLUSIONS

The following conclusions were made from wind-tunnel tests of a 0.0667-scale force model of configuration 1 of the North American X-15 research airplane at transonic speeds:

1. The drag of the configuration was comparatively high. The maximum lift-drag ratios varied from 6.7 at a Mach number of 0.60 to approximately 4.5 at Mach numbers above 1.00.
2. The model was stable longitudinally except at Mach numbers near 0.95 where neutral stability was indicated at approximately zero lift.
3. Satisfactory longitudinal control power was indicated over the Mach number and angle ranges tested.
4. The model was stable directionally and had positive effective dihedral for the conditions investigated.
5. The horizontal tail when differentially deflected was adequate as a roll control, but produced excessively large favorable yawing moments at the lower angles of attack.
6. Differential deflection of the horizontal tail for lateral control had little effect on longitudinal stability and control.
7. Deflecting the speed brakes 45° at a Mach number of 1.43 increased the zero-lift drag by a factor of 5, caused large longitudinal trim changes, increased directional stability by 30 percent, and doubled effective dihedral at low angles of attack.

Langley Research Center,
National Aeronautics and Space Administration,
Langley Field, Va., March 19, 1959.

REFERENCES

1. Boisseau, Peter C.: Investigation of the Low-Speed Stability and Control Characteristics of a 1/7-Scale Model of the North American X-15 Airplane. NACA RM L57D09, 1957.
2. Matthews, Clarence W.: An Investigation of the Adaptation of a Transonic Slotted Tunnel to Supersonic Operation by Enclosing the Slots With Fairings. NACA RM L55H15, 1955.
3. Ritchie, Virgil S., and Pearson, Albin O.: Calibration of the Slotted Test Section of the Langley 8-Foot Transonic Tunnel and Preliminary Experimental Investigation of Boundary-Reflected Disturbances. NACA RM L51K14, 1952.

L
3
7
6

TABLE I

DIMENSIONS OF THE 0.0667-SCALE MODEL OF THE
NORTH AMERICAN X-15 RESEARCH AIRPLANE

Wing:

Airfoil section	Modified NACA 66-005	
Total area, sq in.		127.744
Exposed area, sq in.		67.287
Total span, in.		17.870
Exposed span, in.		10.933
Total aspect ratio		2.50
Exposed aspect ratio		1.78
Leading-edge sweepback, deg		36.75
Quarter-chord-line sweepback, deg		25.64
Trailing-edge sweepforward, deg		17.75
Root chord at center line, in.		11.926
Exposed root chord, in.		8.798
Tip chord, in.		2.387
Total taper ratio		0.20
Exposed taper ratio		0.27
\bar{c} based on total area, in.		8.207
Dihedral		0
Incidence, deg		0

Horizontal tail:

Hinge line, percent exposed \bar{c}		37
Airfoil section	Modified NACA 66-005	
Total area in plane of surface, sq in.		70.853
Exposed area in plane of surface, sq in.		32.406
Total projected span, in.		14.108
Exposed projected span, in.		8.442
Total aspect ratio based on projected span and area in plane of surface		2.81
Exposed aspect ratio based on projected span and area in plane of surface		2.20
Leading-edge sweepback, deg		50.58
Quarter-chord-line sweepback, deg		45.00
Trailing-edge sweepback, deg		19.28
Root chord at center line, in.		8.017
Exposed root chord, in.		5.562
Tip chord, in.		1.685
Total taper ratio		0.21
Exposed taper ratio		0.30
\bar{c} based on total area, in.		5.539
\bar{c} based on exposed area, in.		3.969
Longitudinal distance from total wing 0.25 \bar{c} to exposed tail 0.25 \bar{c} , in.		11.872
Dihedral, deg		-15.00

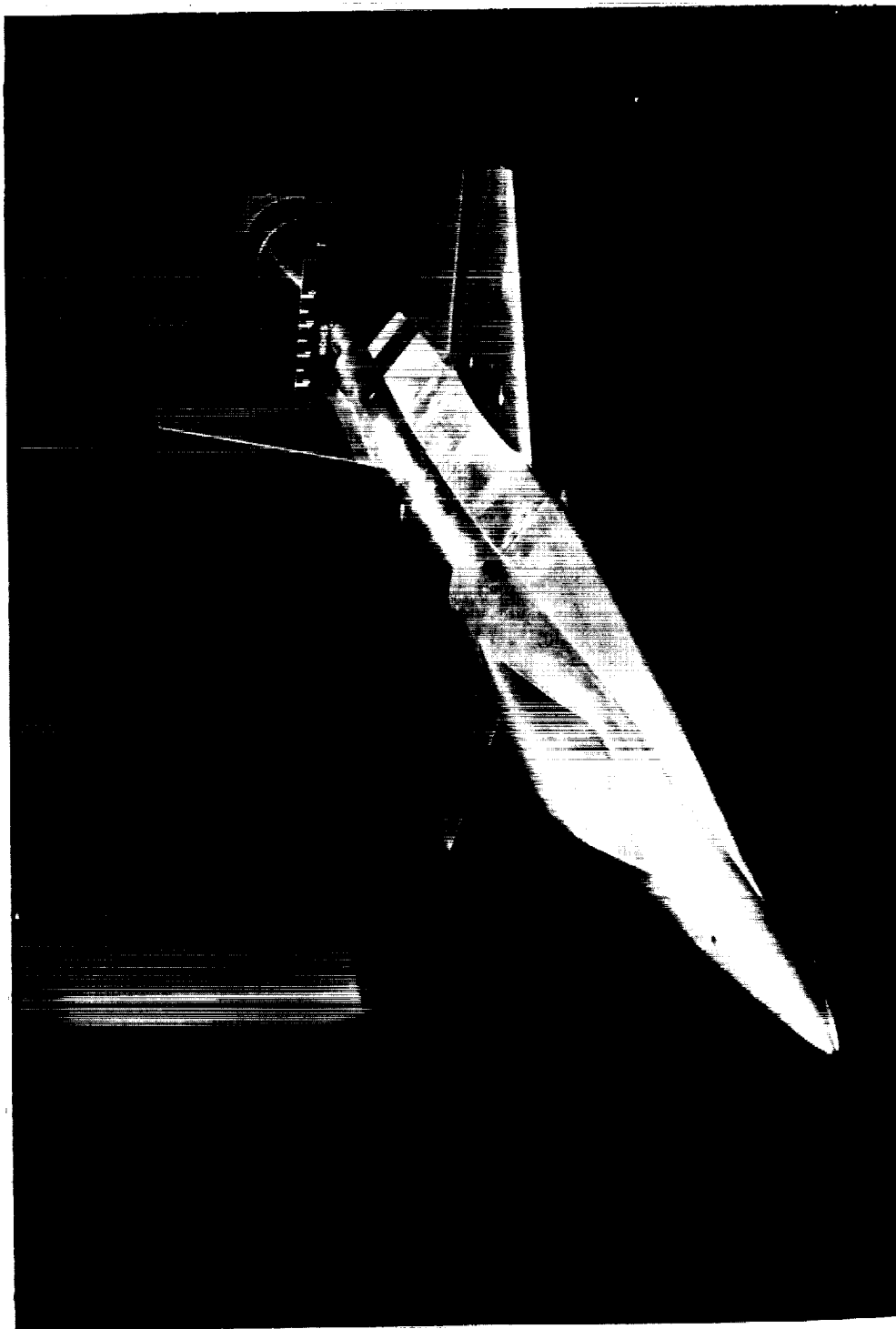
TABLE I
DIMENSIONS OF THE 0.0667-SCALE MODEL OF THE NORTH
AMERICAN X-15 RESEARCH AIRPLANE - Concluded

Upper vertical tail:	
Airfoil section	Modified 10° double wedge
Exposed area, sq in.	24.166
Exposed span, in.	5.510
Exposed aspect ratio	1.26
Leading-edge sweepback, deg	32.14
Quarter-chord-line sweepback, deg	21.99
Maximum-thickness sweepback, deg	0
Exposed root chord, in.	6.819
Tip chord, in.	1.953
Exposed taper ratio	0.29
\bar{c} based on exposed area	4.840
Longitudinal distance from total wing 0.25 \bar{c} to exposed tail 0.25 \bar{c} , in.	9.657
Speed brakes:	
Total surface area, sq in.	17.632
Span, in.	5.067
Root chord, in.	2.503
Tip chord, in.	0.977
Deflection, closed, deg	-4.38
Deflection, open, deg	45.00
Hinge-line sweepback, deg	0
Lower vertical tail:	
Airfoil section	Modified 15° double wedge
Exposed area, sq in.	8.757
Exposed span, in.	1.500
Exposed aspect ratio	0.26
Leading-edge sweepback, deg	60.00
Quarter-chord-line sweepback, deg	52.41
Maximum-thickness sweepback, deg	0
Exposed root chord, in.	6.900
Tip chord, in.	4.383
Exposed taper ratio	0.63
\bar{c} based on exposed area	5.740
Longitudinal distance from total wing 0.25 \bar{c} to exposed tail 0.25 \bar{c} , in.	10.292
Speed brakes:	
Total surface area, sq in.	7.644
Span, in.	1.500
Root chord, in.	2.666
Tip chord, in.	2.666
Deflection, closed, deg	-4.32
Deflection, open, deg	45.00
Hinge-line sweepback, deg	0
Fuselage:	
Length, in.	39.200
Maximum cross-sectional area of basic fuselage, sq in.	9.805
Maximum cross-sectional area of fuselage with side fairings, sq in.	13.005
Fineness ratio of basic fuselage	11.09
Fineness ratio of fuselage with side fairings	9.63
Fuselage base area, sq in.	8.042

TABLE II

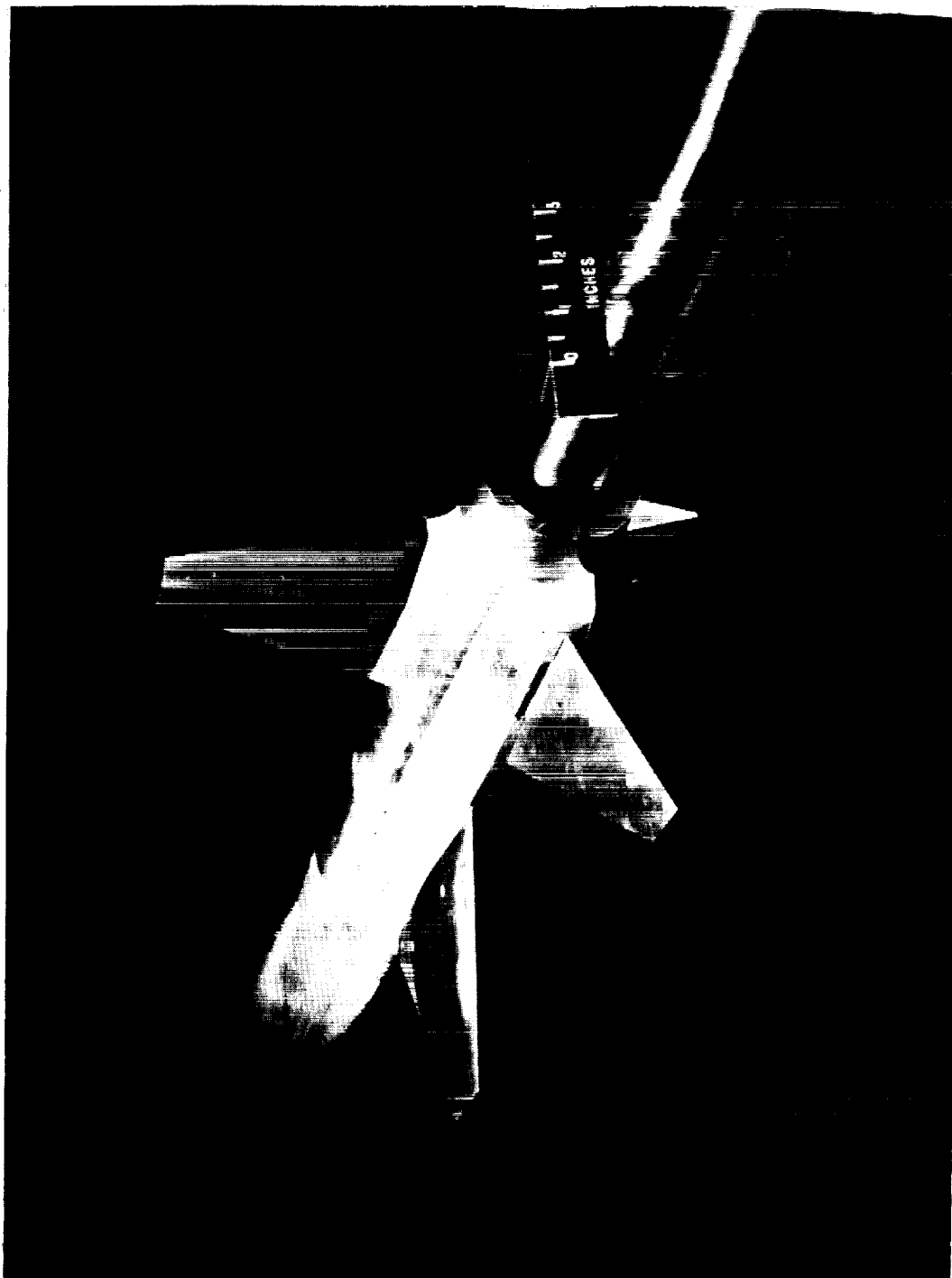
TEST PROGRAM AND LIST OF FIGURES PRESENTING BASIC DATA

Configuration	M	β , deg	Basic-data figures
Complete model; $\delta_e = 0^\circ$, $\delta_a = 0^\circ$	0.60 to 1.43	0, 2, 5.1	6 to 9
Complete model; $\delta_e = -3^\circ$, $\delta_a = 6^\circ$	0.60 to 1.43	0	6, 9
Complete model; $\delta_e = -6^\circ$, $\delta_a = 0^\circ$	0.60 to 1.43	0	6
Complete model; speed brakes open	1.43	0, 2, 5.1	10
Model less horizontal tail	0.60 to 1.18, 1.43	0	6
Model less horizontal tail and side fairing	1.43	0, 2, 5.1	6, 11
Model less vertical tail	1.43	0, 2, 5.1	12
Model less horizontal tail and vertical tail	0.60 to 1.18	0, 2, 5.1	13, 14
	0.60 to 1.43	0, 2, 5.1	15, 16



L-93849
Figure 1.- Photographs of the 0.0667-scale model of the X-15 installed in the Langley 8-foot transonic pressure tunnel.

L-376



L-93850

Figure 1.- Concluded.

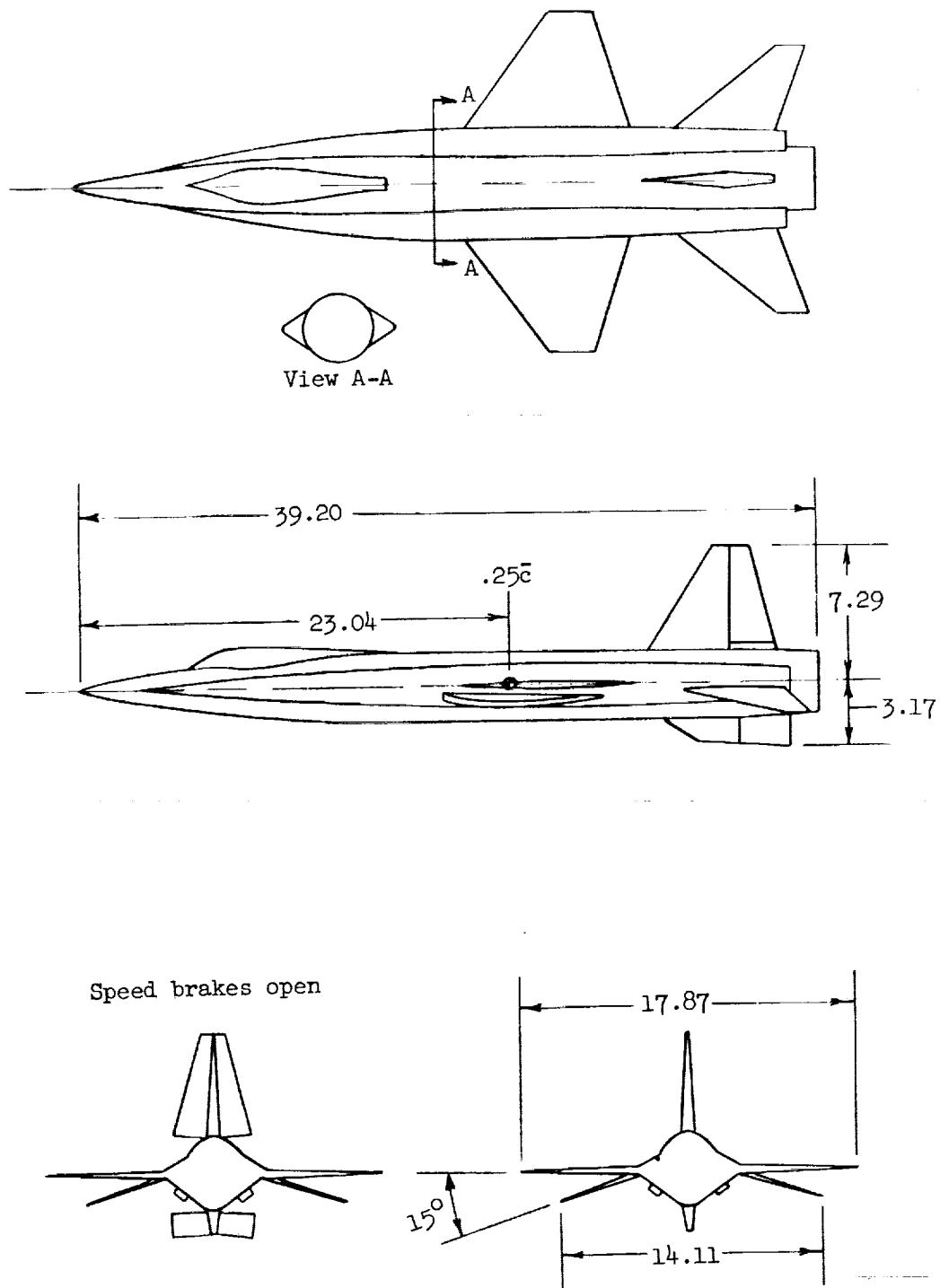


Figure 2.- Drawing of the 0.0667-scale model of the X-15. All dimensions are in inches and speed brakes closed unless otherwise noted.

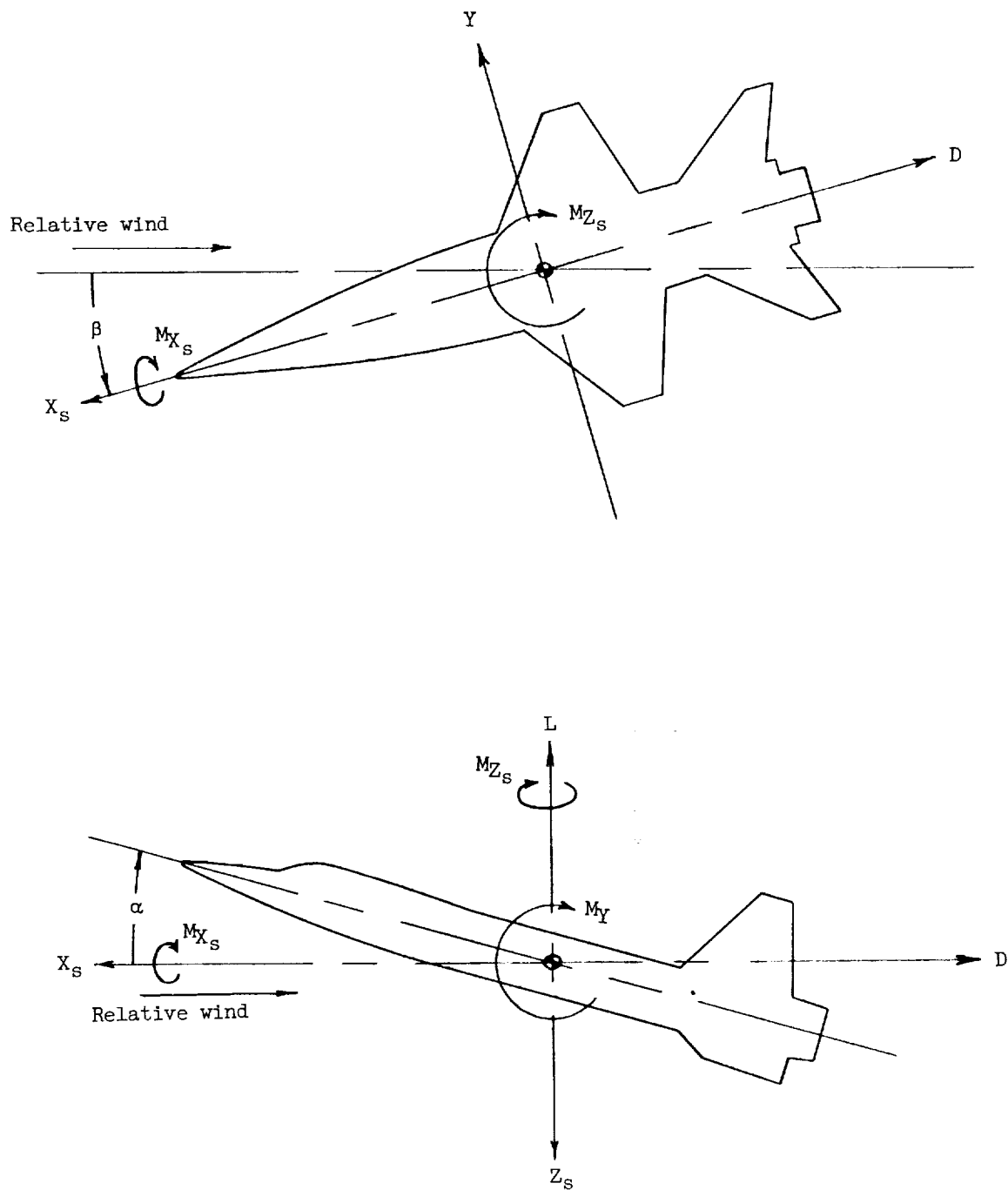


Figure 3.- System of stability axes. Arrows indicate positive directions.

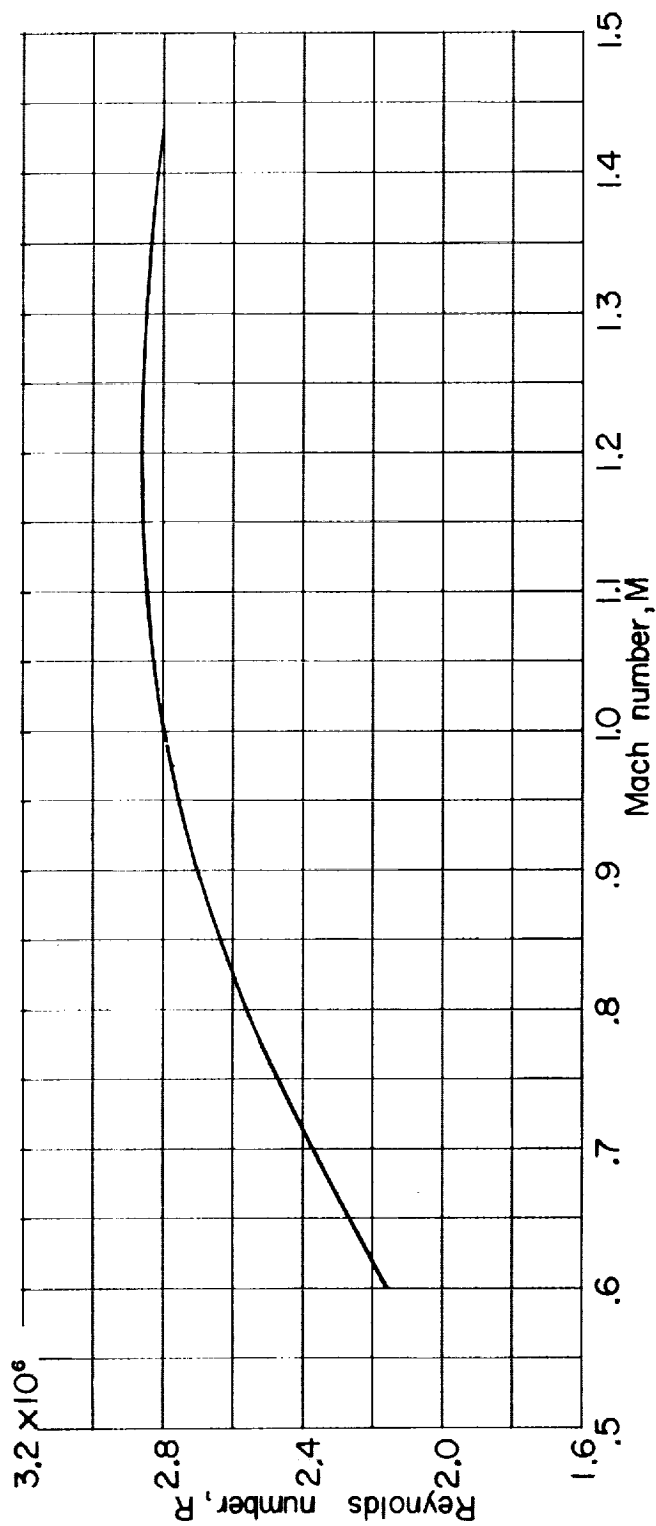


Figure 4.- Variation with Mach number of test Reynolds number based on $\bar{c} = 8.207$ inches.

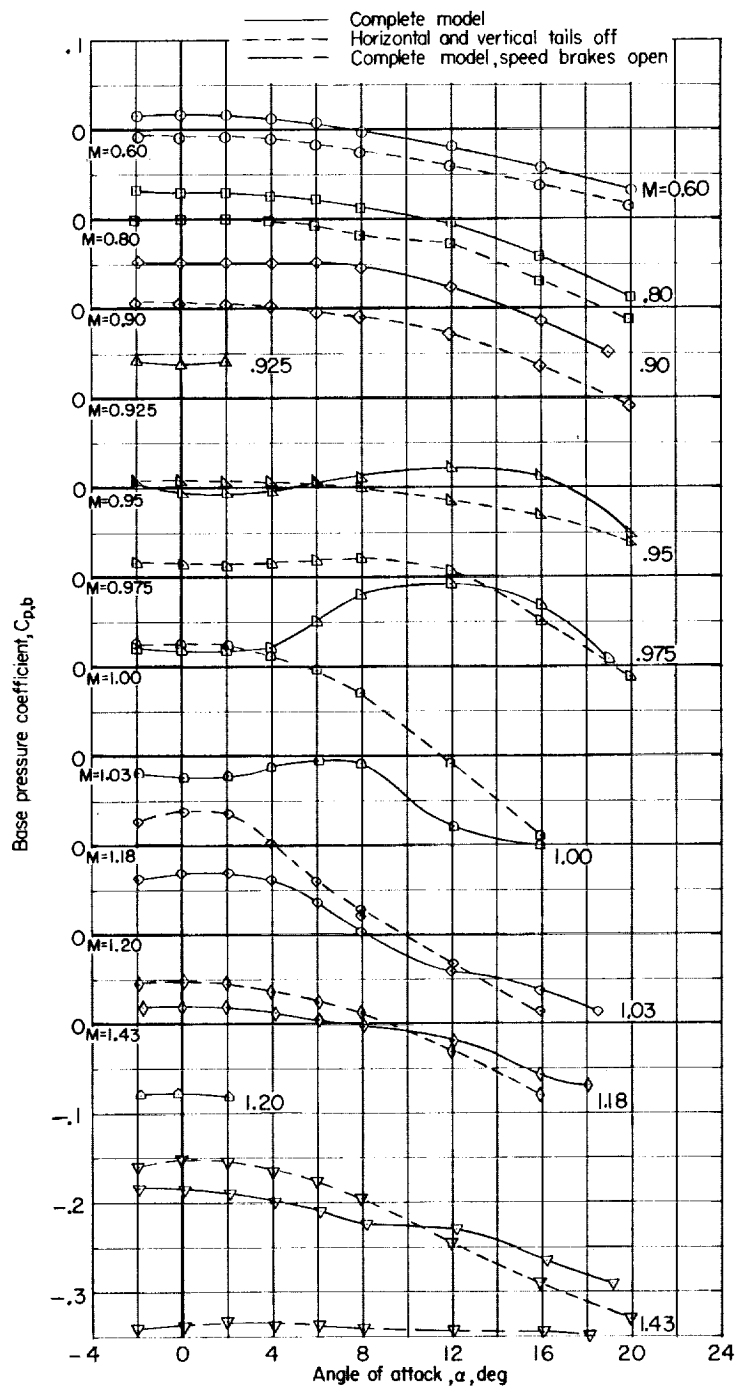


Figure 5.- Base pressure coefficients for the complete model and for the model with the horizontal and vertical tails off at zero sideslip. Surfaces undeflected unless otherwise noted.

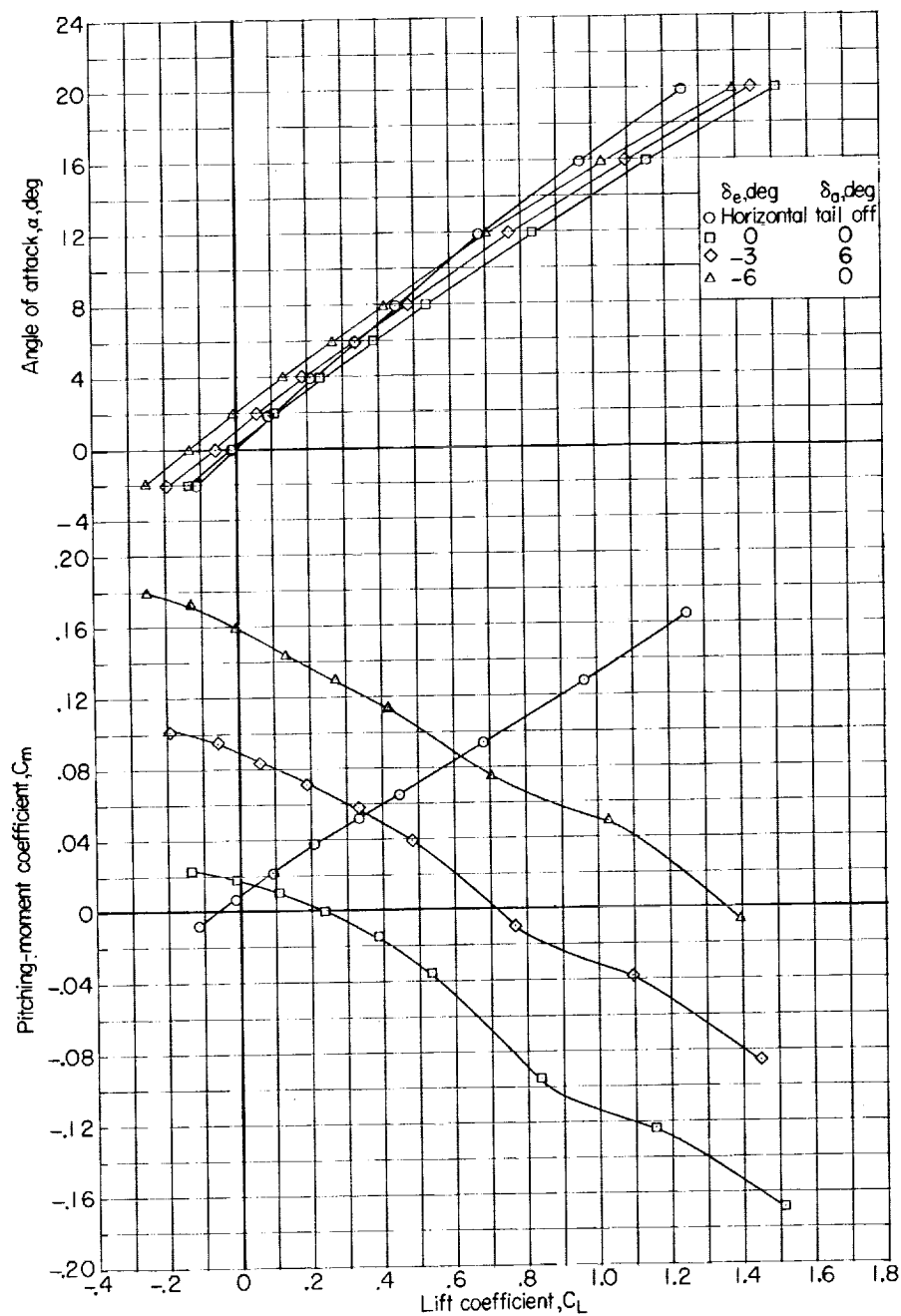
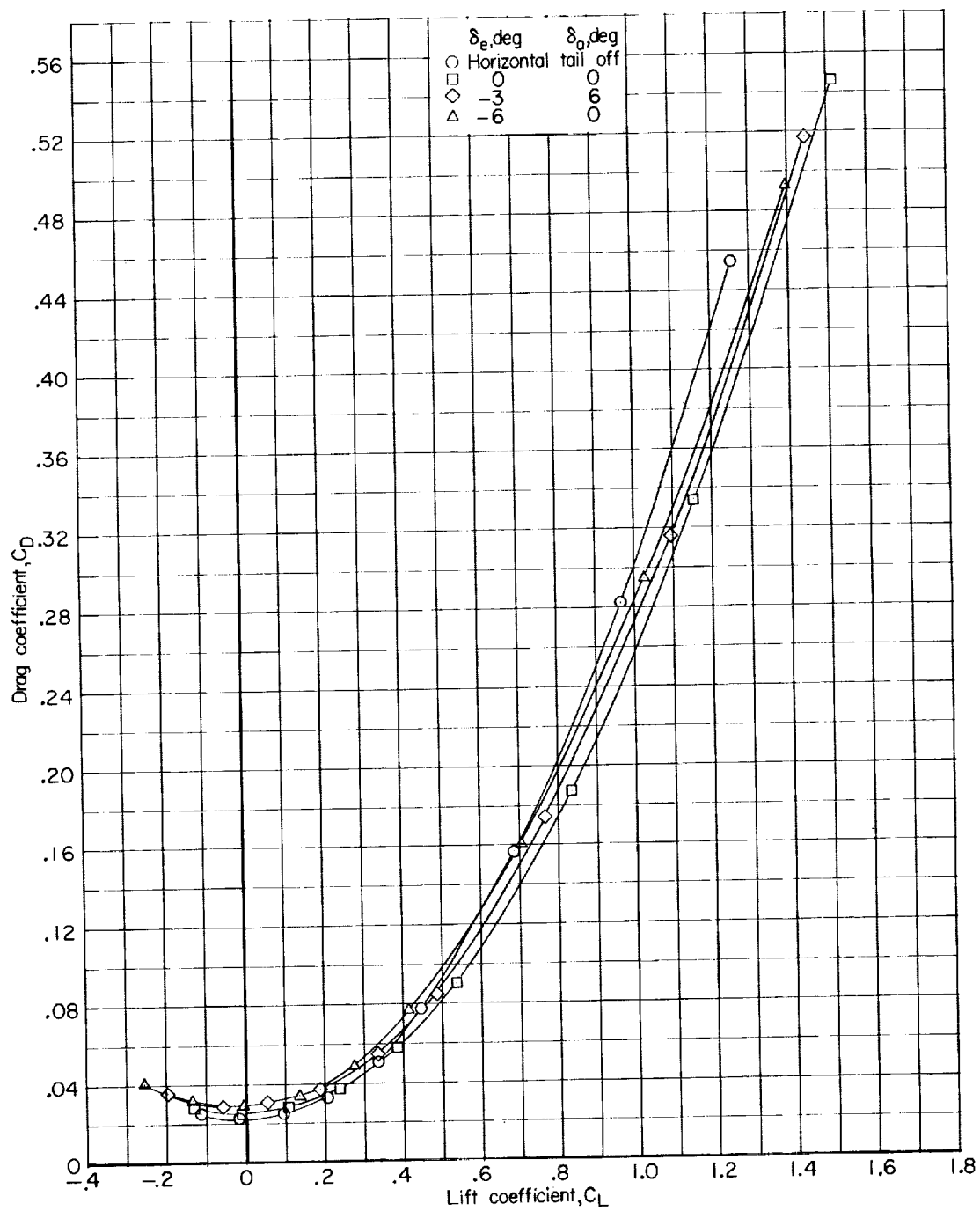
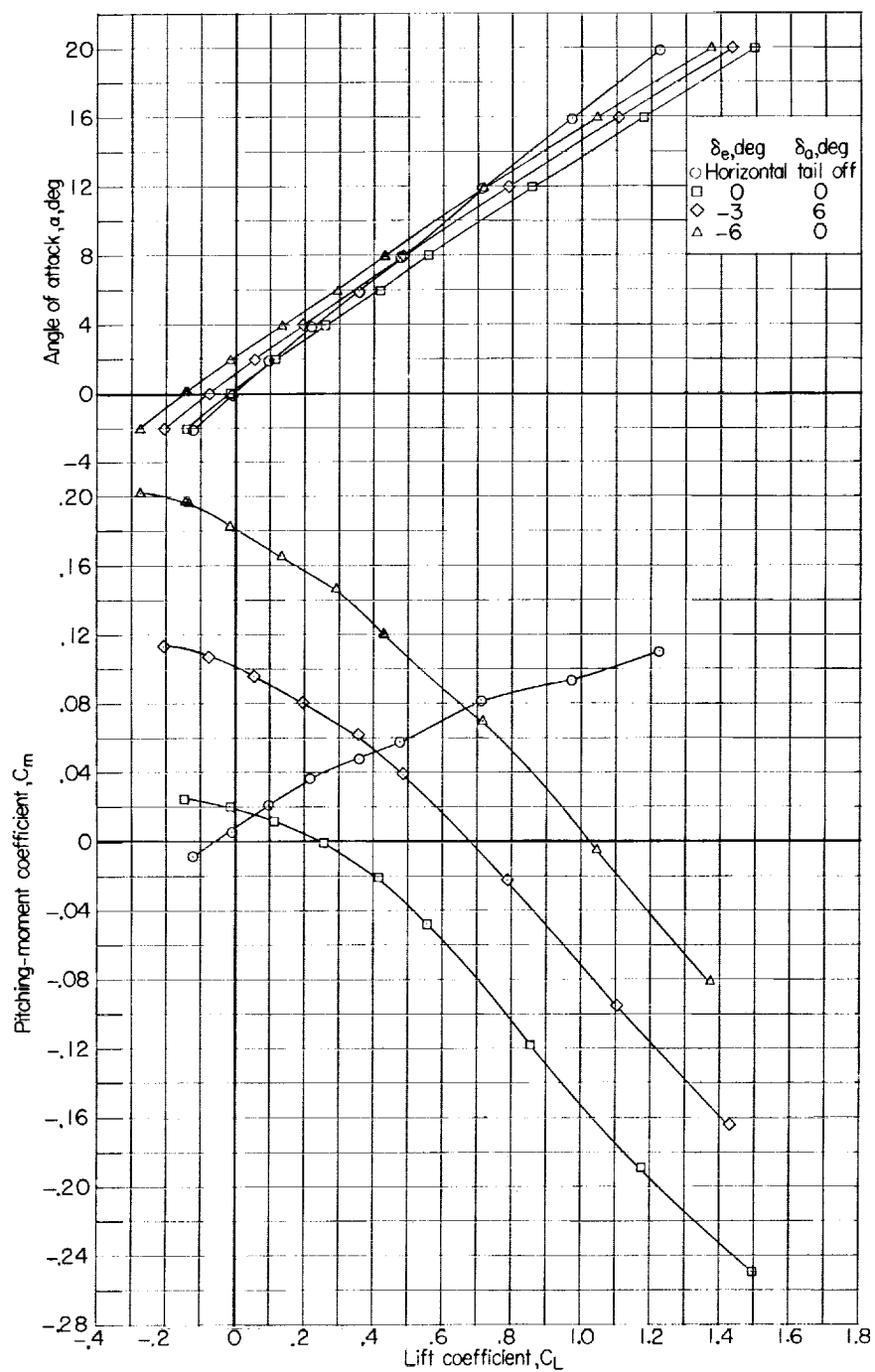
(a) $M = 0.60$.

Figure 6.- Longitudinal characteristics of the complete model with various horizontal-tail deflections and of the model with the horizontal tail off at zero sideslip.



(a) Concluded.

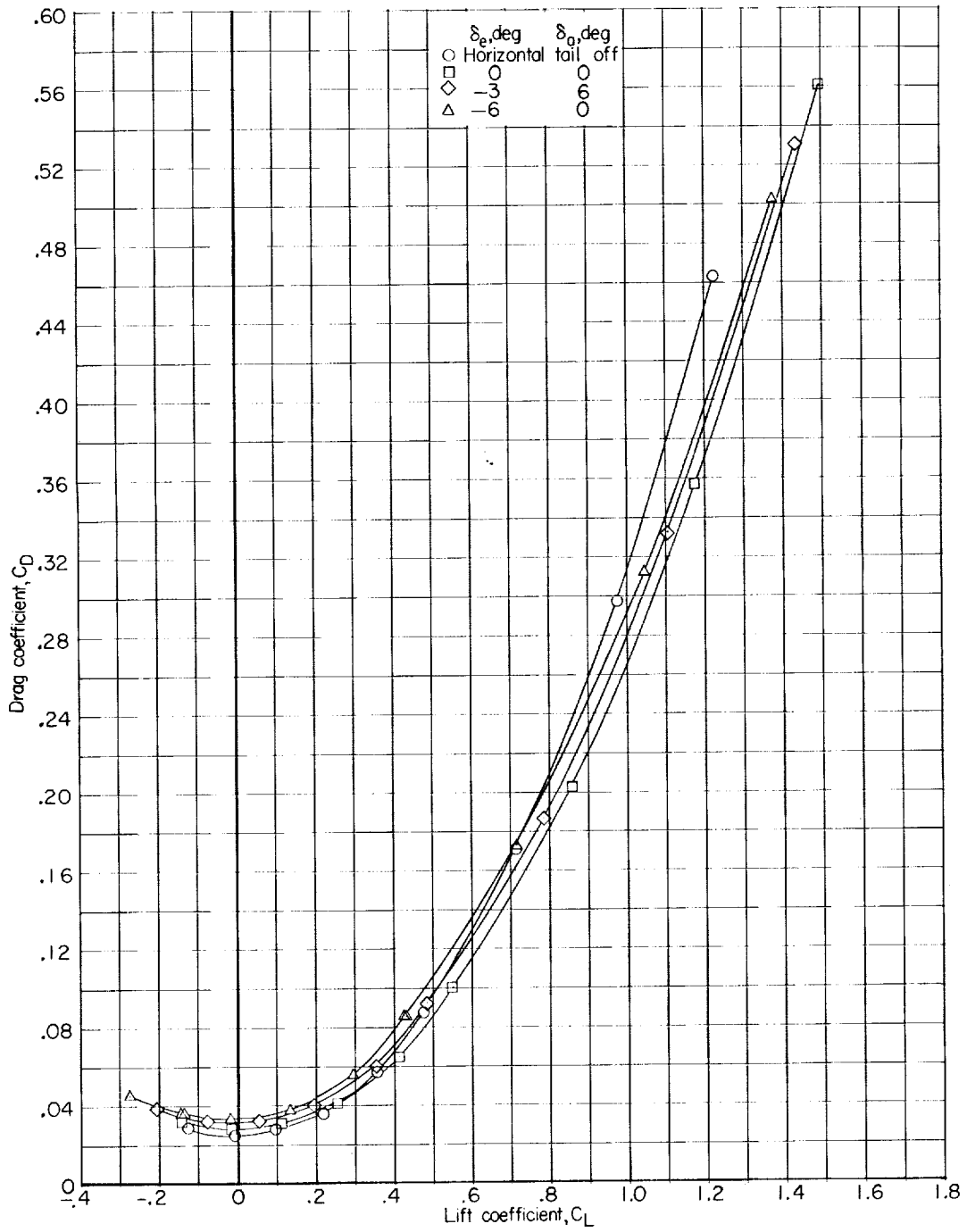
Figure 6.- Continued.



(b) $M = 0.80$.

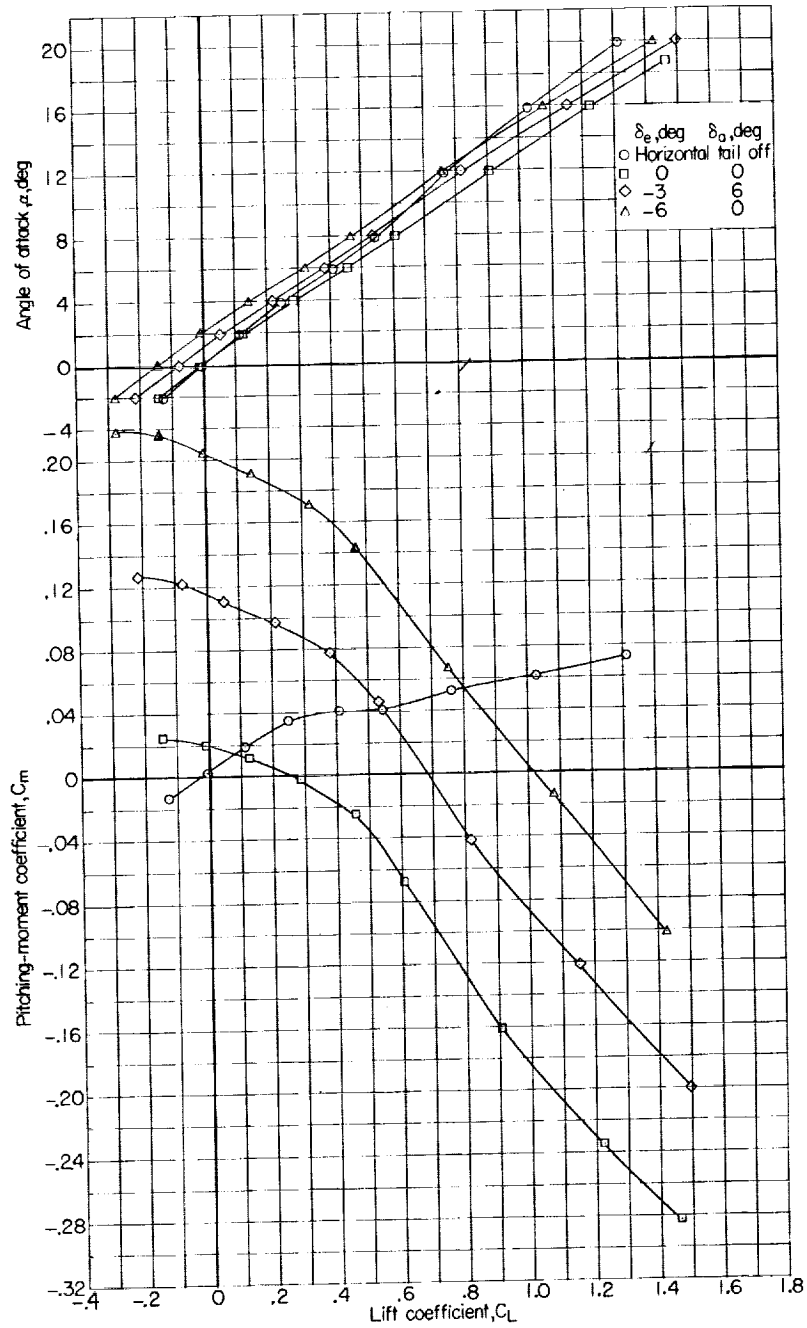
Figure 6.- Continued.

L-376



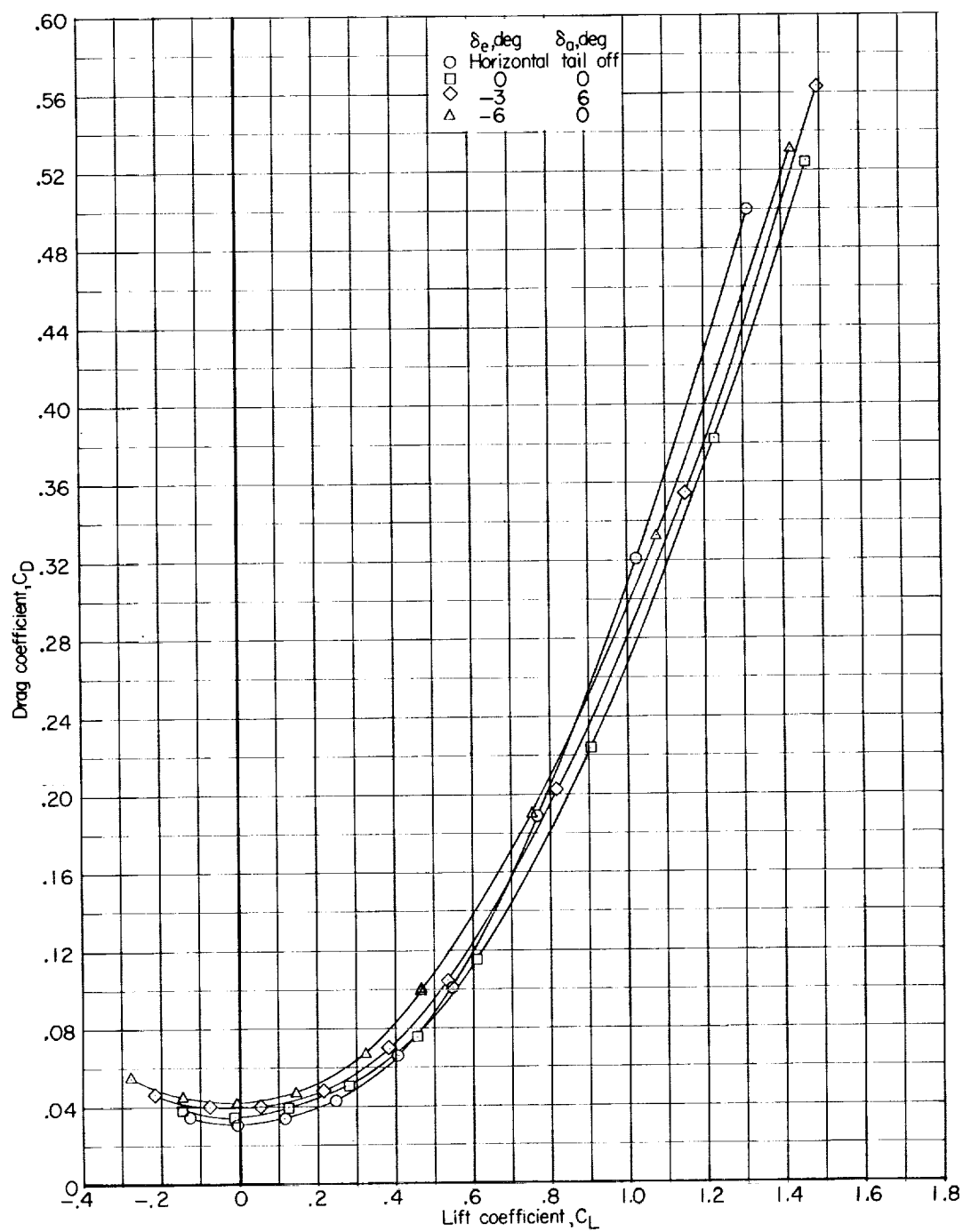
(b) Concluded.

Figure 6.- Continued.



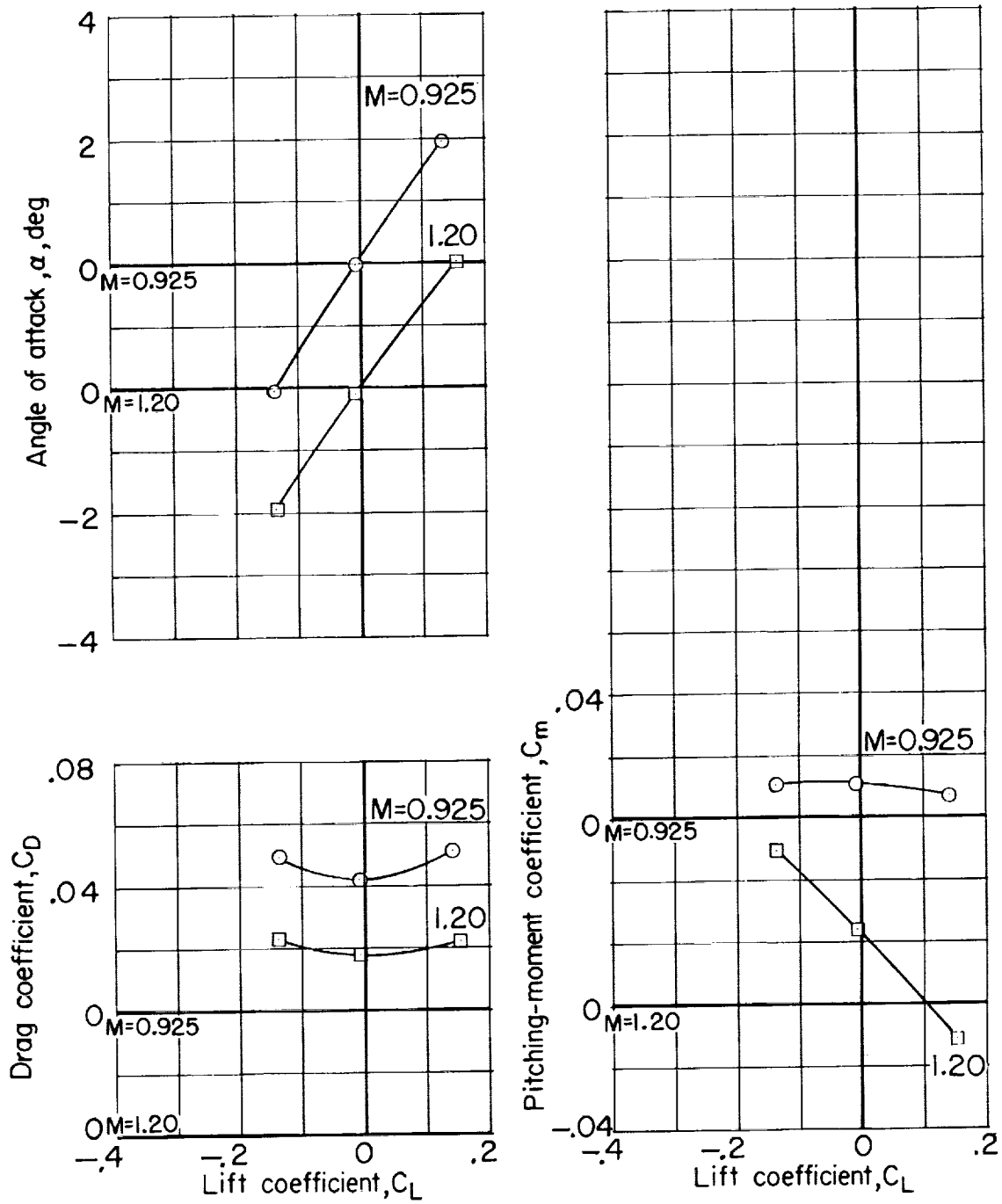
(c) $M = 0.90$.

Figure 6.- Continued.



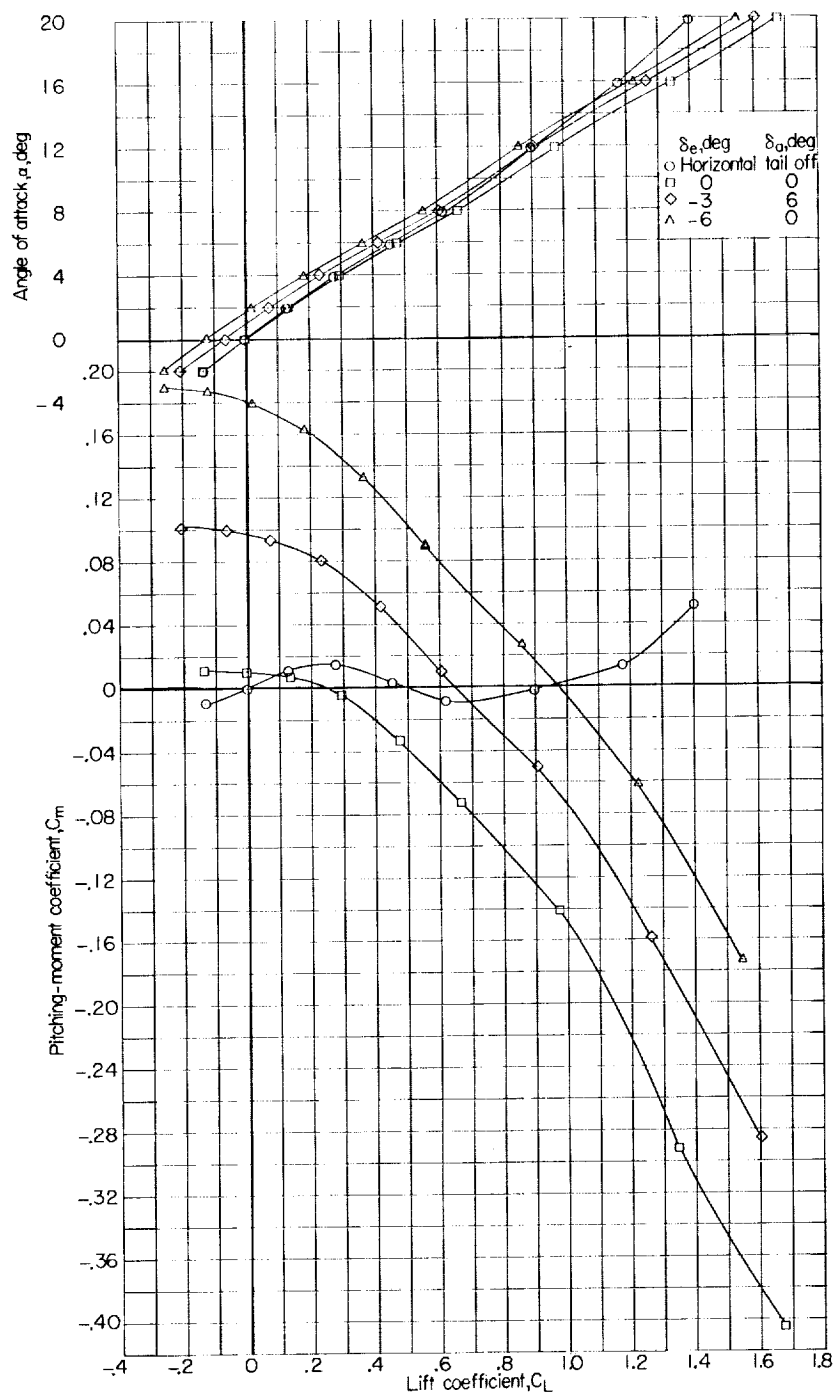
(c) Concluded.

Figure 6.- Continued.



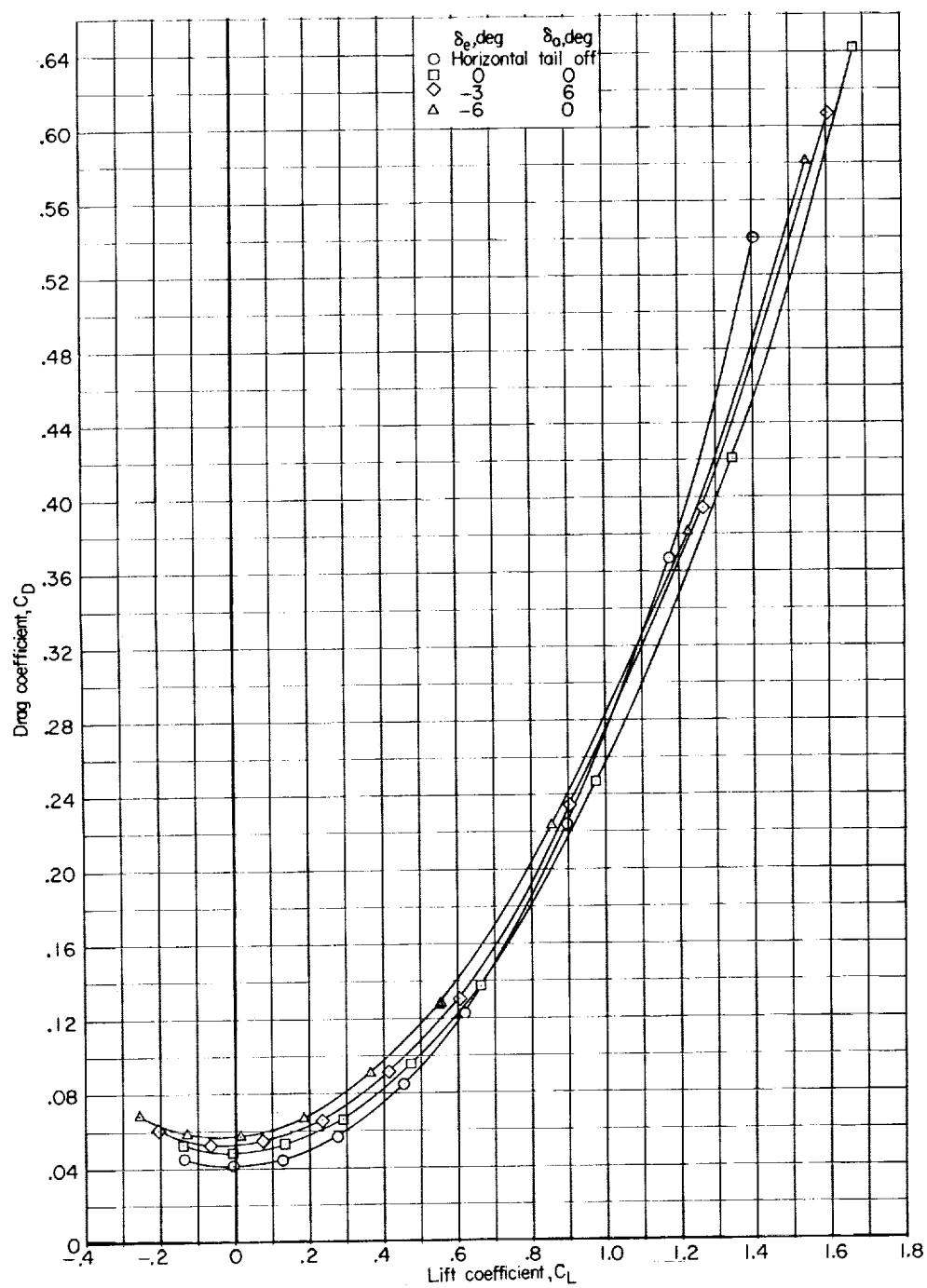
(d) $M = 0.925$ and 1.20 ; $\delta_e = 0^\circ$; $\delta_a = 0^\circ$.

Figure 6.- Continued.



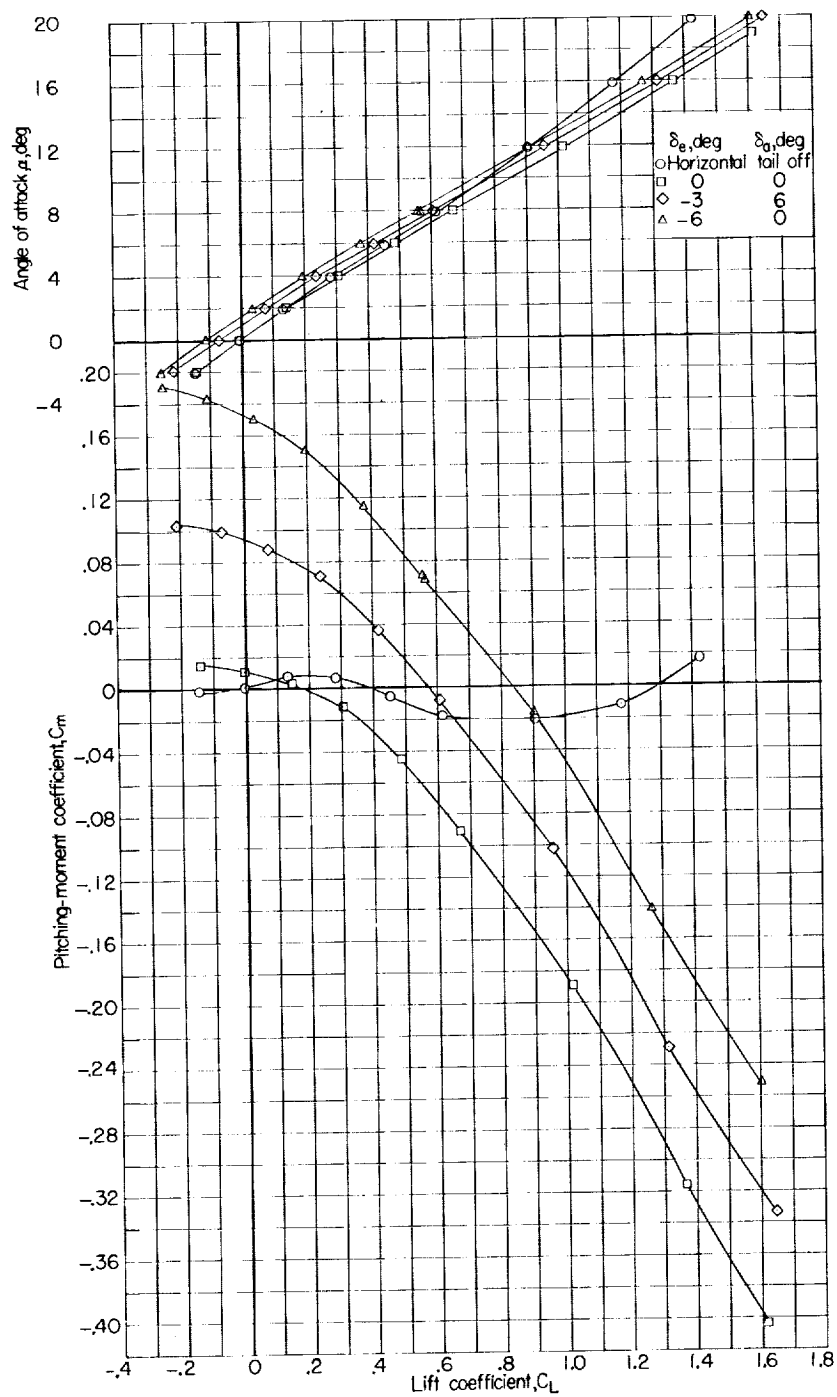
(e) $M = 0.95$.

Figure 6.- Continued.



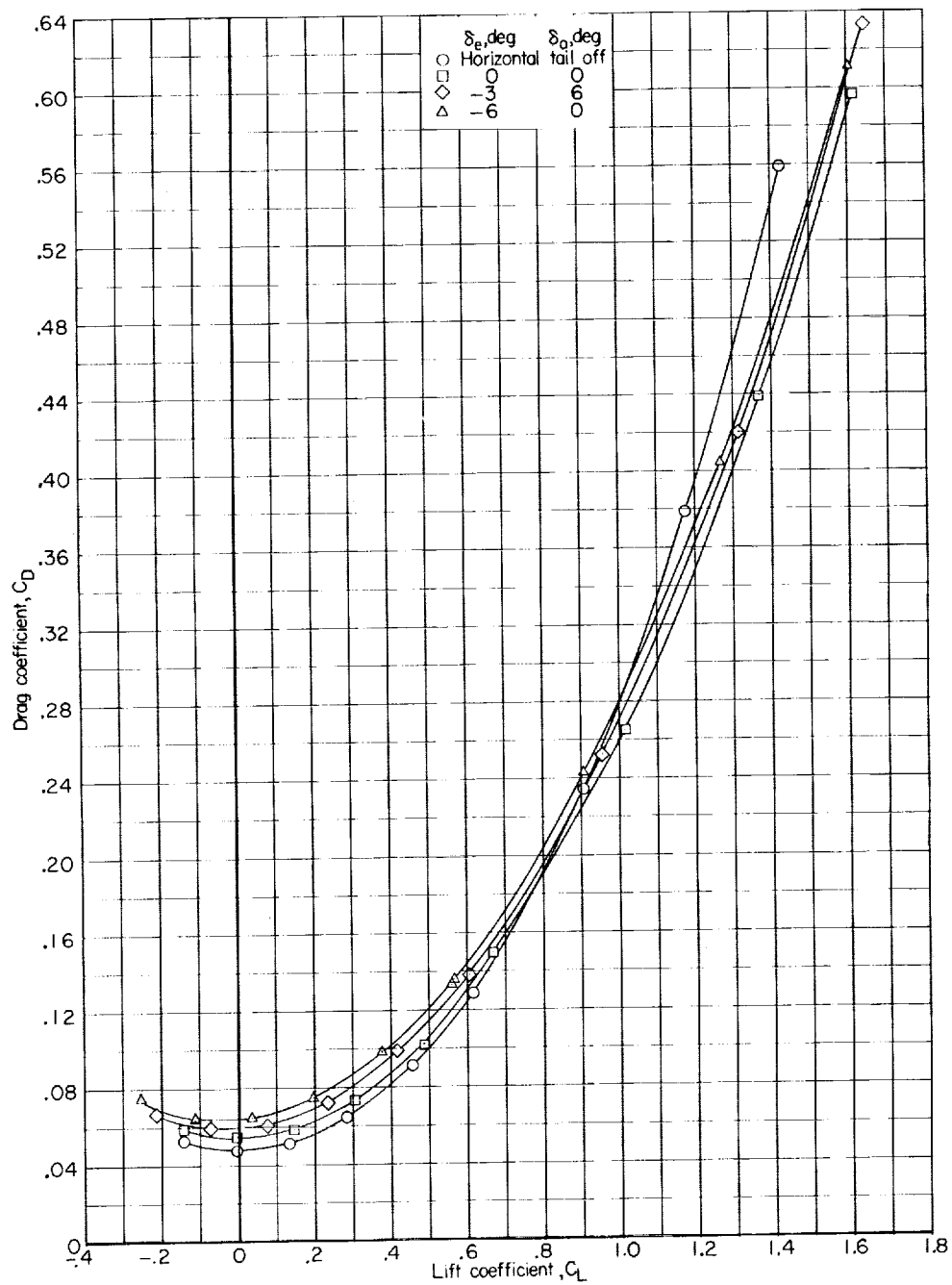
(e) Concluded.

Figure 6.- Continued.



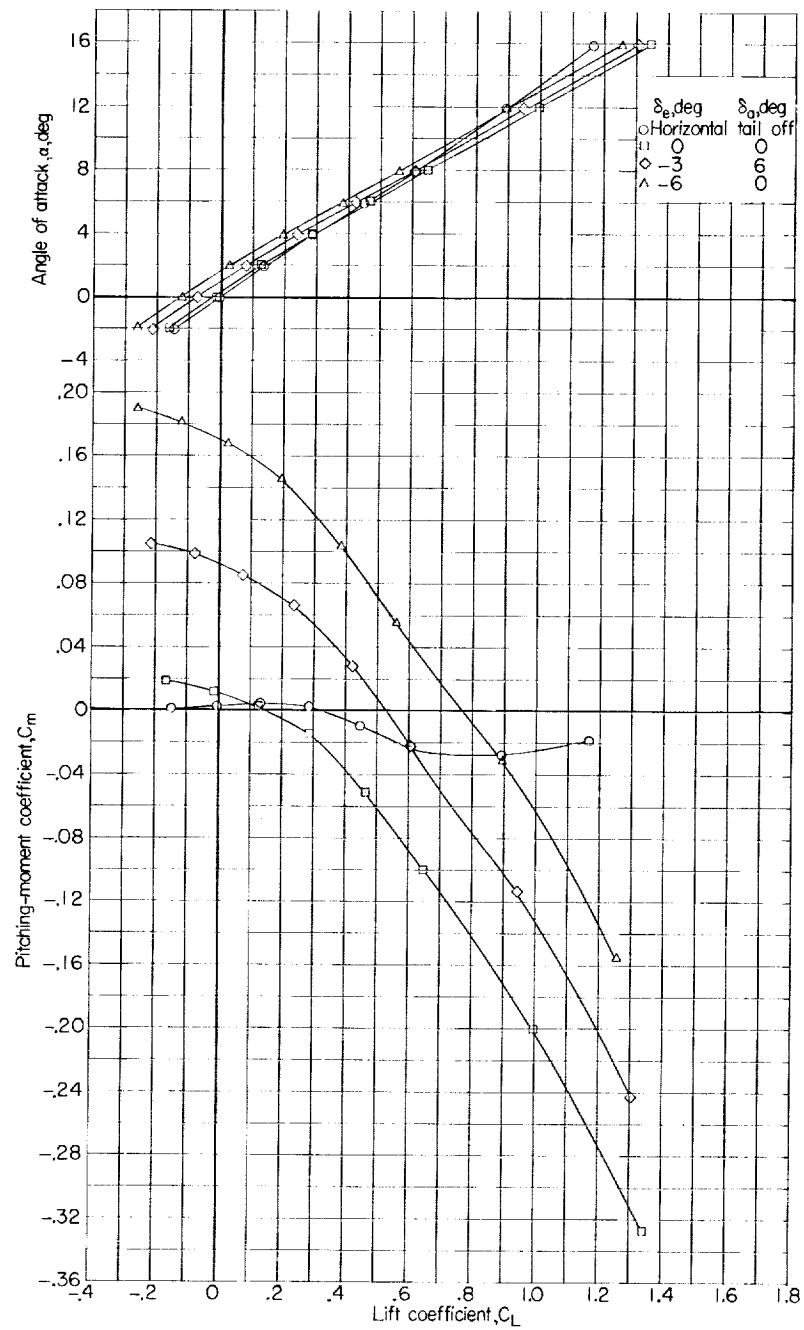
(f) $M = 0.975$.

Figure 6.- Continued.



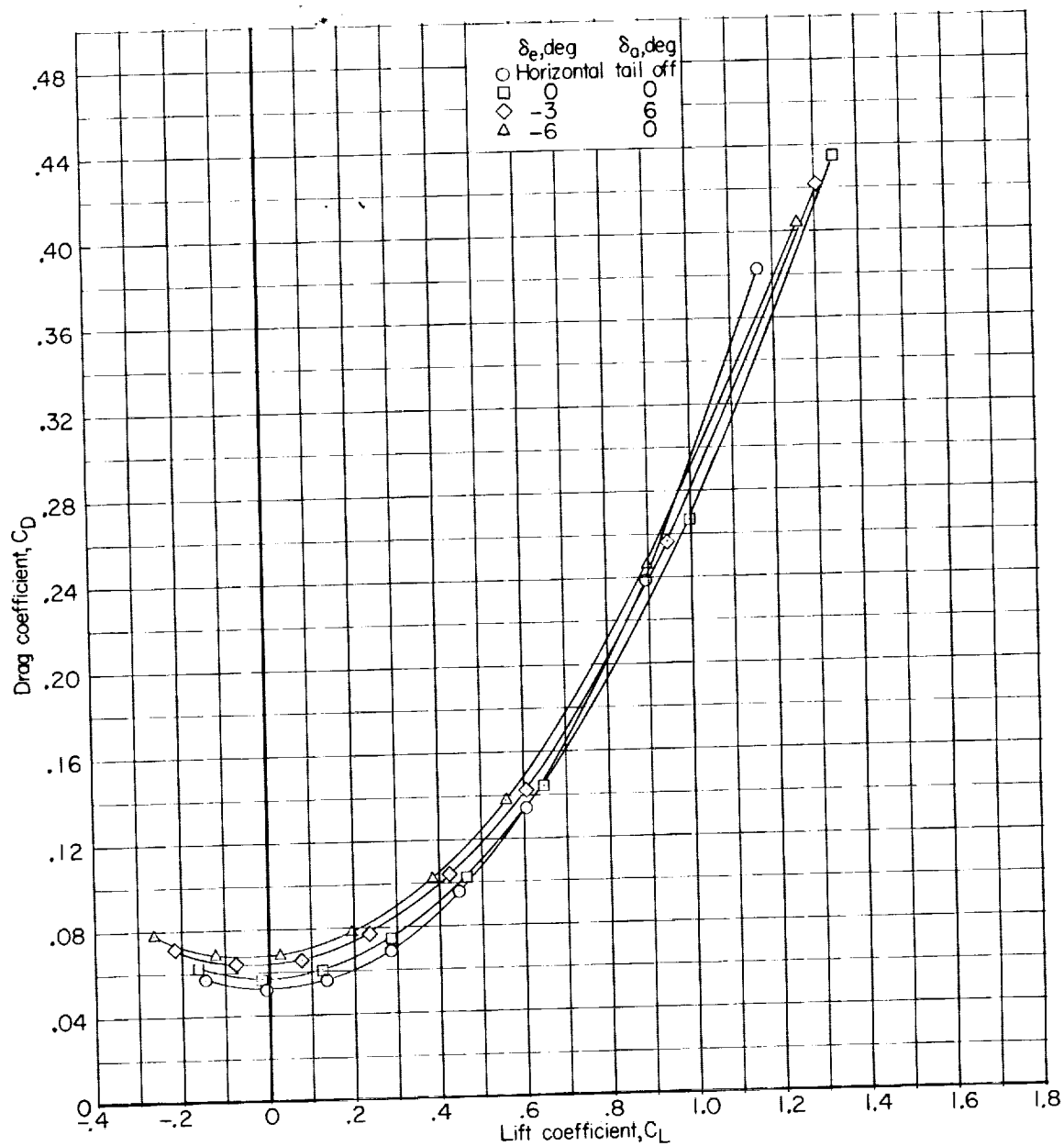
(f) Concluded.

Figure 6.- Continued.



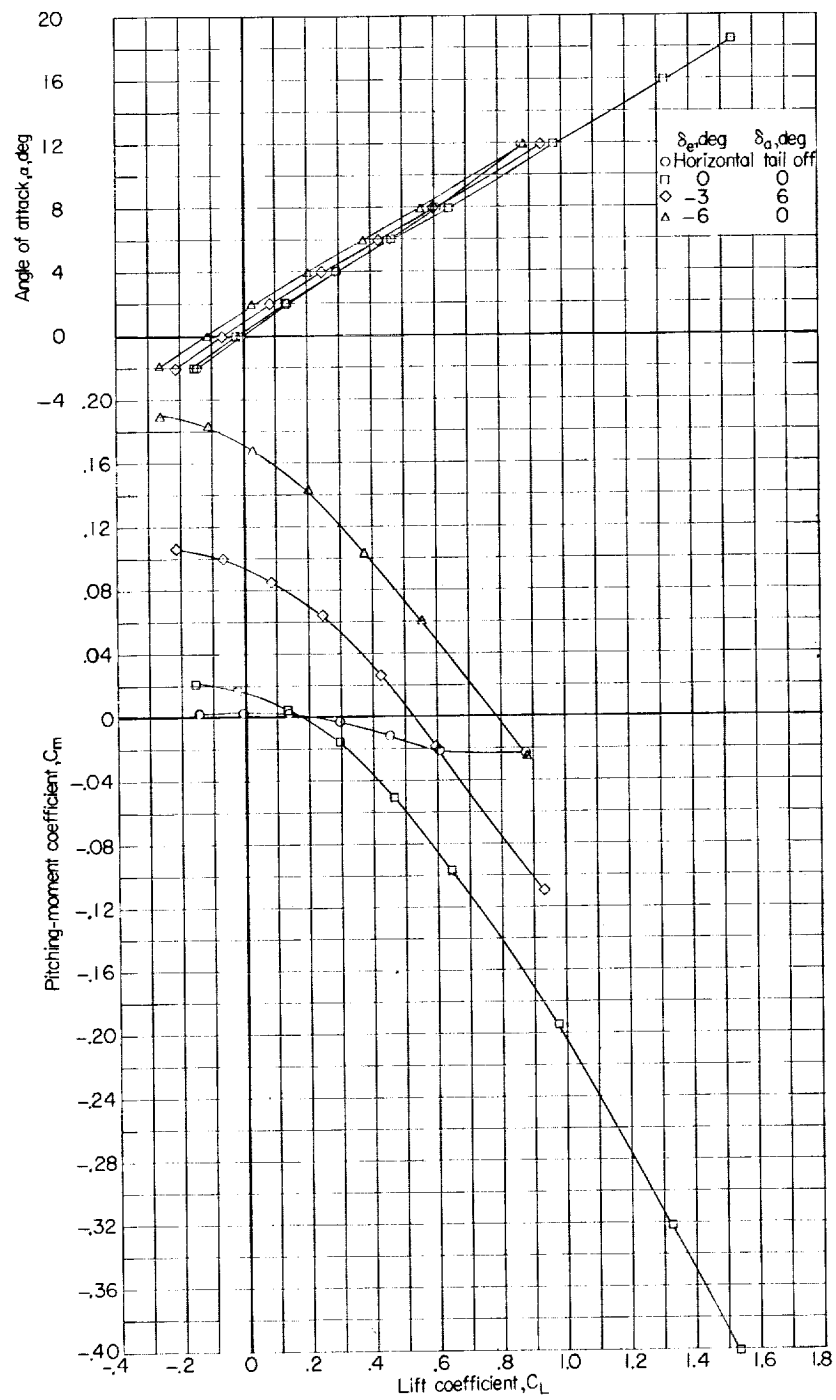
(g) $M = 1.00$.

Figure 6.- Continued.



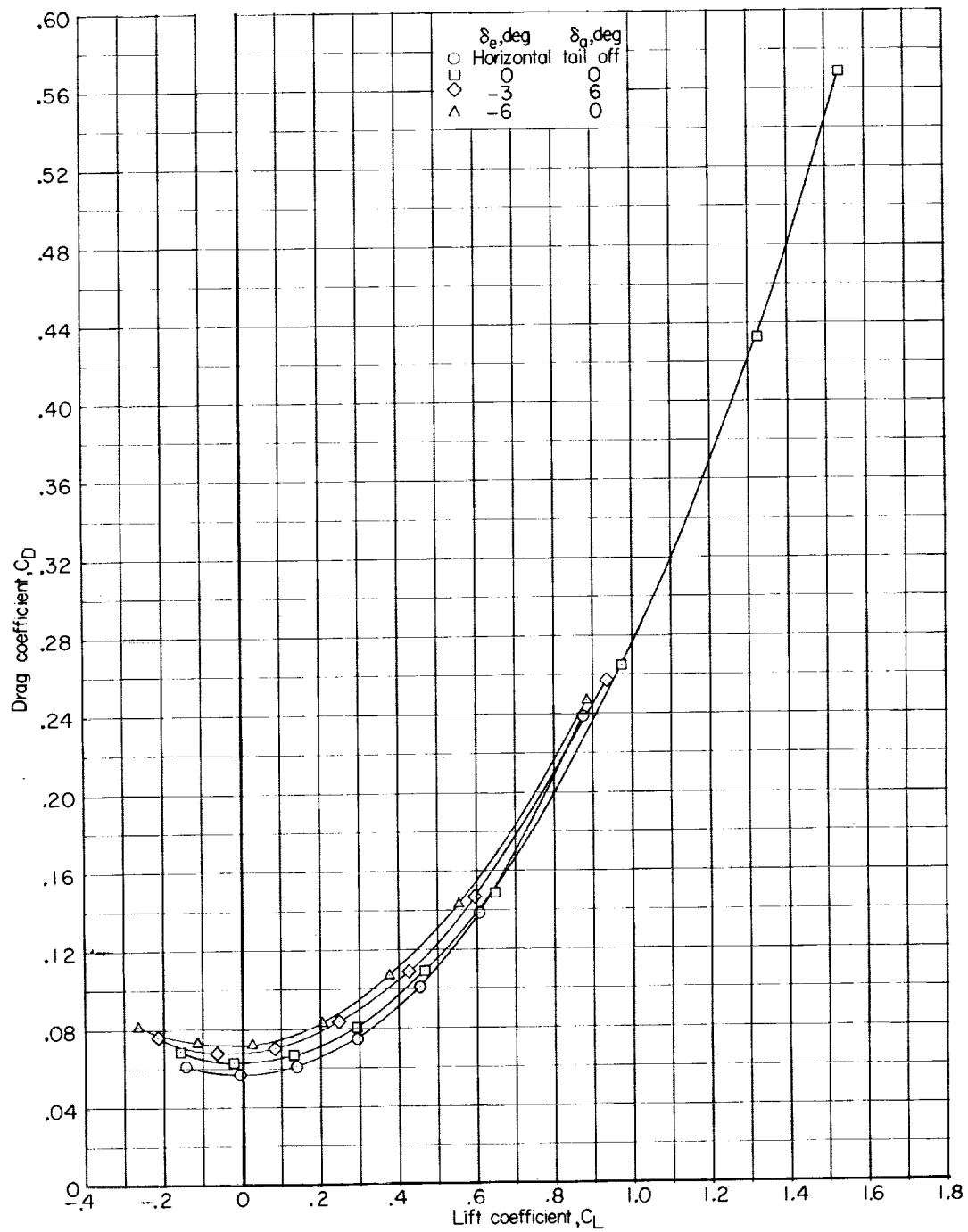
(g) Concluded.

Figure 6.- Continued.



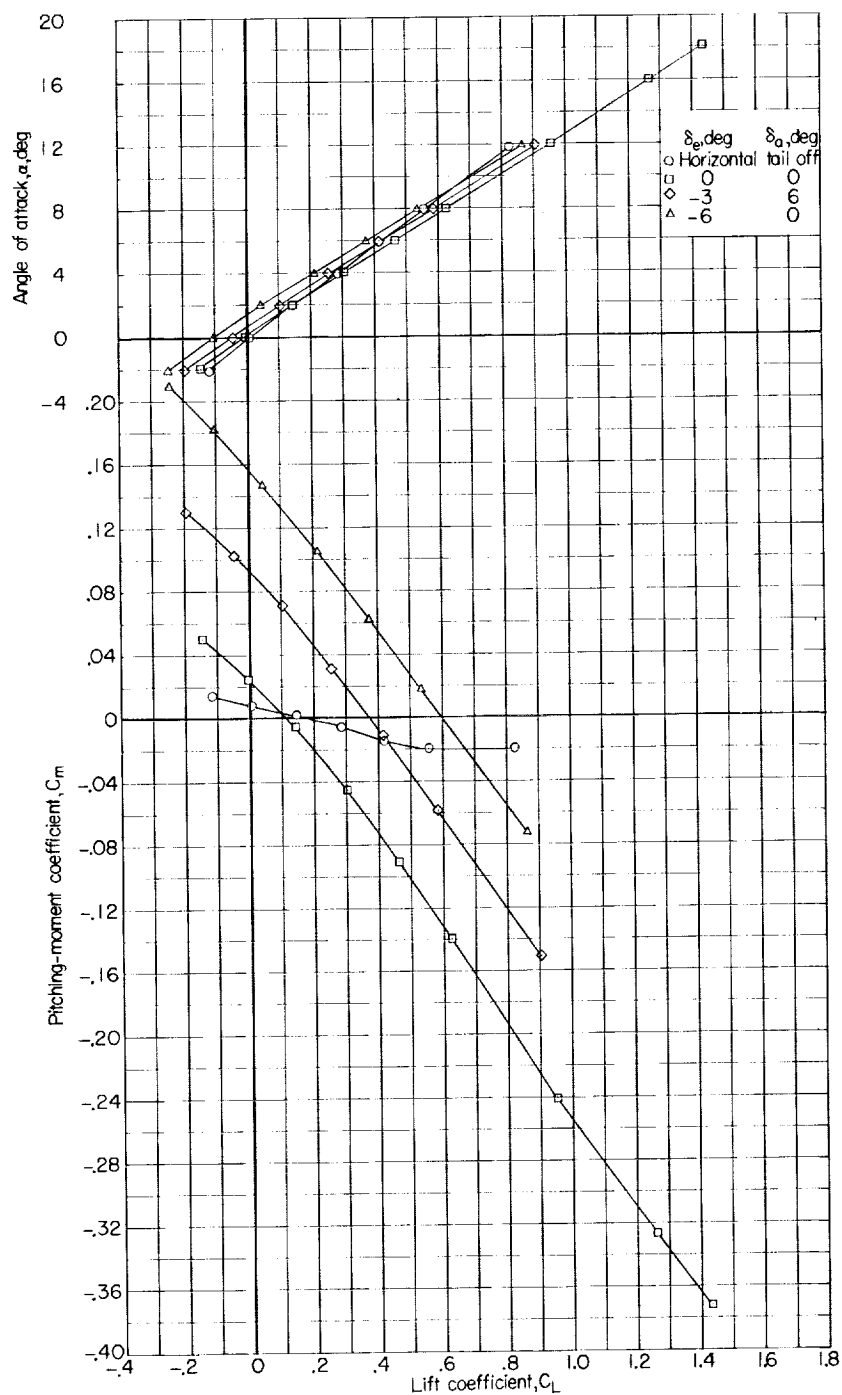
(h) $M = 1.03$.

Figure 6.- Continued.



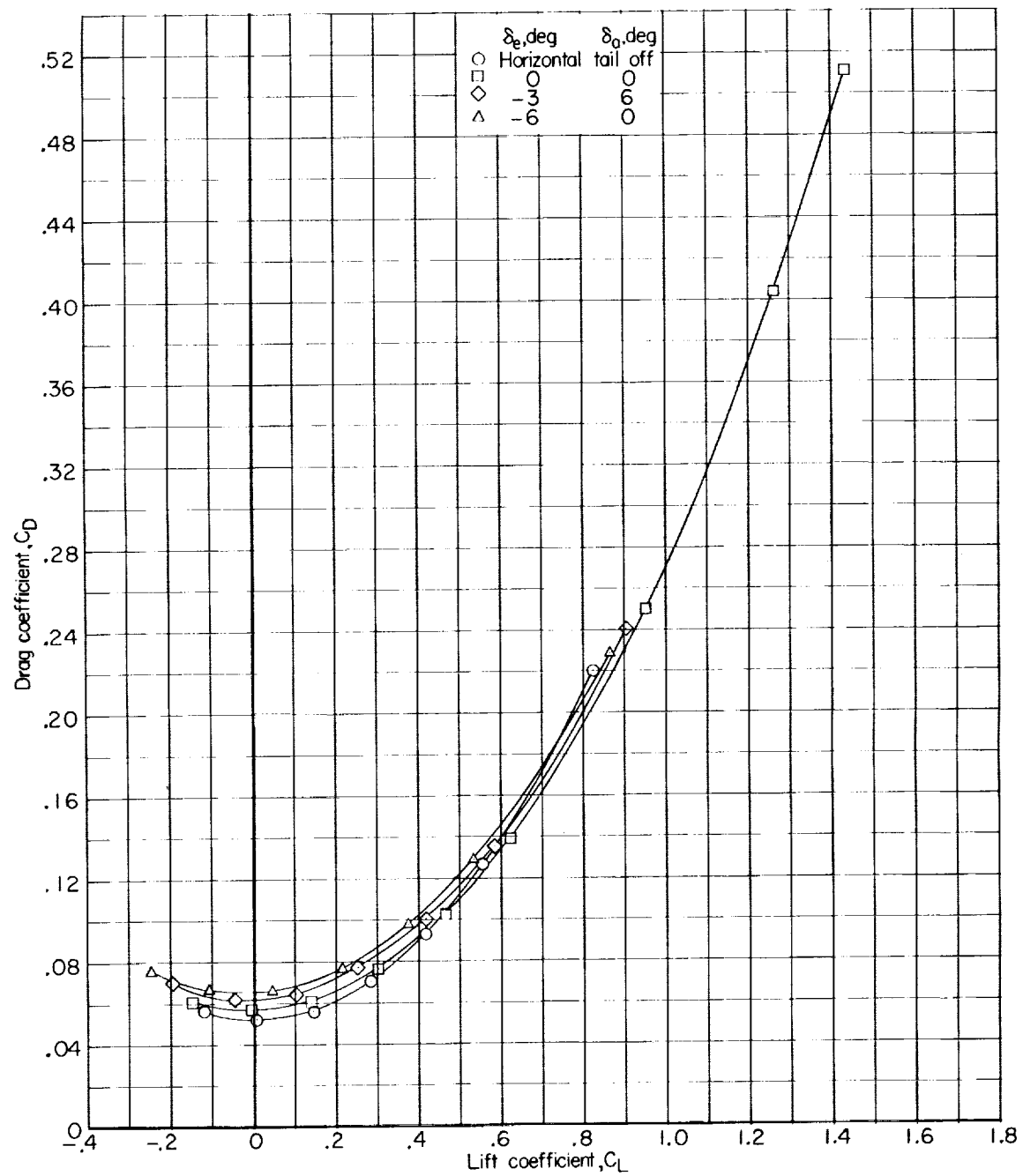
(h) Concluded.

Figure 6.- Continued.



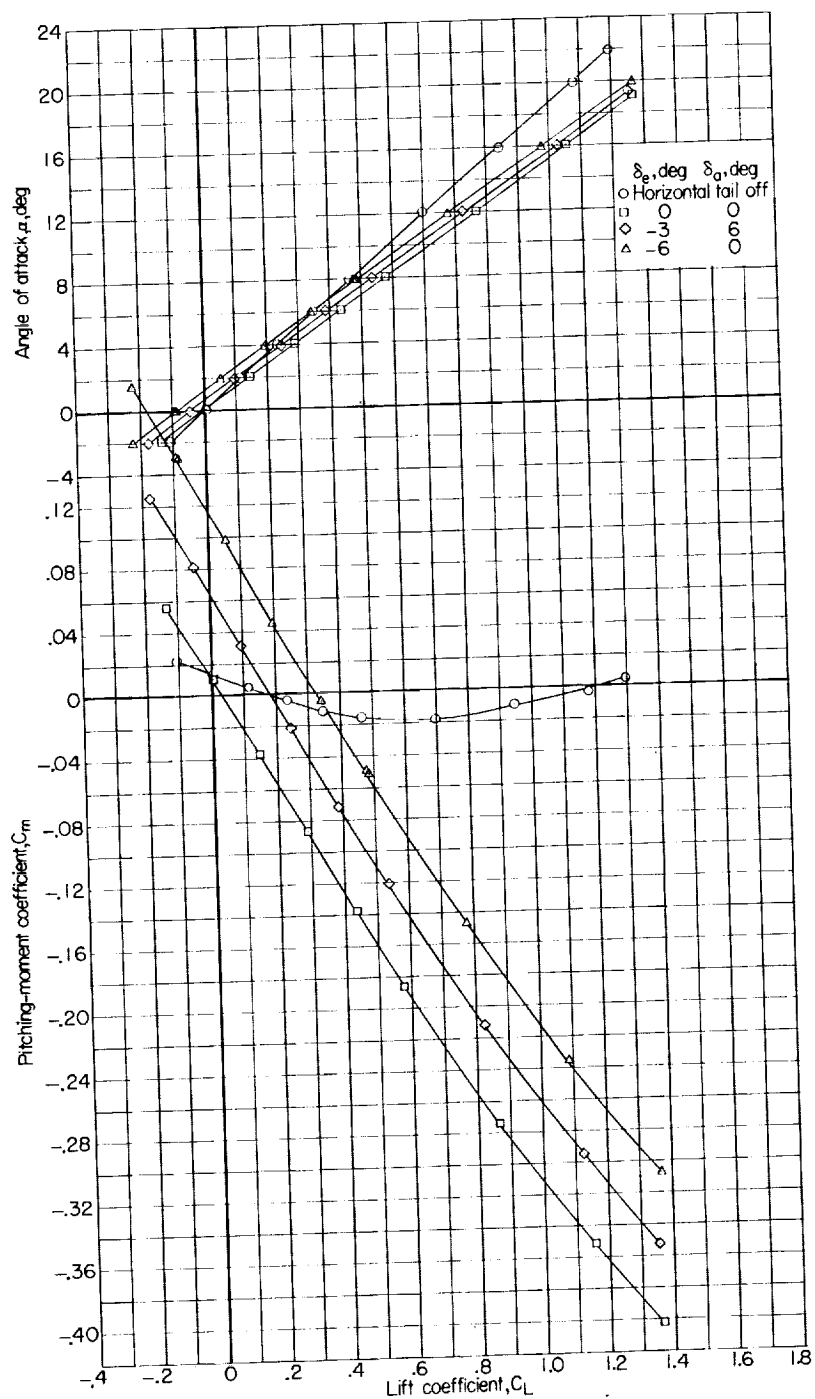
(i) $M = 1.18$.

Figure 6.- Continued.



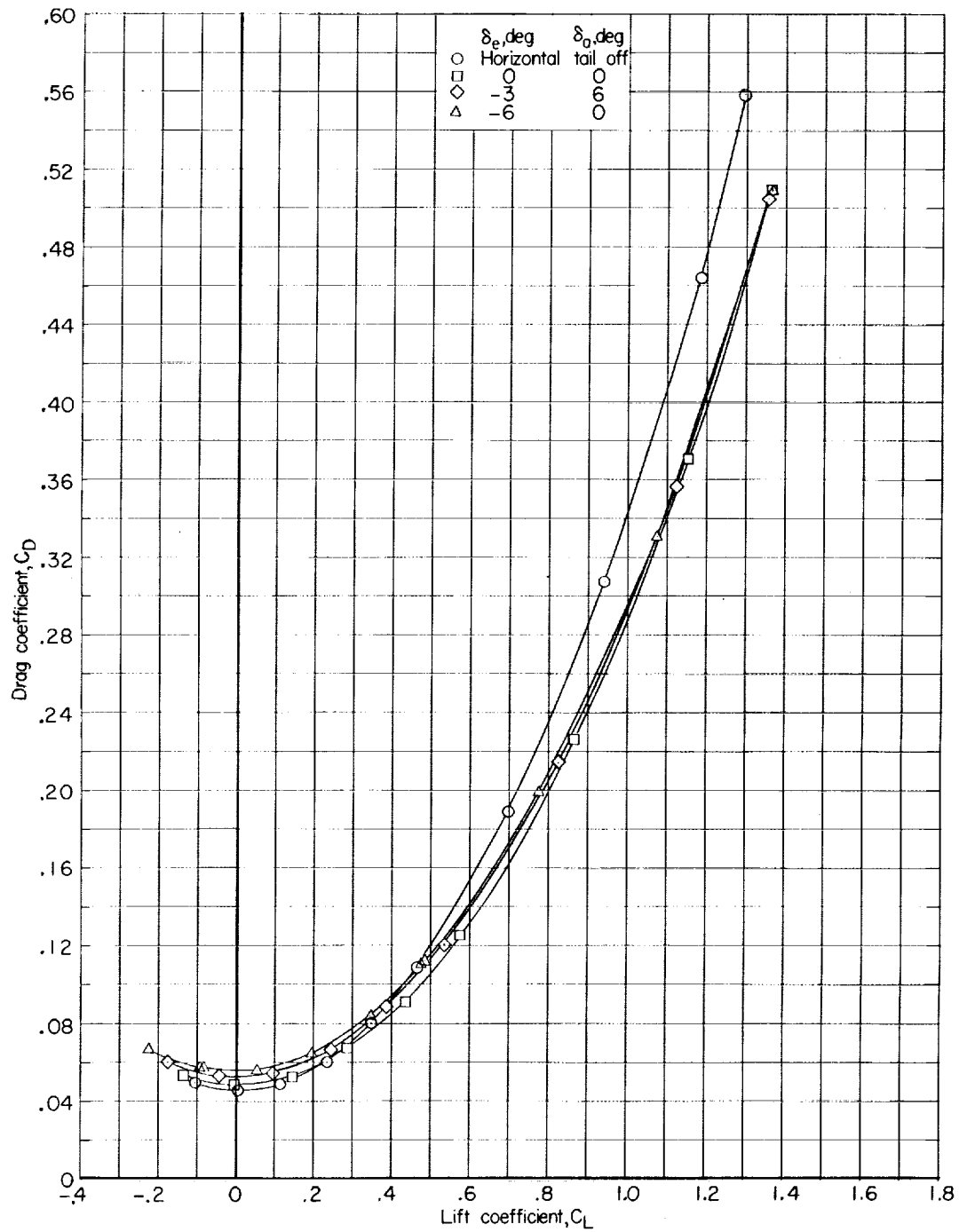
(i) Concluded.

Figure 6.- Continued.



(j) $M = 1.43$.

Figure 6.- Continued.



(j) Concluded.

Figure 6.- Concluded.

L-376

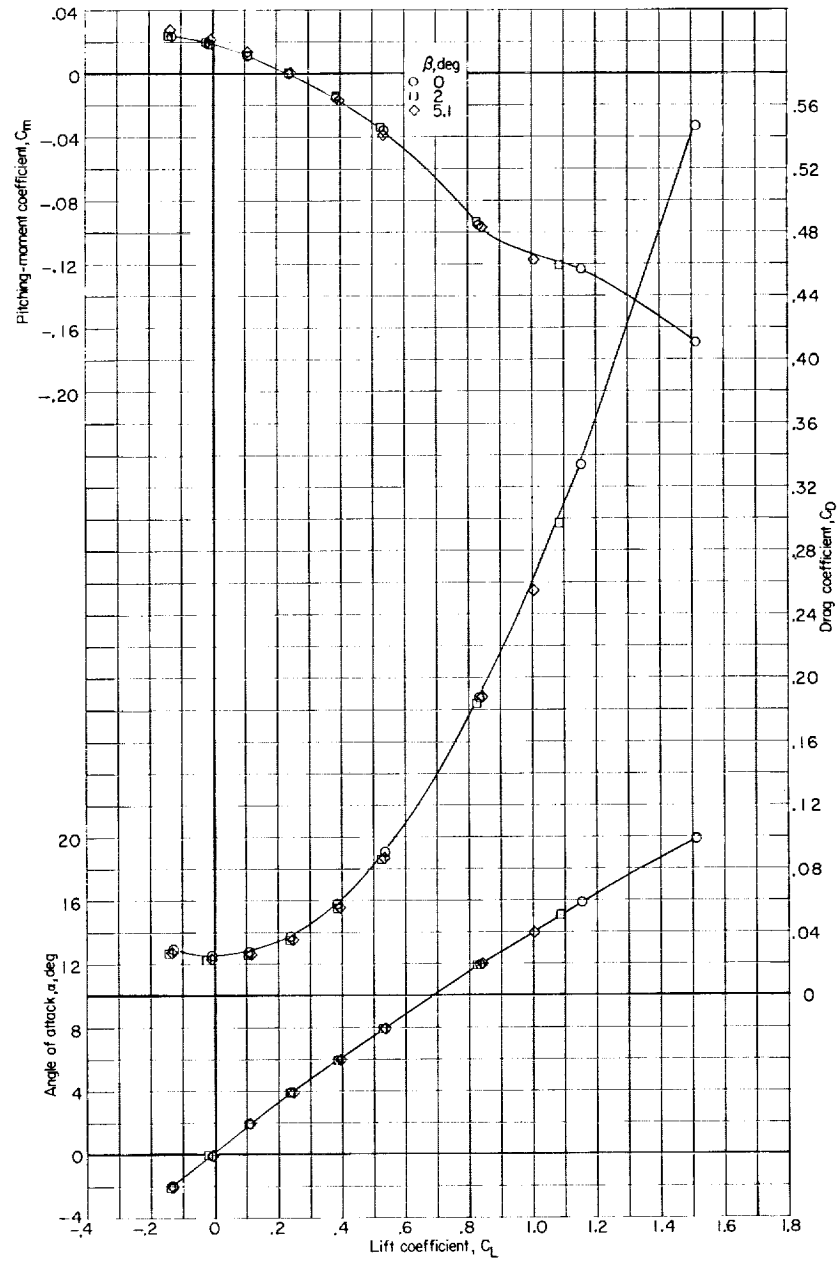
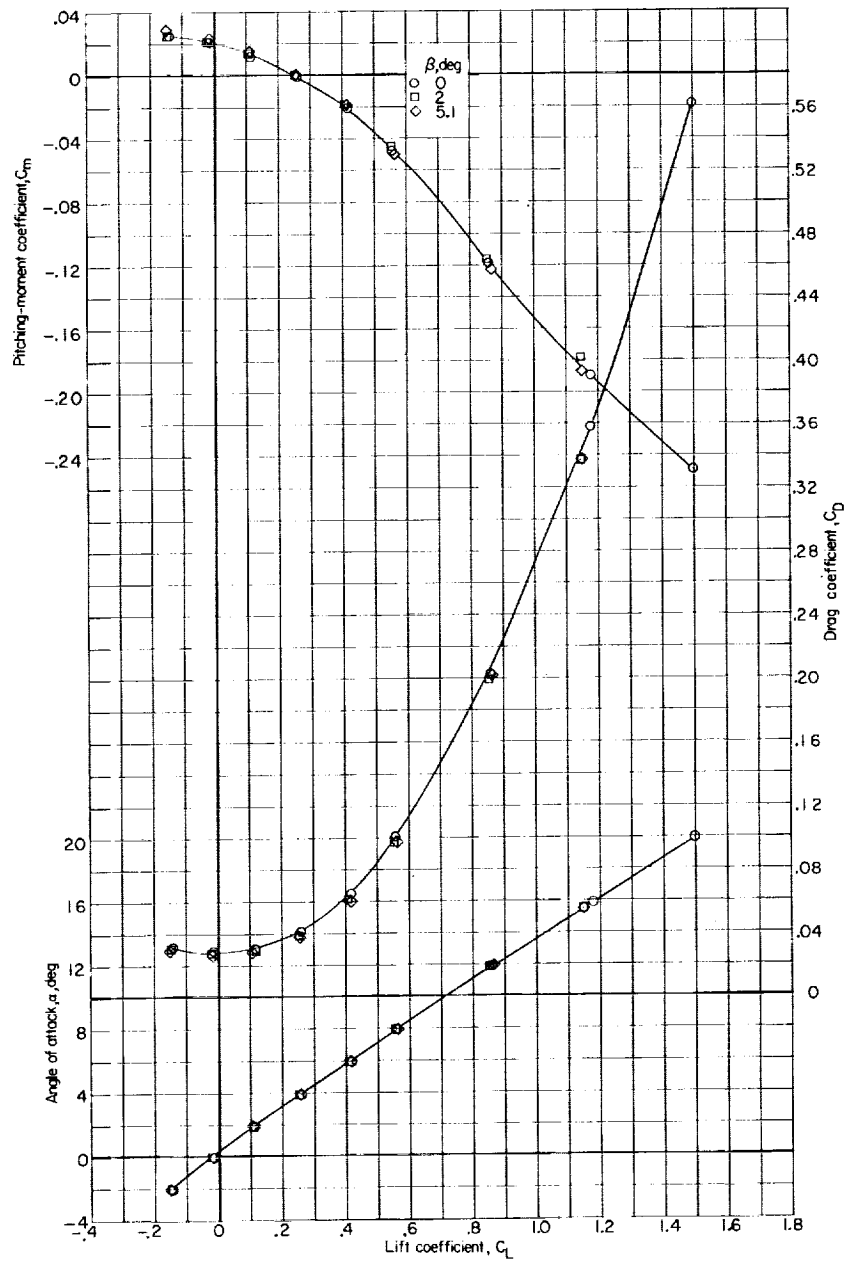
(a) $M = 0.60$

Figure 7.- Longitudinal characteristics of the complete model at various angles of sideslip. Surfaces undeflected.



(b) $M = 0.80$.

Figure 7.- Continued.

1-376

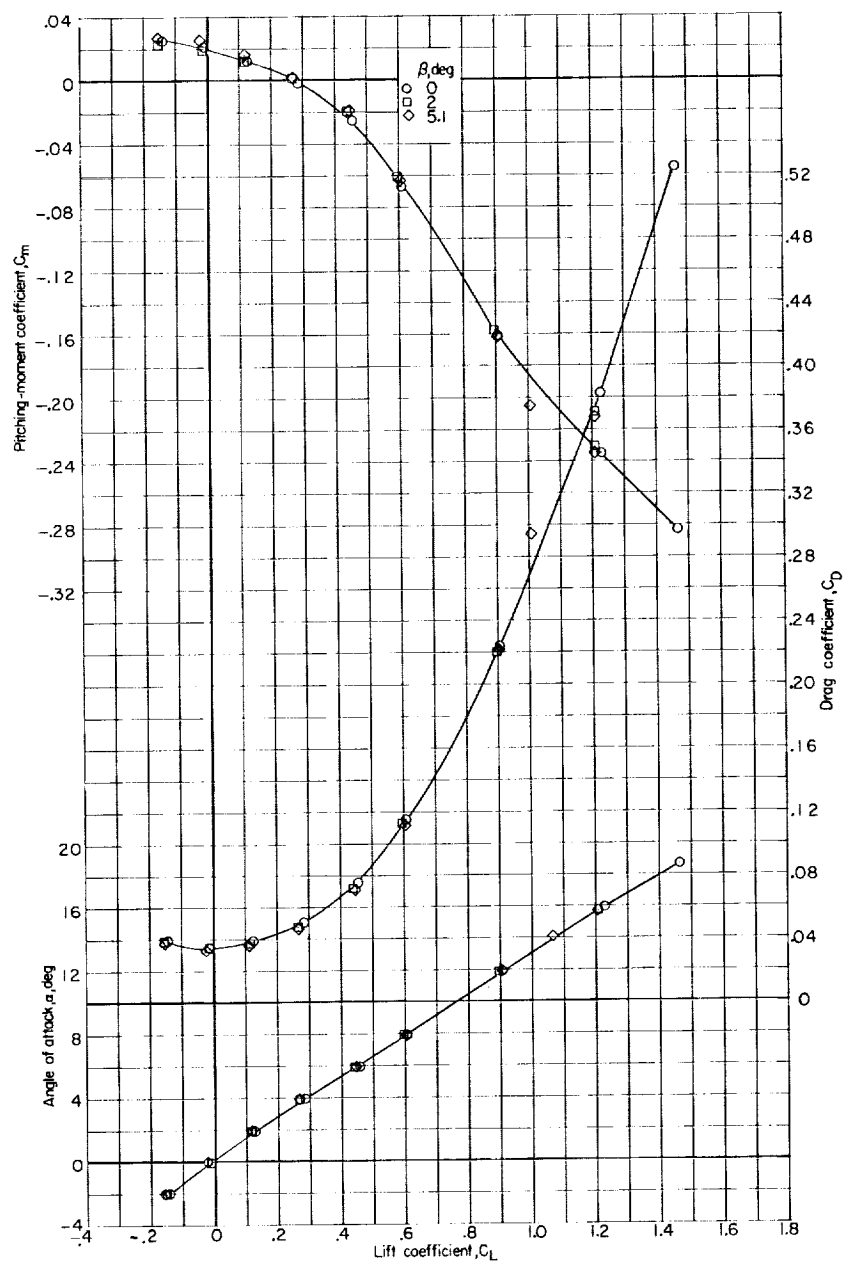
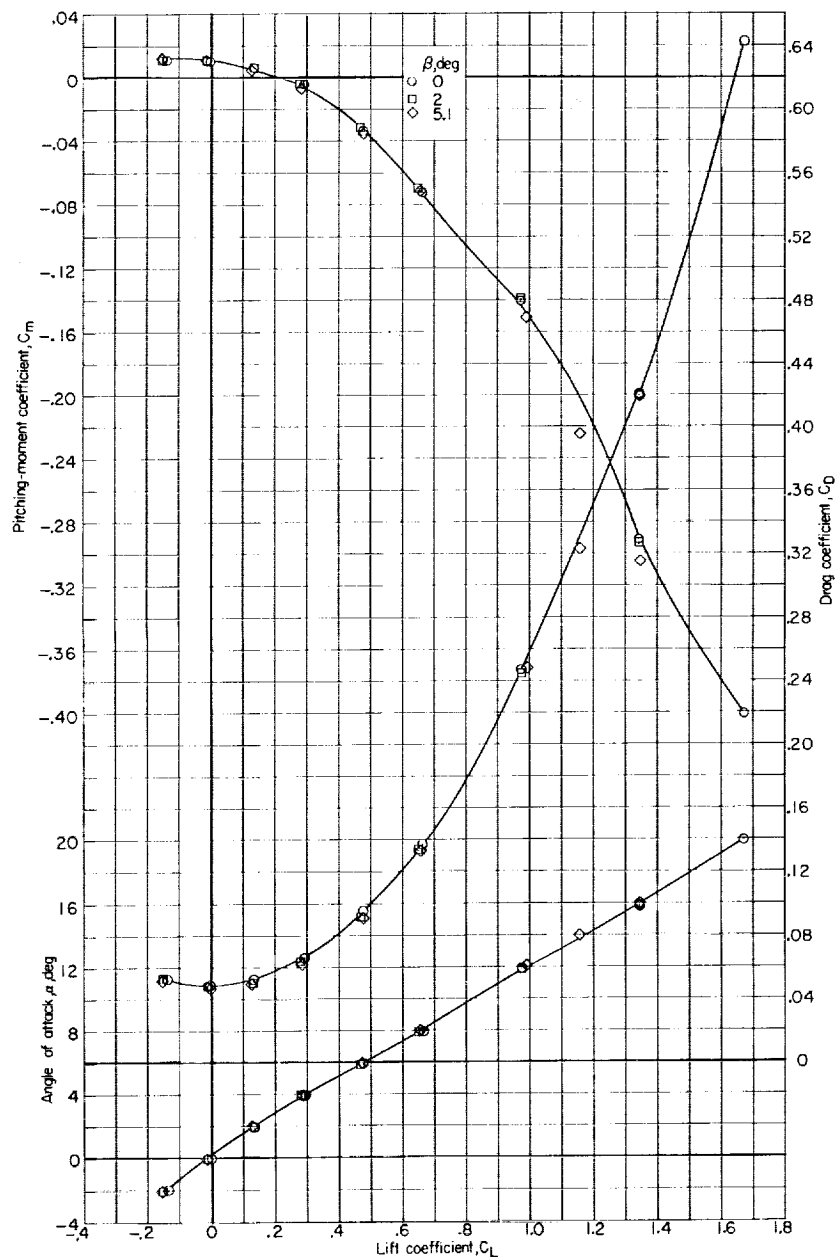
(c) $M = 0.90$.

Figure 7.- Continued.



(d) $M = 0.95$.

Figure 7.- Continued.

L-376

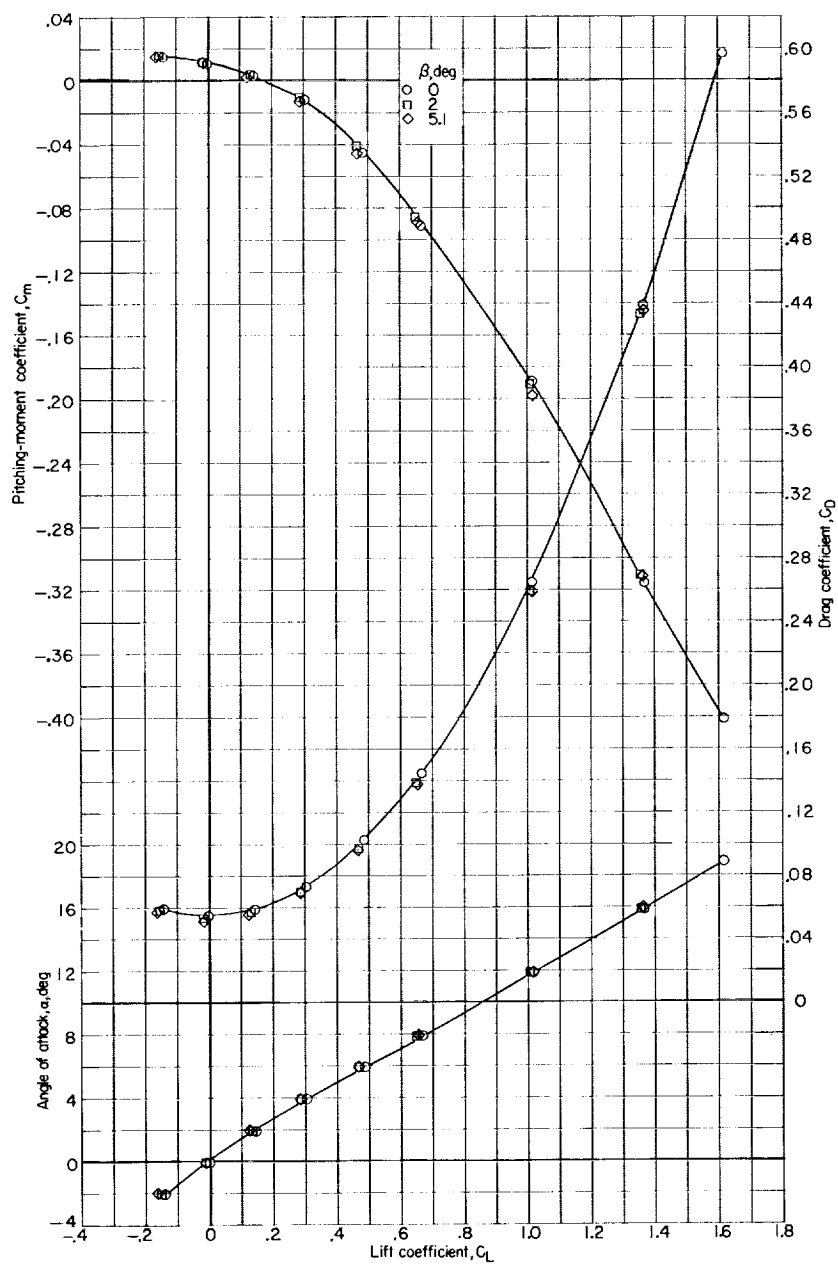
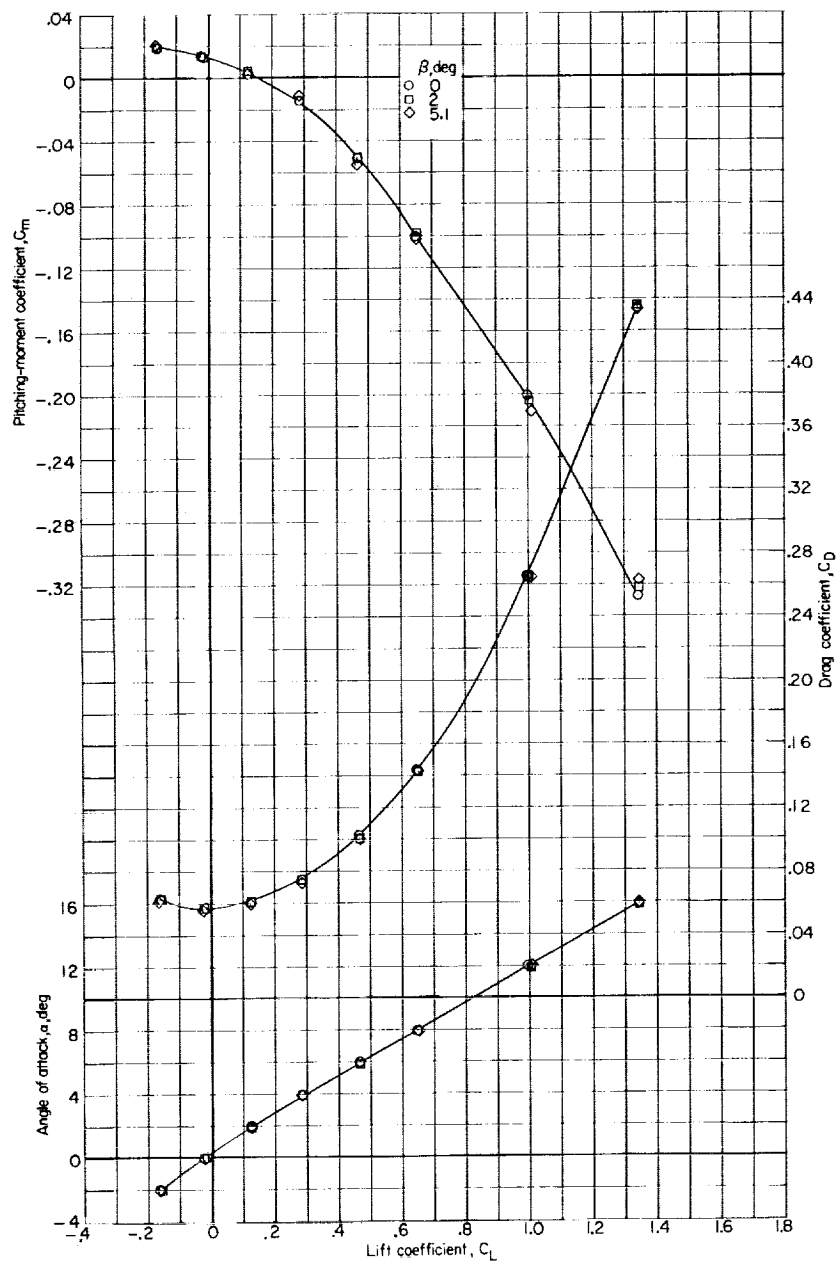
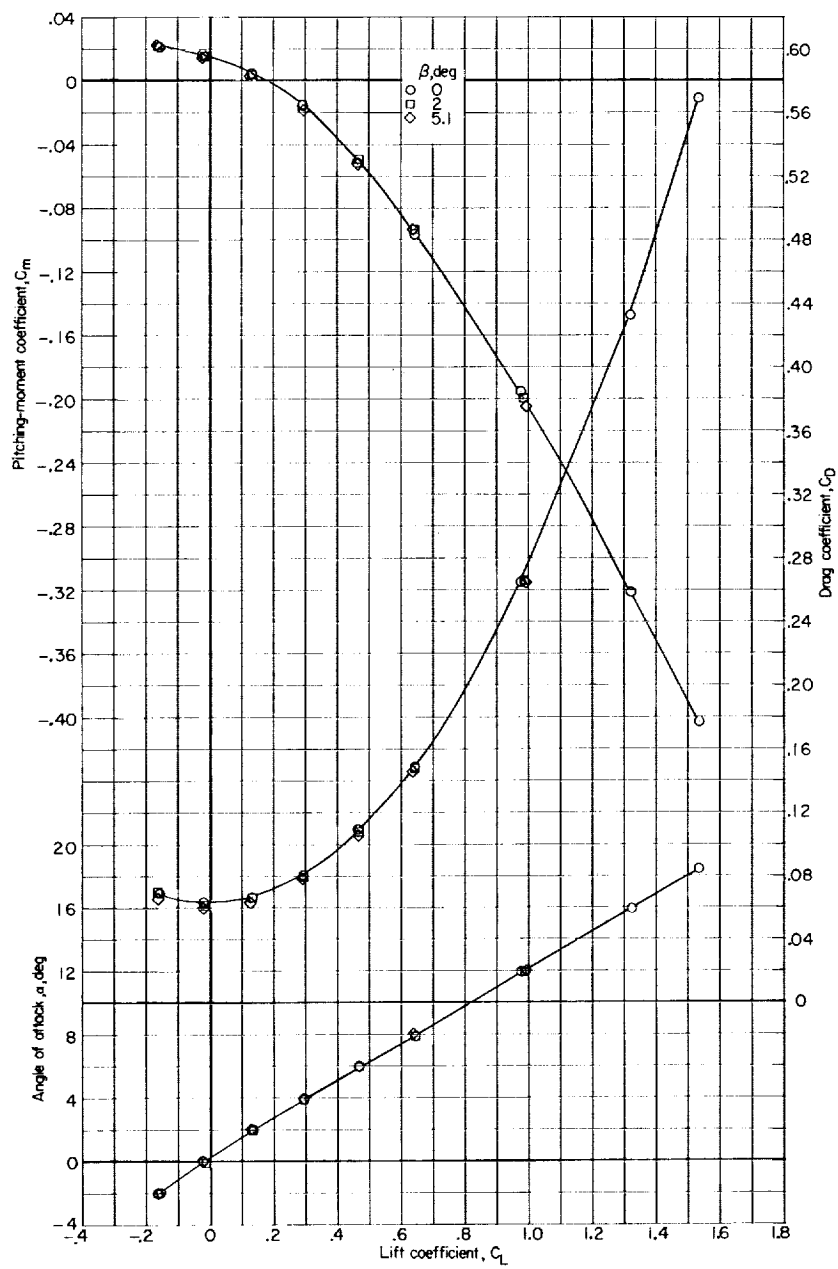
(e) $M = 0.975$.

Figure 7.- Continued.



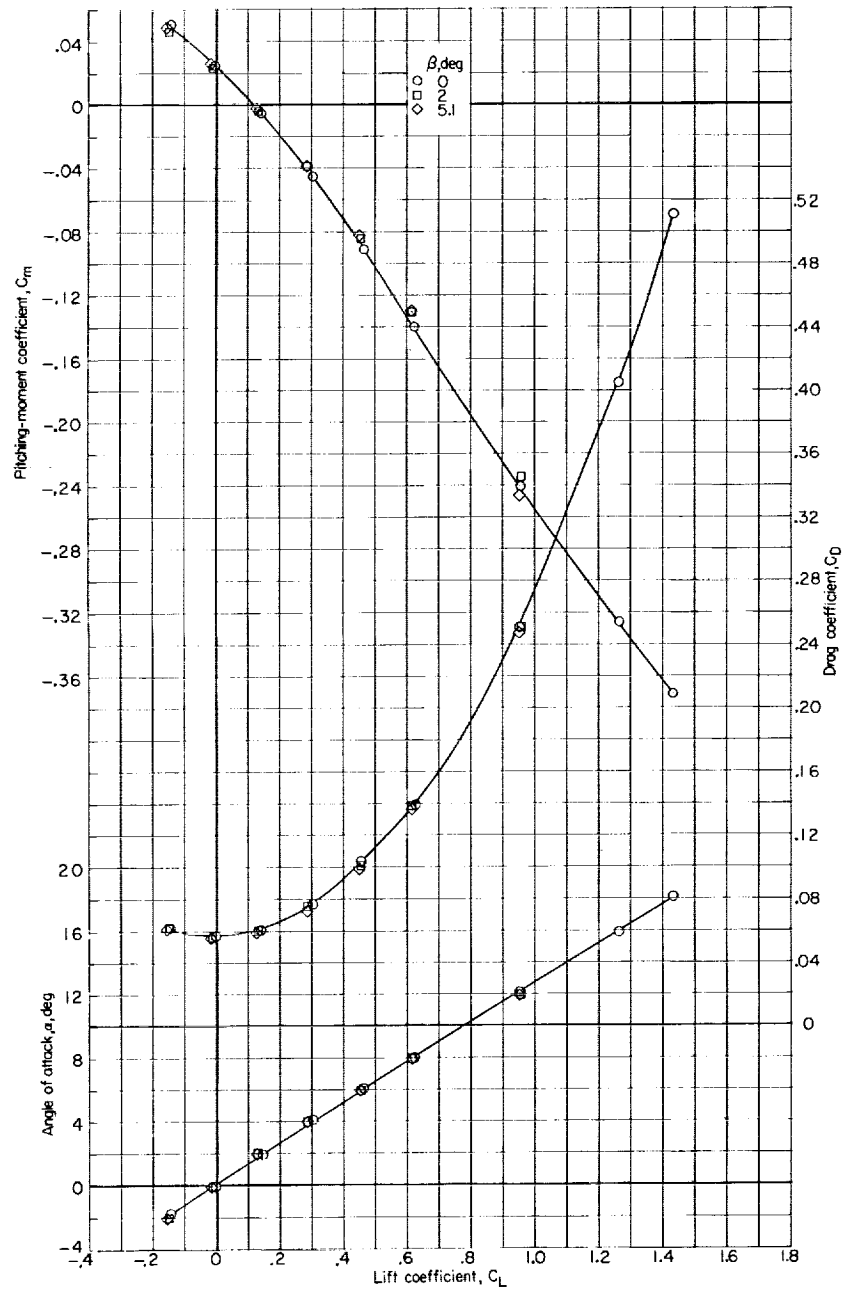
(f) $M = 1.00$.

Figure 7.- Continued.



(g) $M = 1.03$.

Figure 7.- Continued.



(h) $M = 1.18$.

Figure 7.- Continued.

L-376

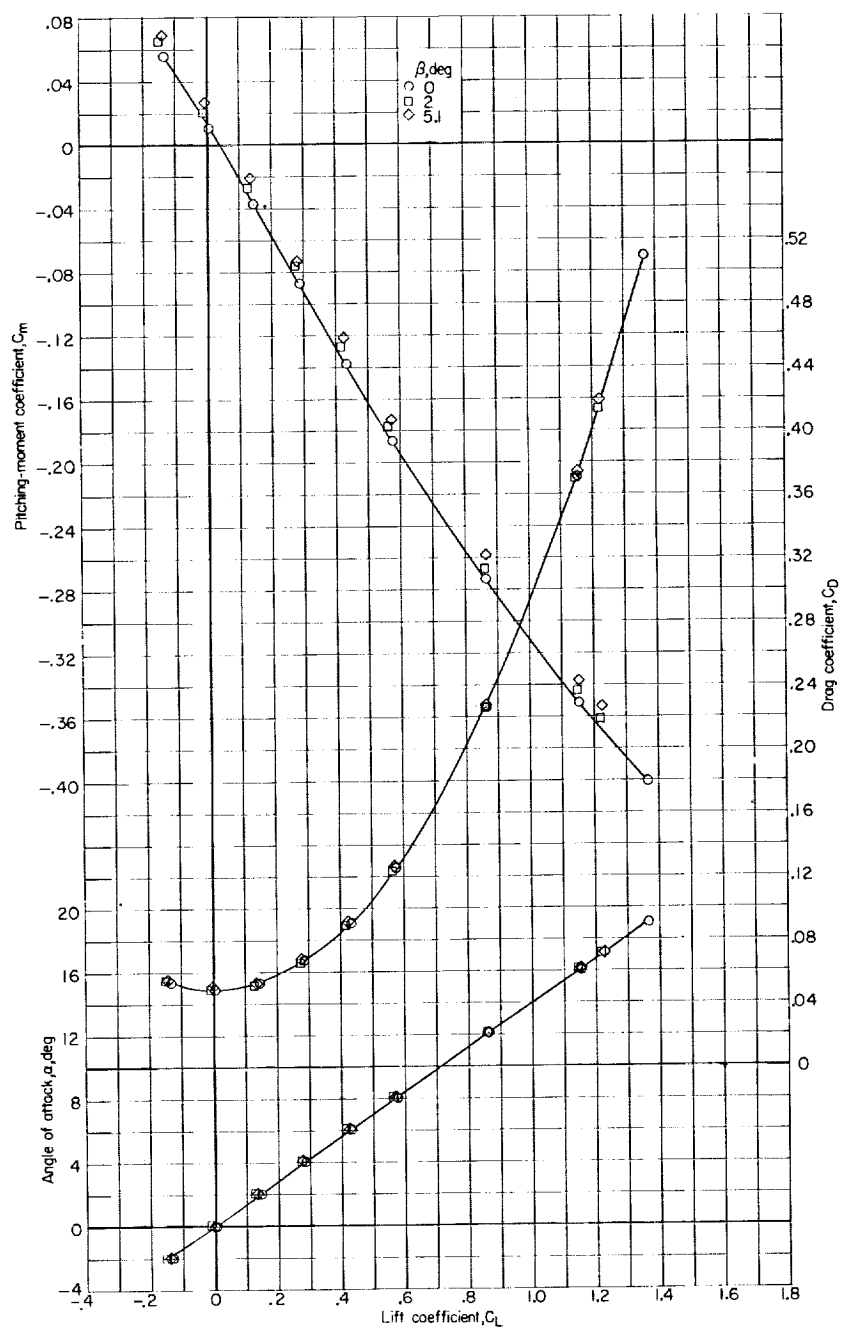
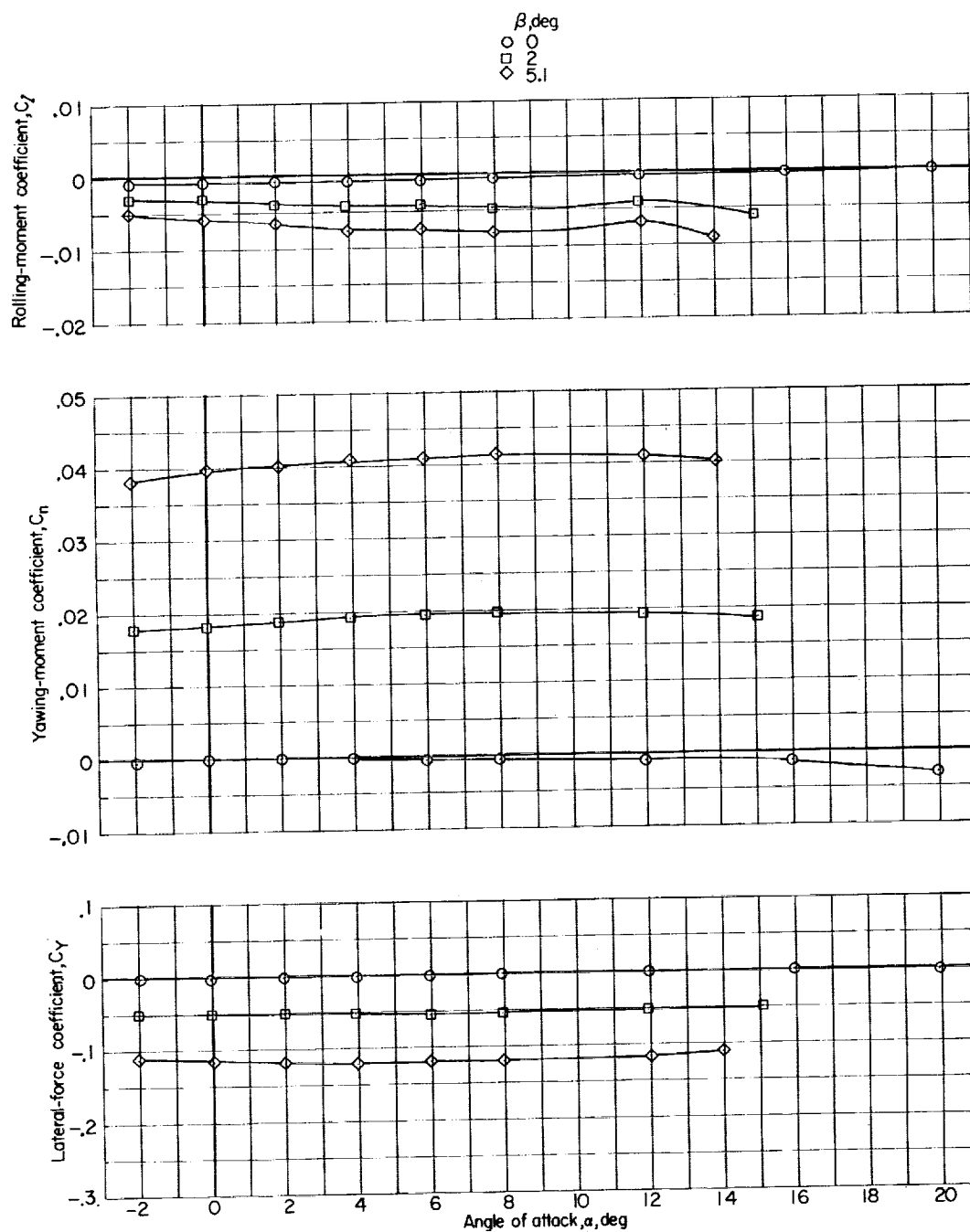
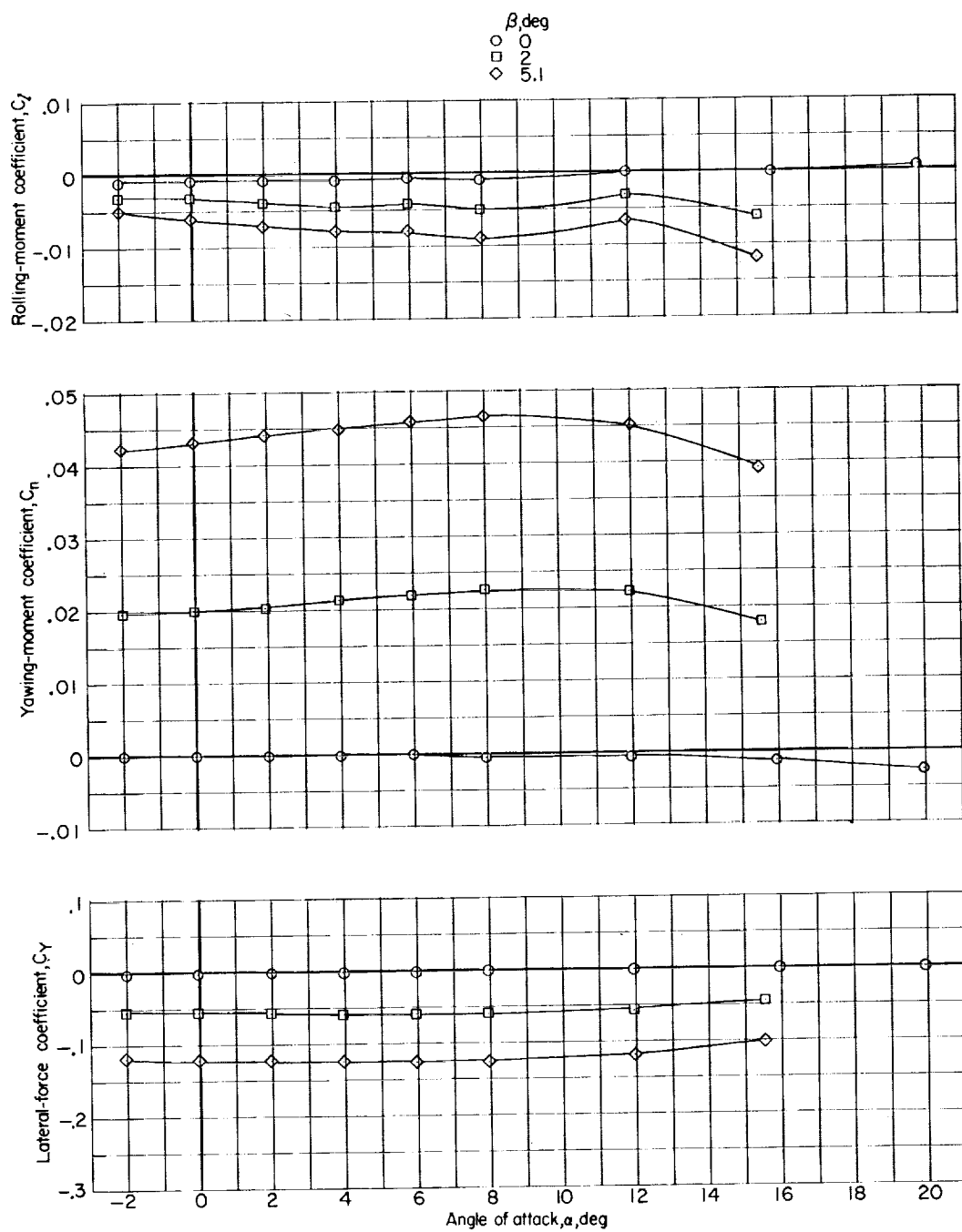
(i) $M = 1.43$.

Figure 7.- Concluded.



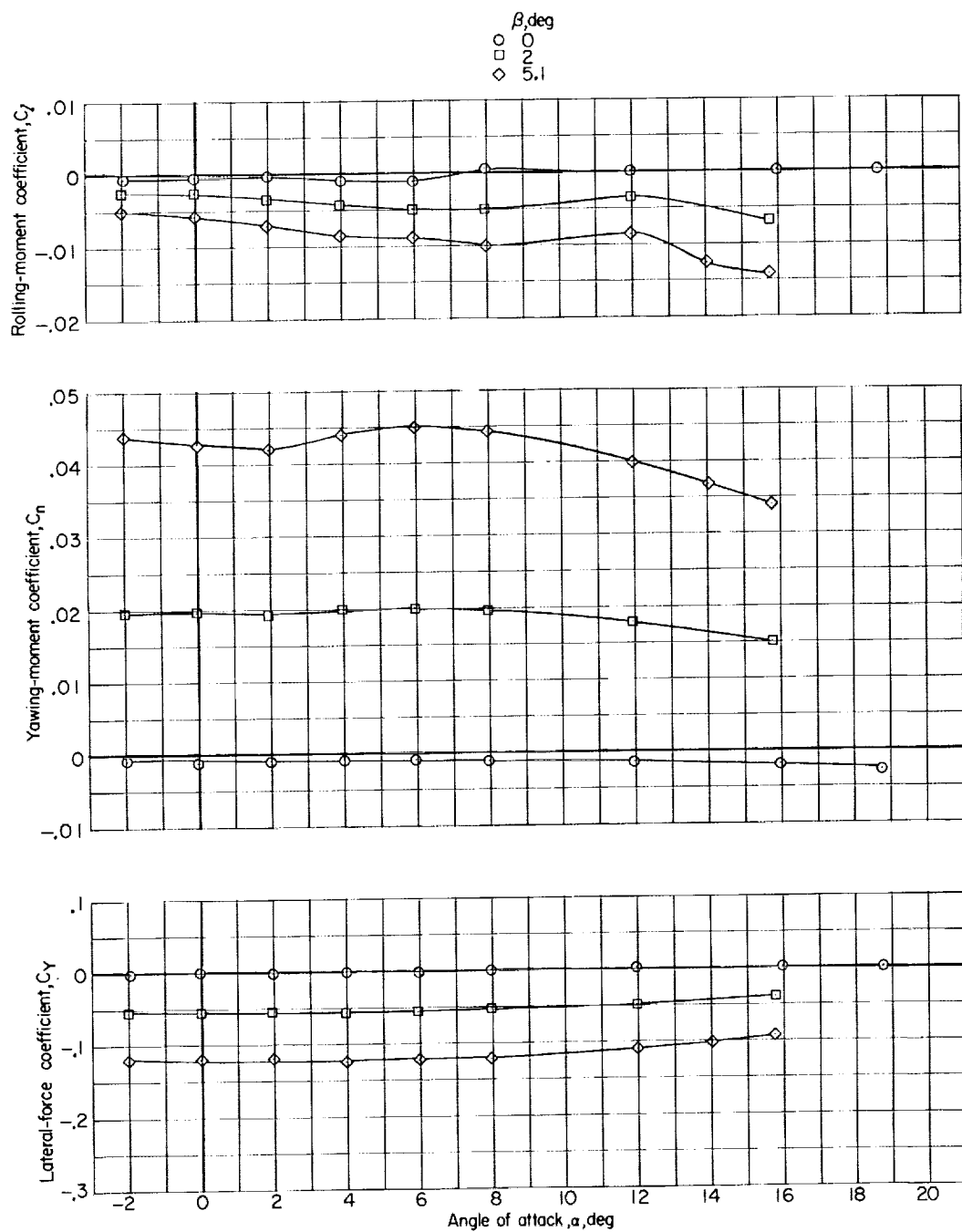
(a) $M = 0.60$.

Figure 8.- Lateral-directional characteristics of the complete model at various angles of sideslip. Surfaces undeflected.



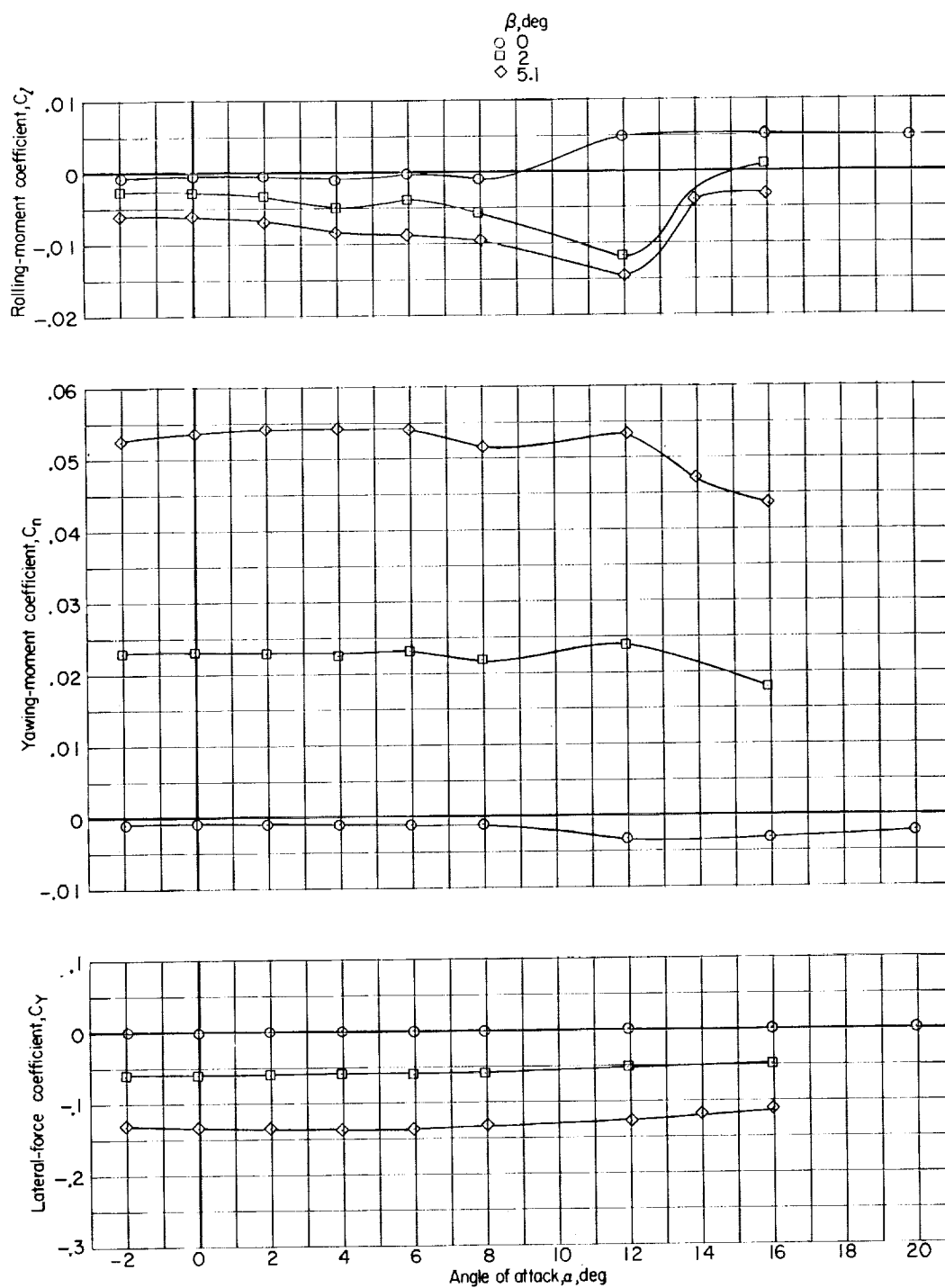
(b) $M = 0.80$.

Figure 8.- Continued.



(c) $M = 0.90$.

Figure 8.- Continued.



(d) $M = 0.95$.

Figure 8.- Continued.

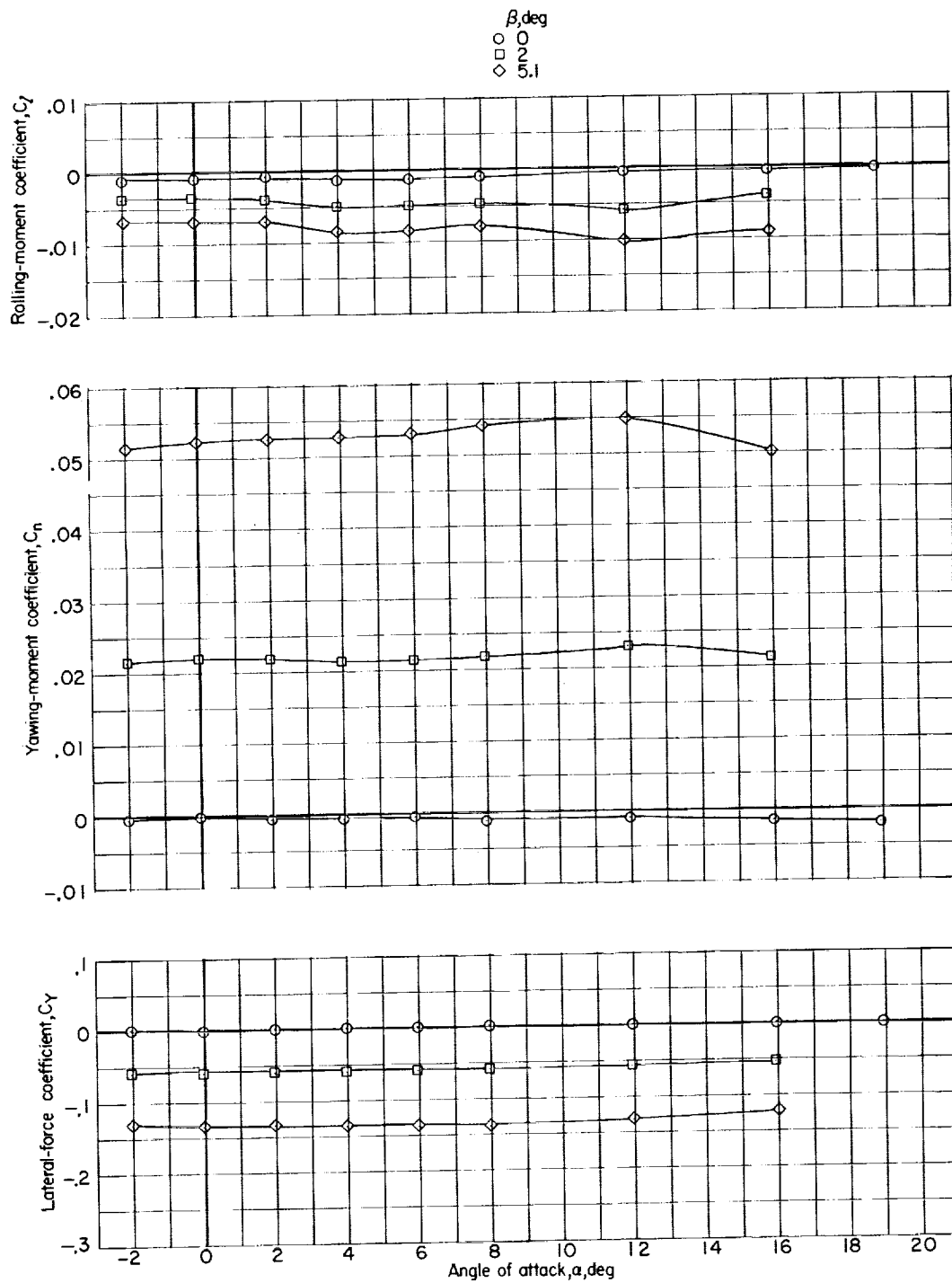
(e) $M = 0.975$.

Figure 8.- Continued.

L-376

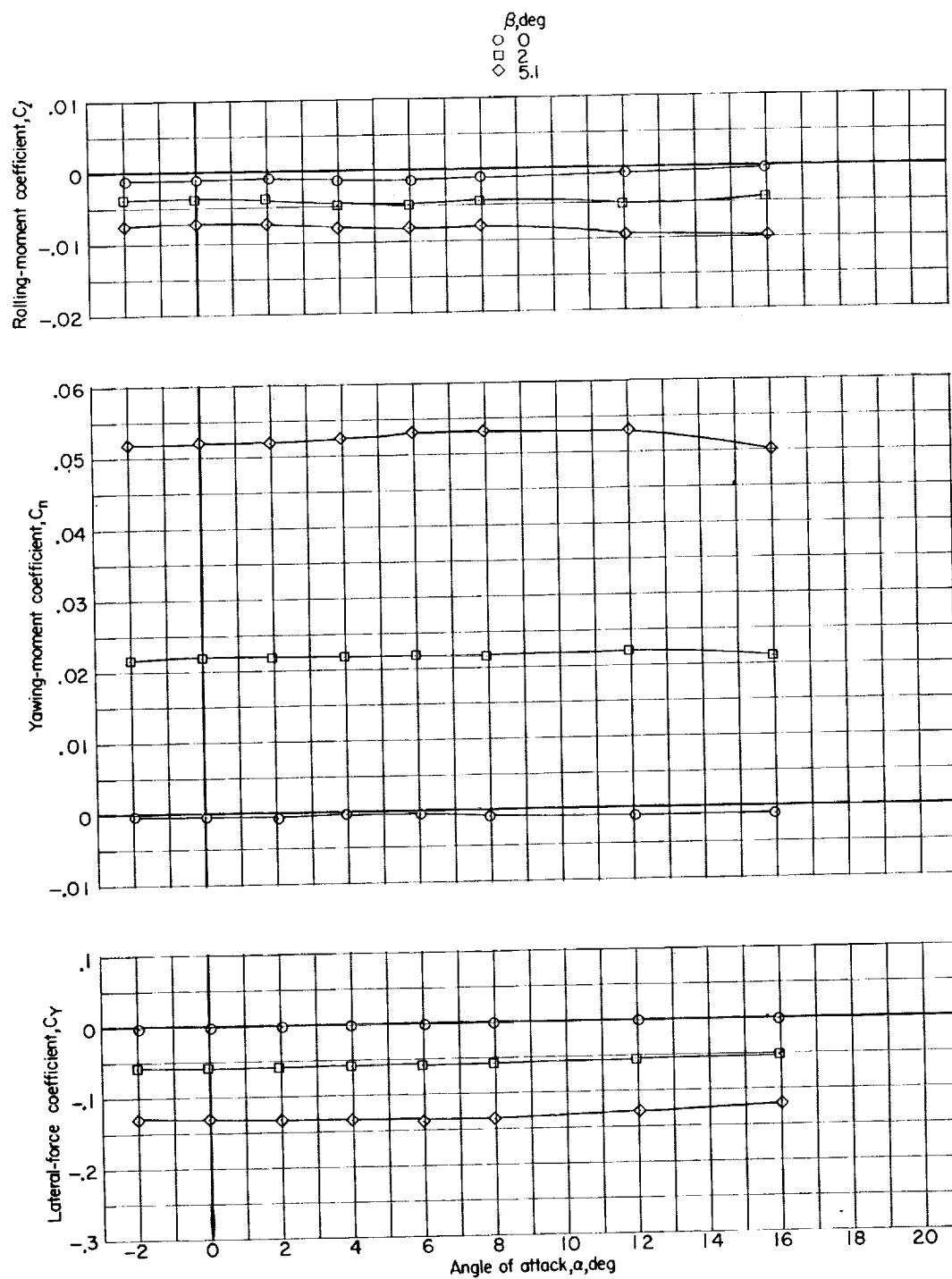
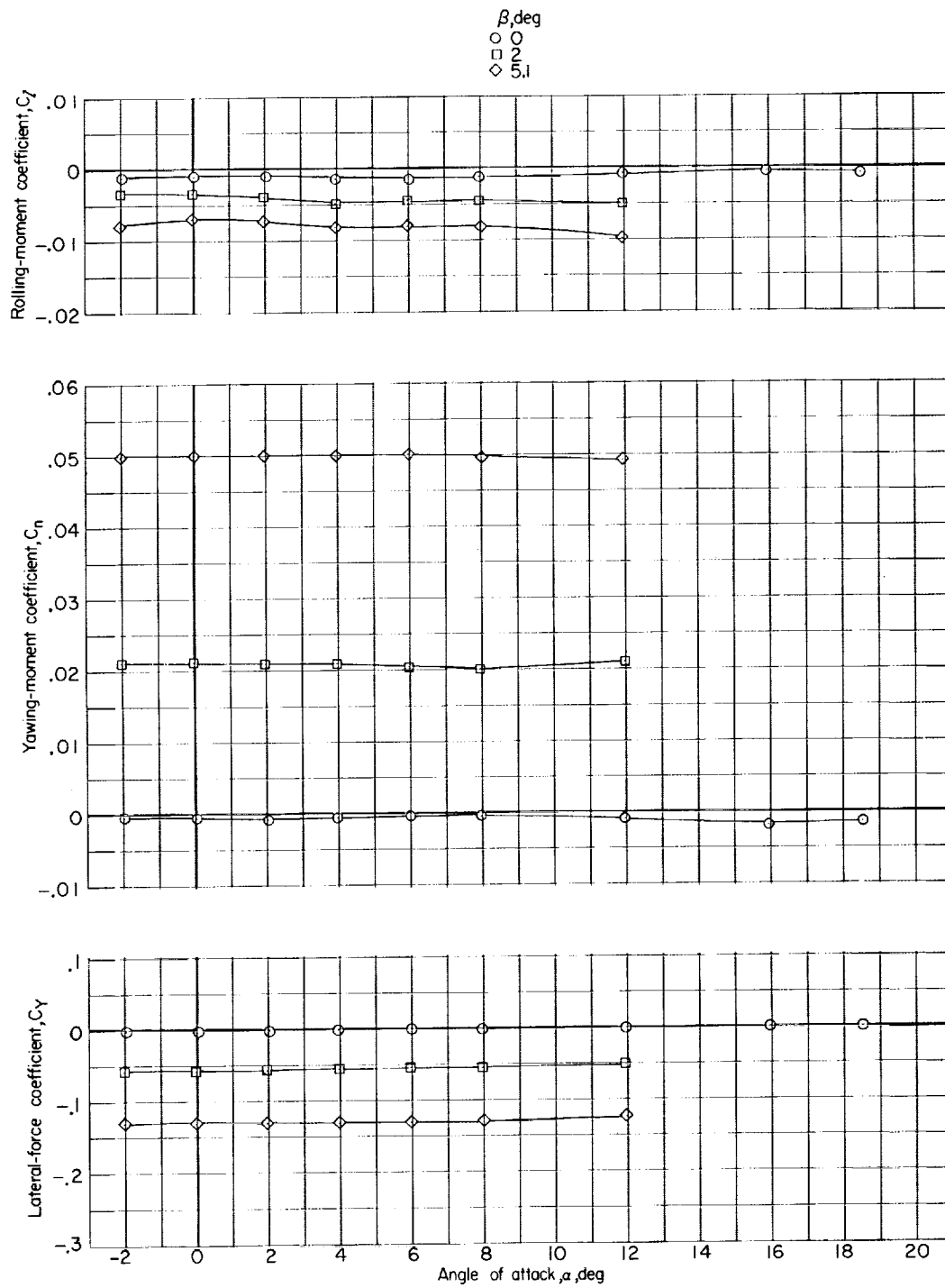
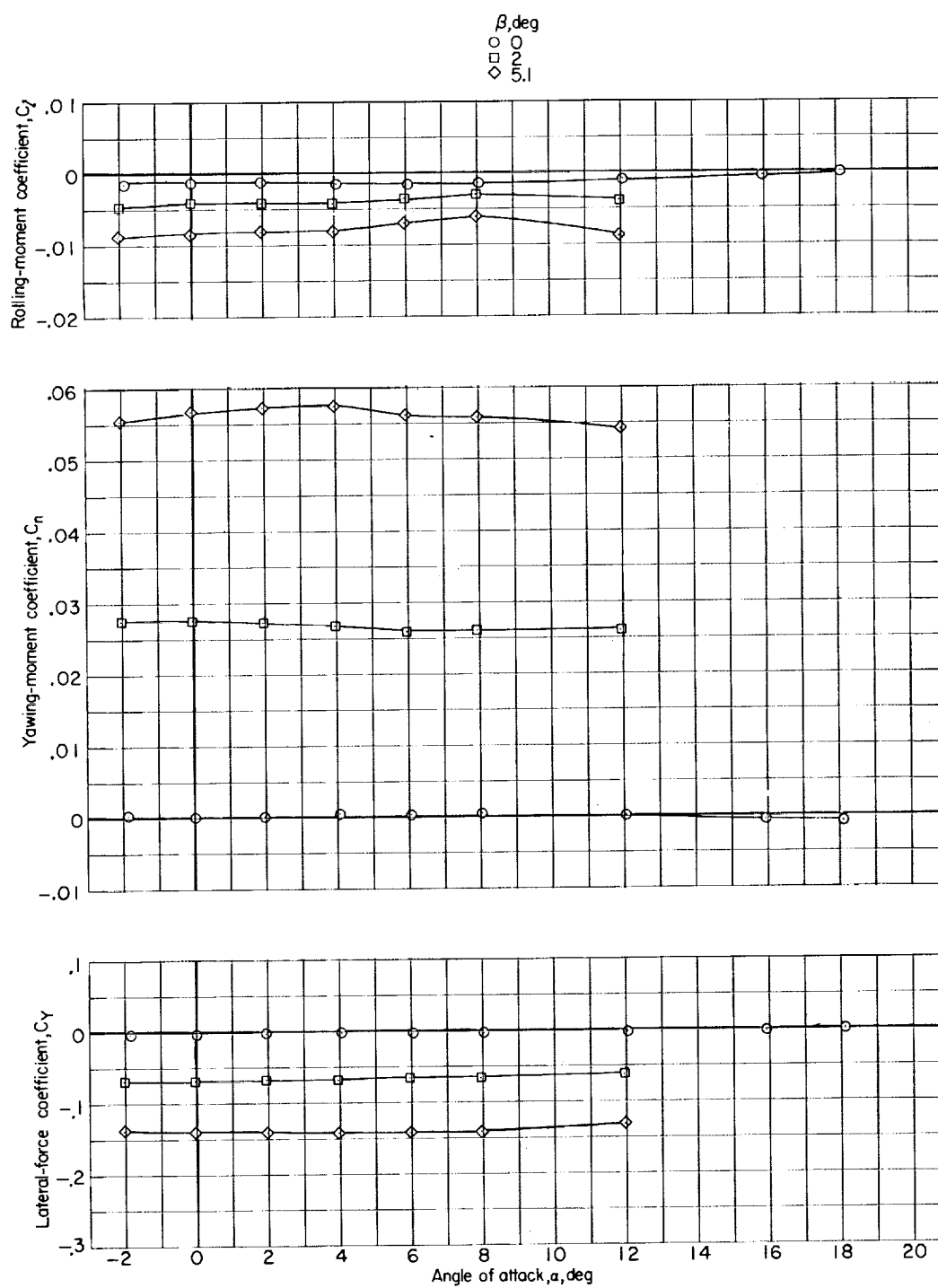
(f) $M = 1.00$.

Figure 8.- Continued.



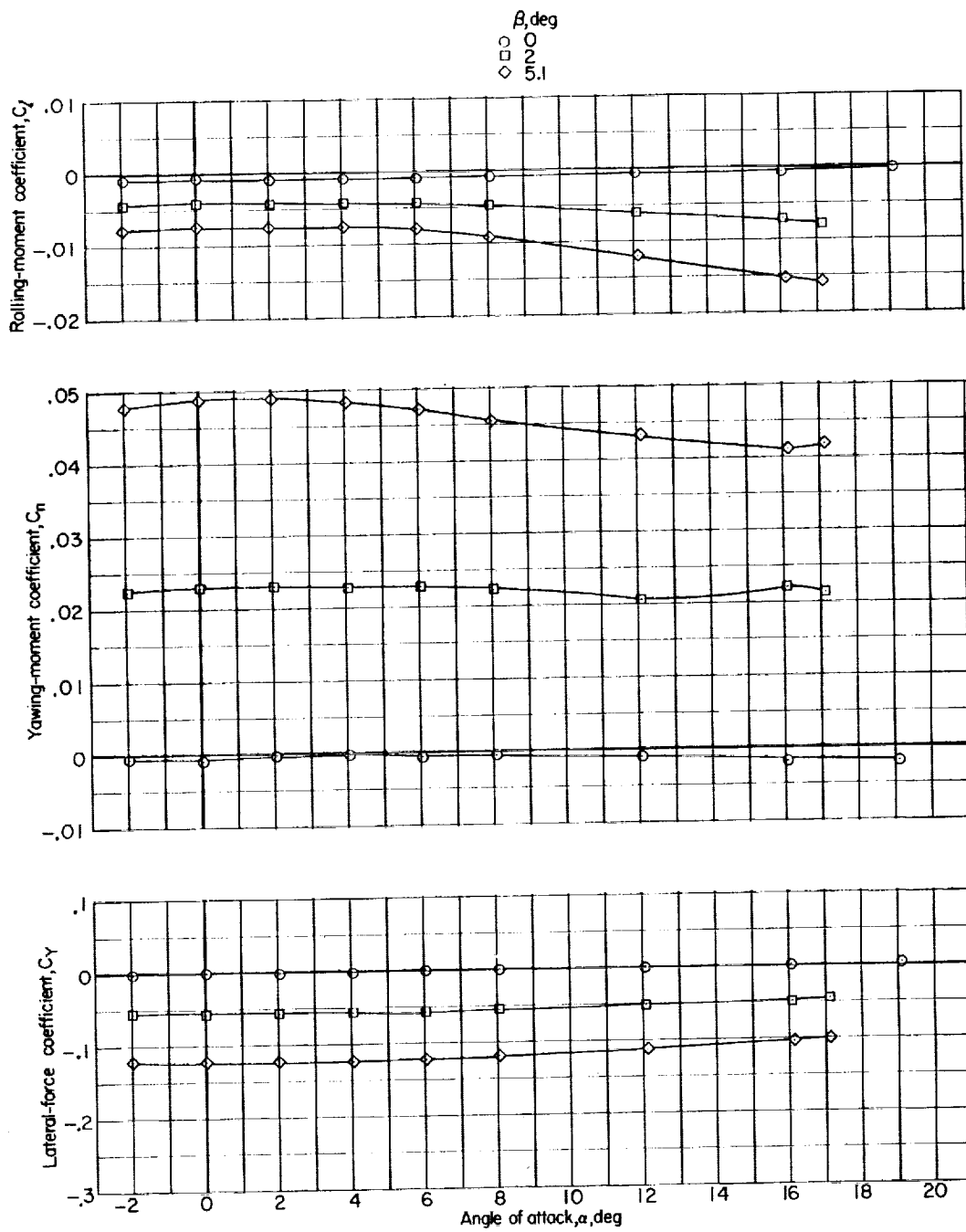
(g) $M = 1.03$.

Figure 8.- Continued.



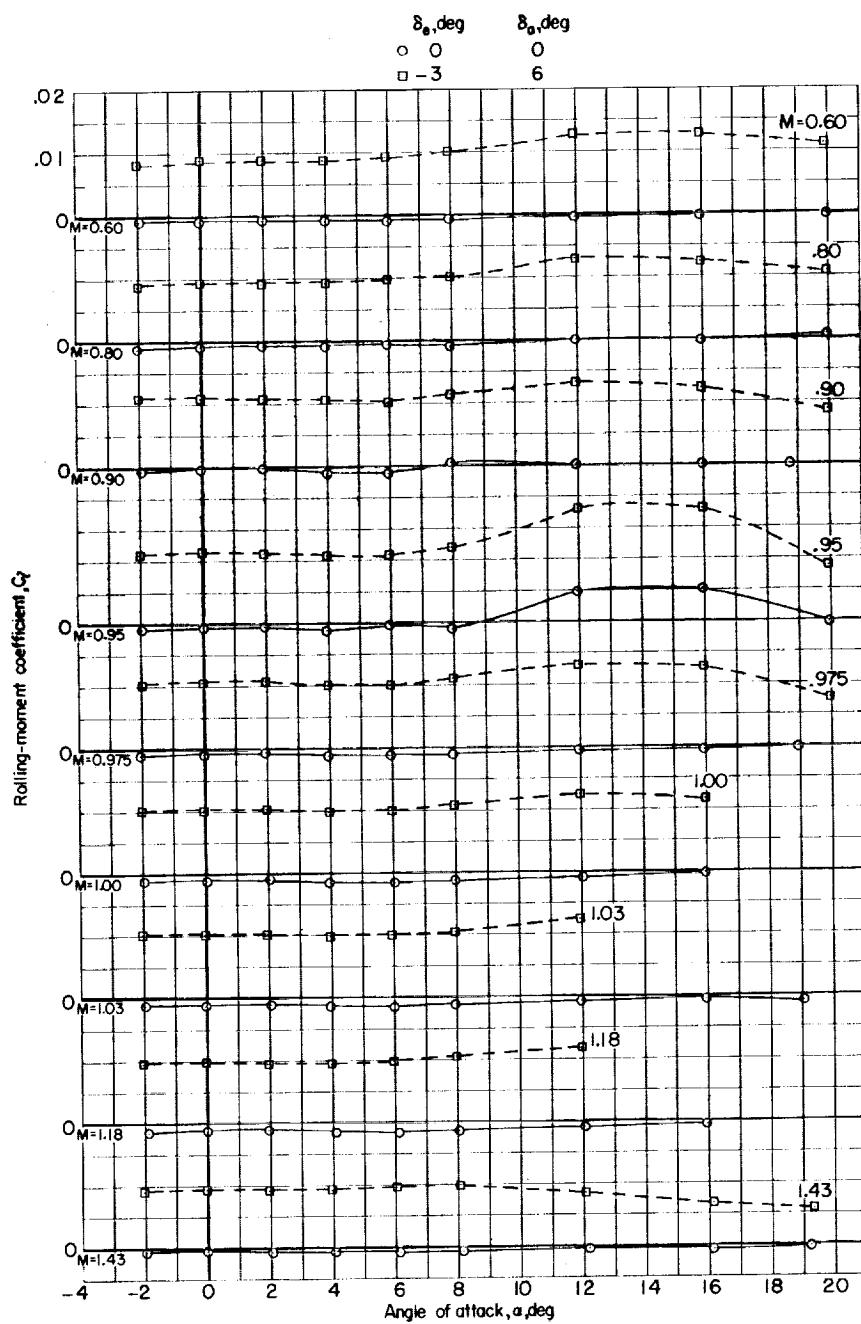
(h) $M = 1.18$.

Figure 8.- Continued.



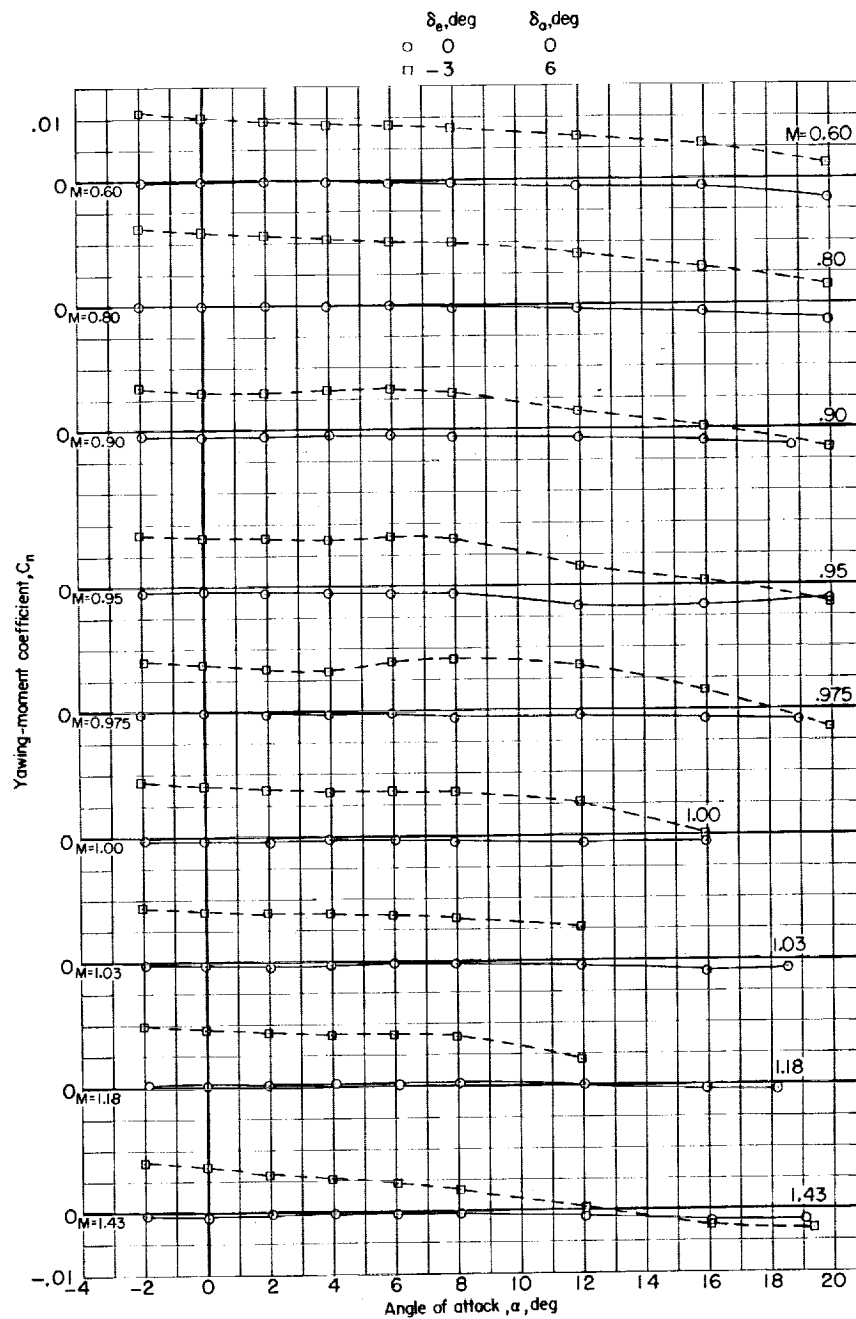
(1) $M = 1.43$.

Figure 8.- Concluded.



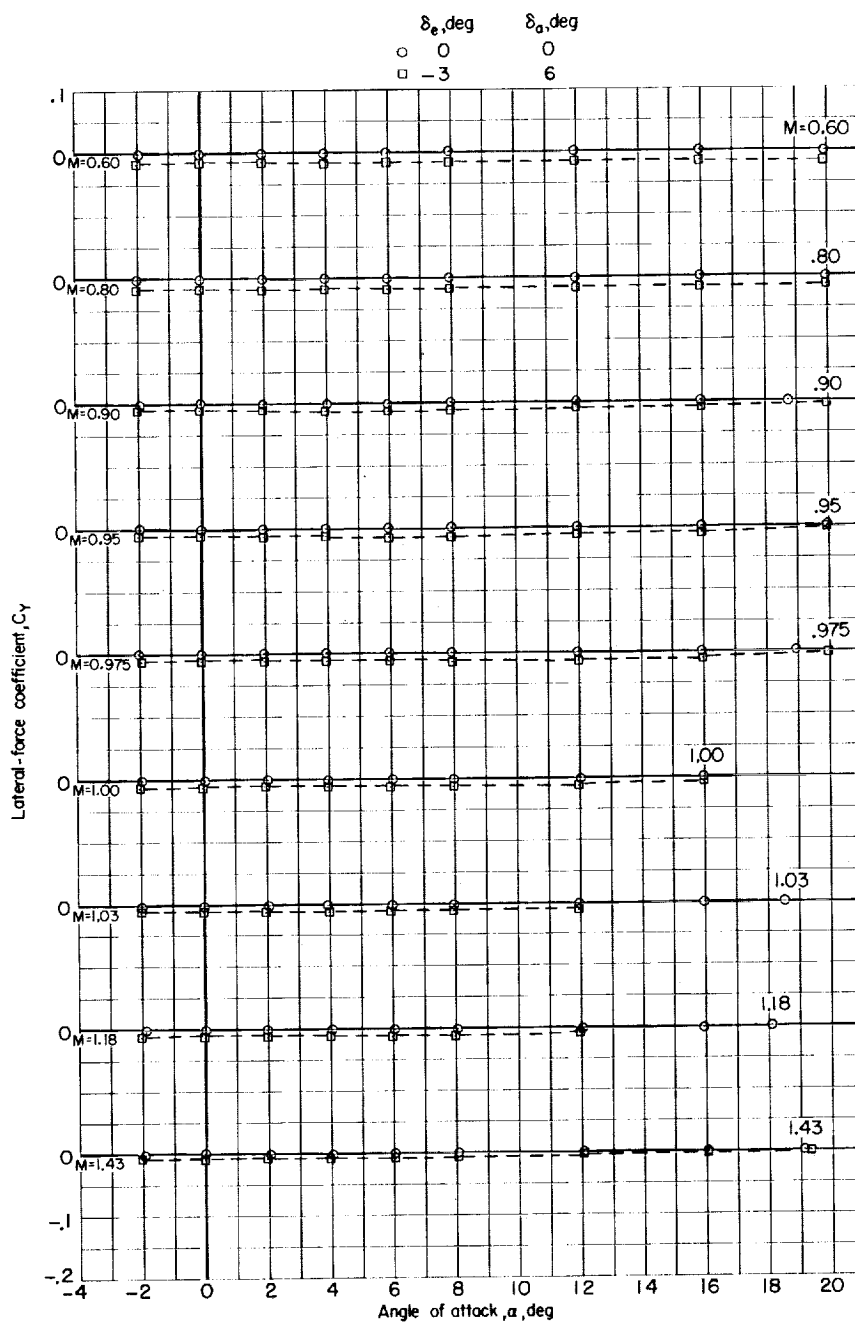
(a) Rolling moment.

Figure 9.- Lateral-directional characteristics of the complete model with the horizontal tail deflected for lateral control at zero sideslip.



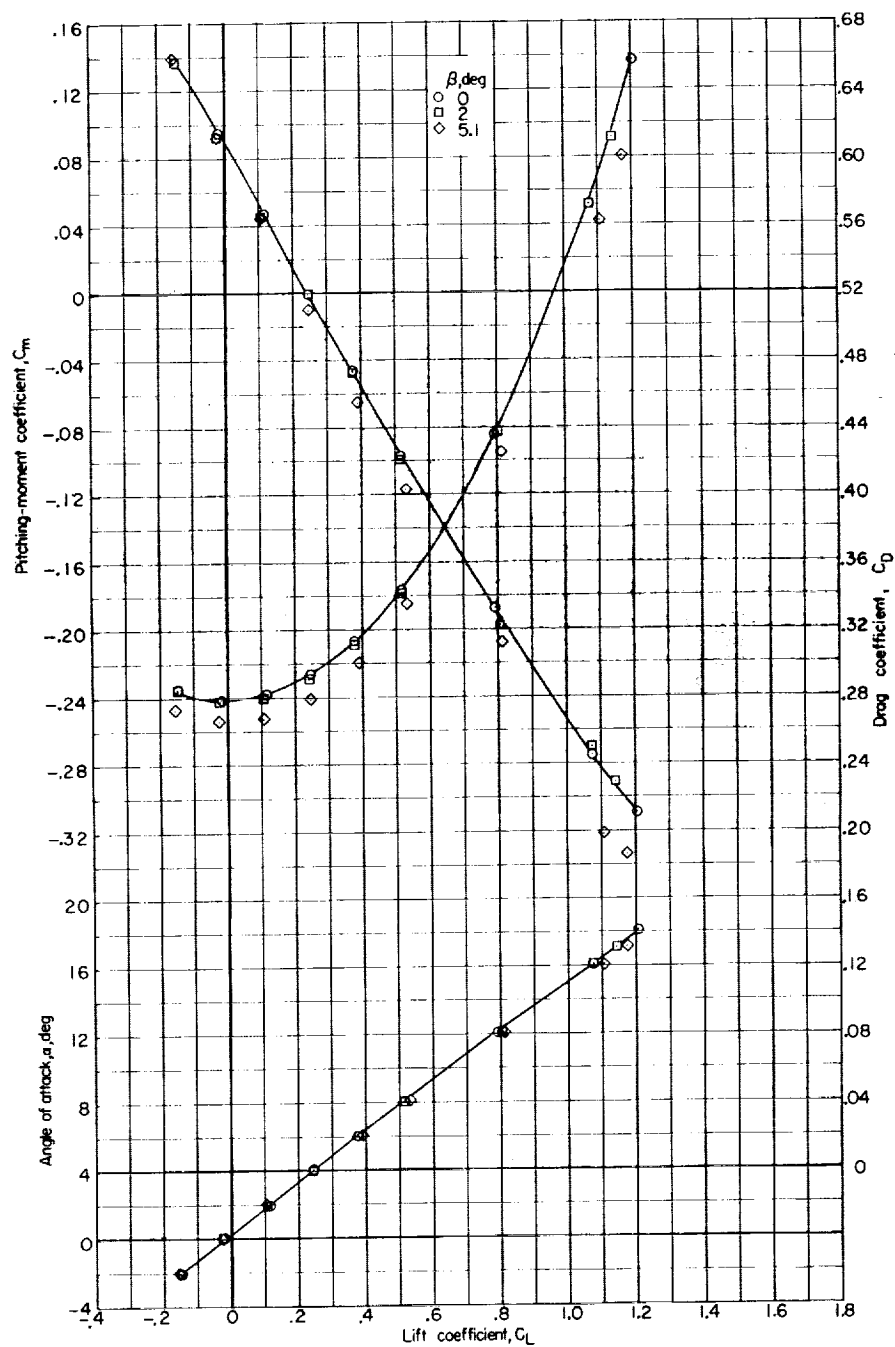
(b) Yawing moment.

Figure 9.- Continued.



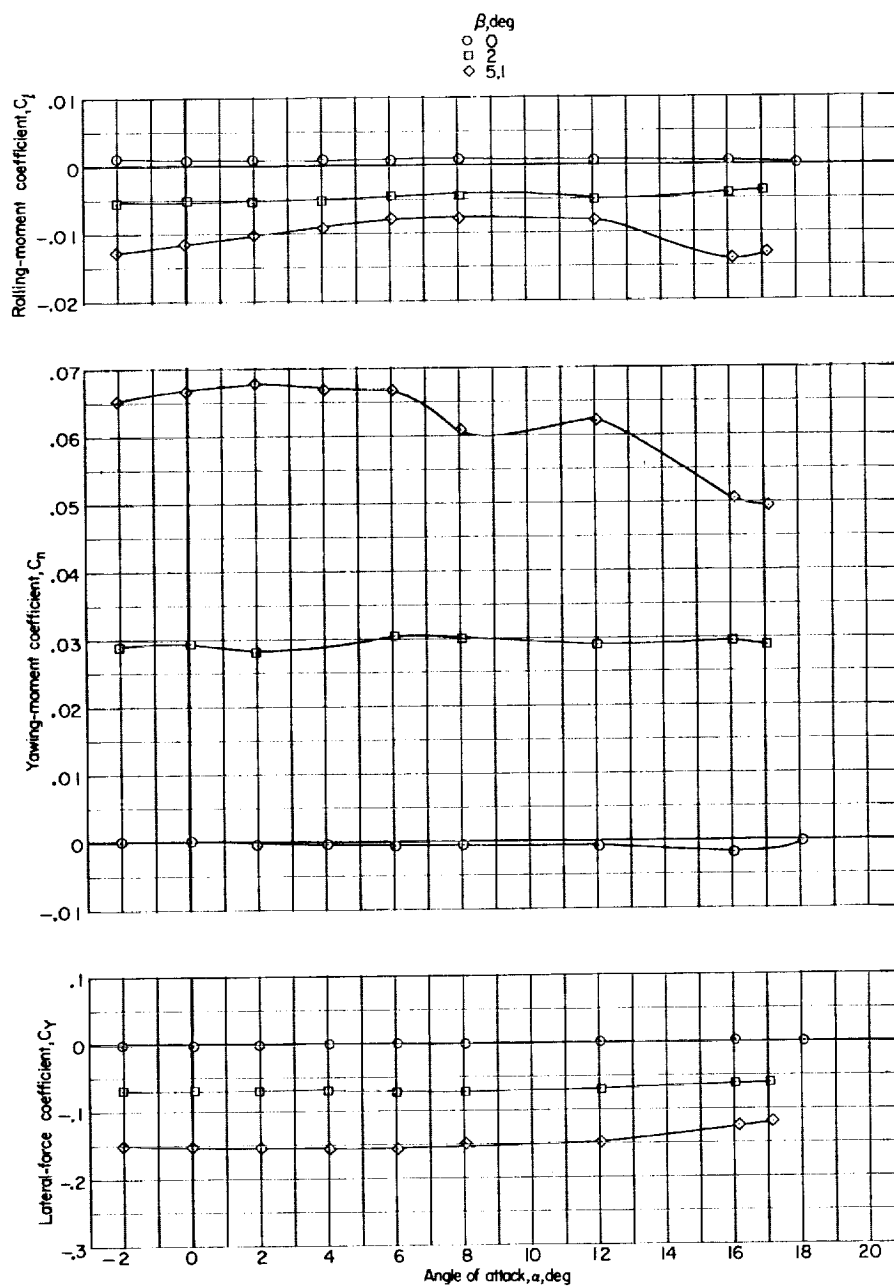
(c) Lateral force.

Figure 9.- Concluded.



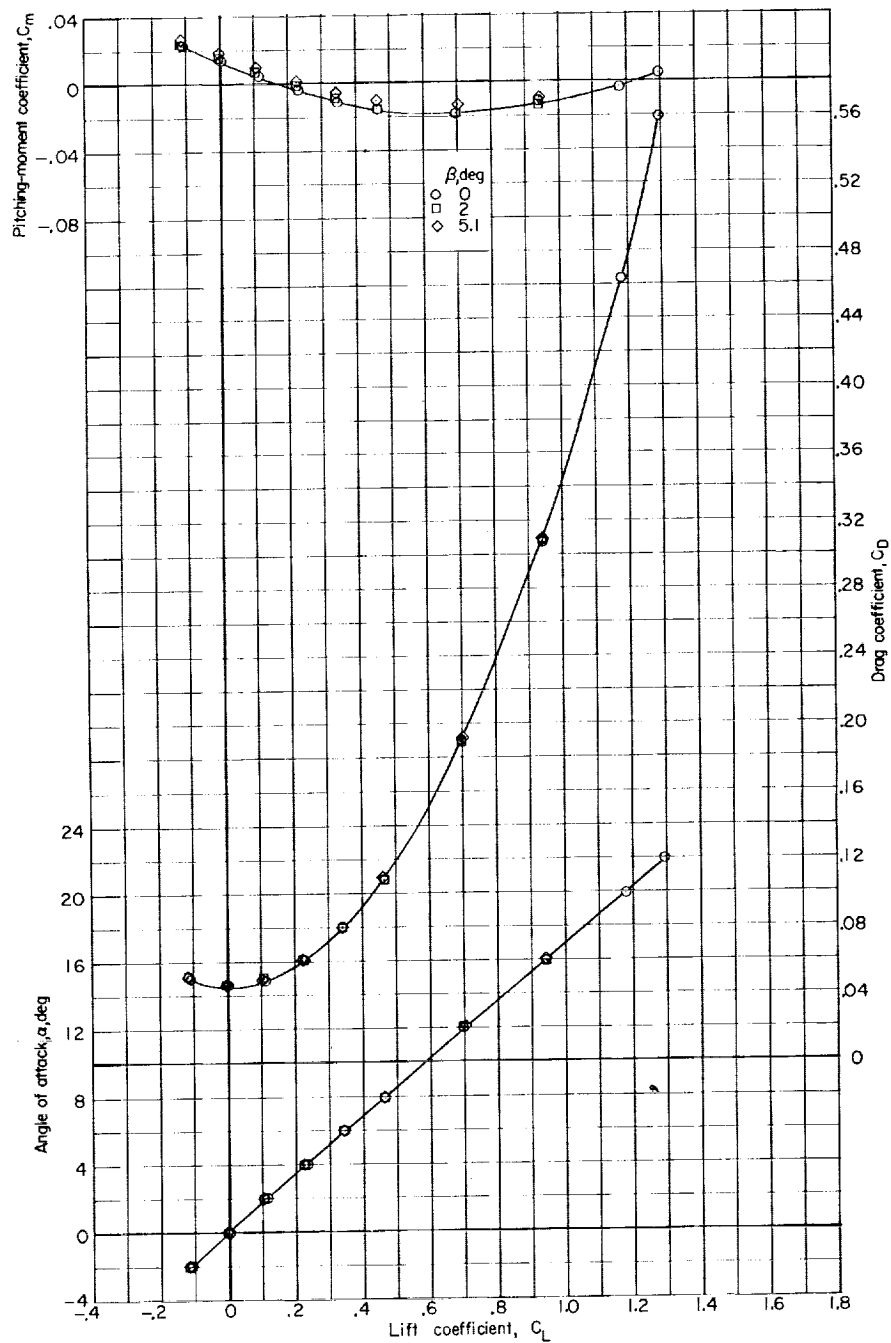
(a) Longitudinal characteristics.

Figure 10.- Longitudinal and lateral-directional characteristics of the complete model with speed brakes deflected 45° at various angles of sideslip. $M = 1.43$; $\delta_e = 0^\circ$; $\delta_a = 0^\circ$.



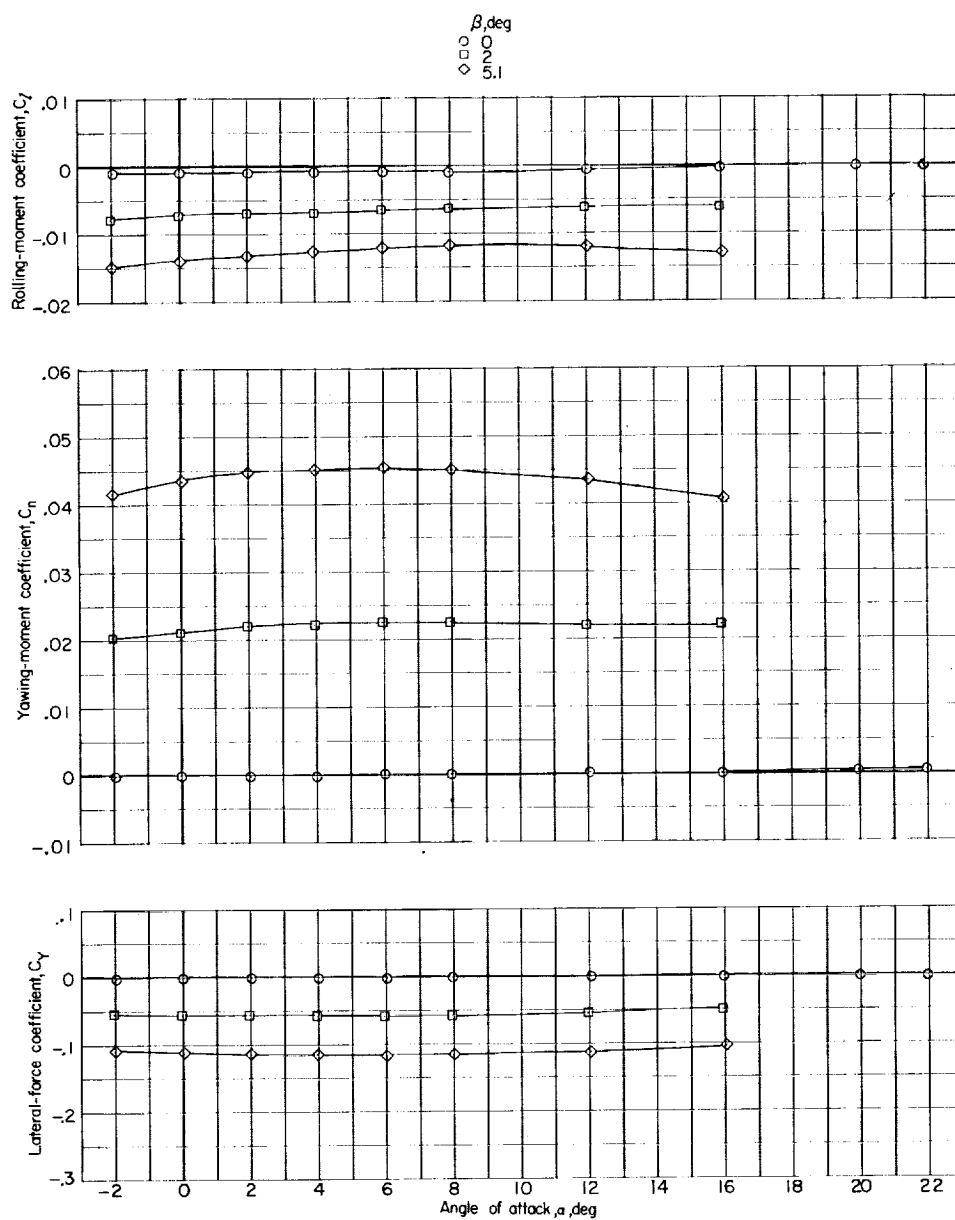
(b) Lateral-directional characteristics.

Figure 10.- Concluded.



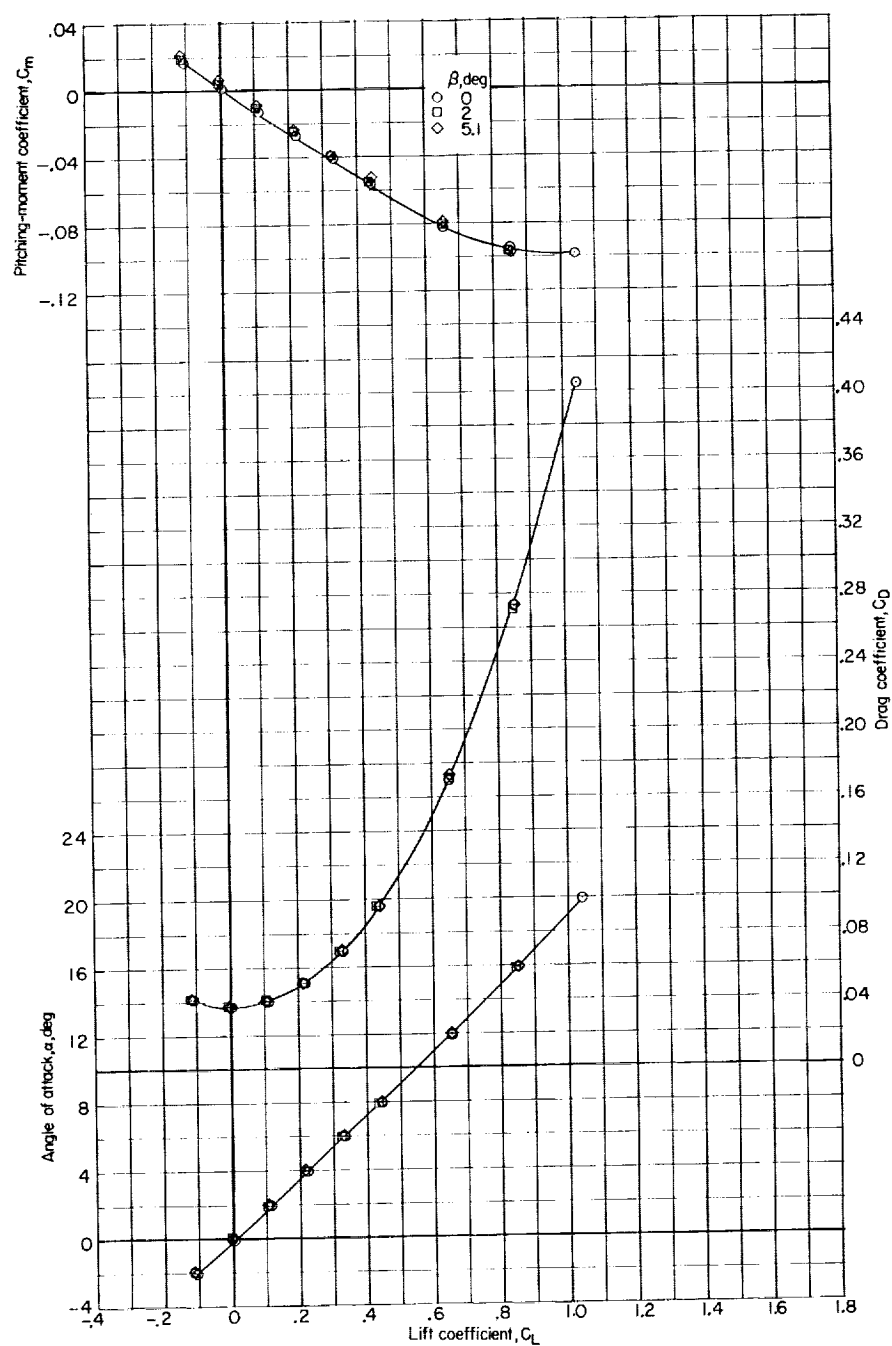
(a) Longitudinal characteristics.

Figure 11.- Longitudinal and lateral-directional characteristics of the model with the horizontal tail off at various angles of sideslip.
 $M = 1.43$.



(b) Lateral-directional characteristics.

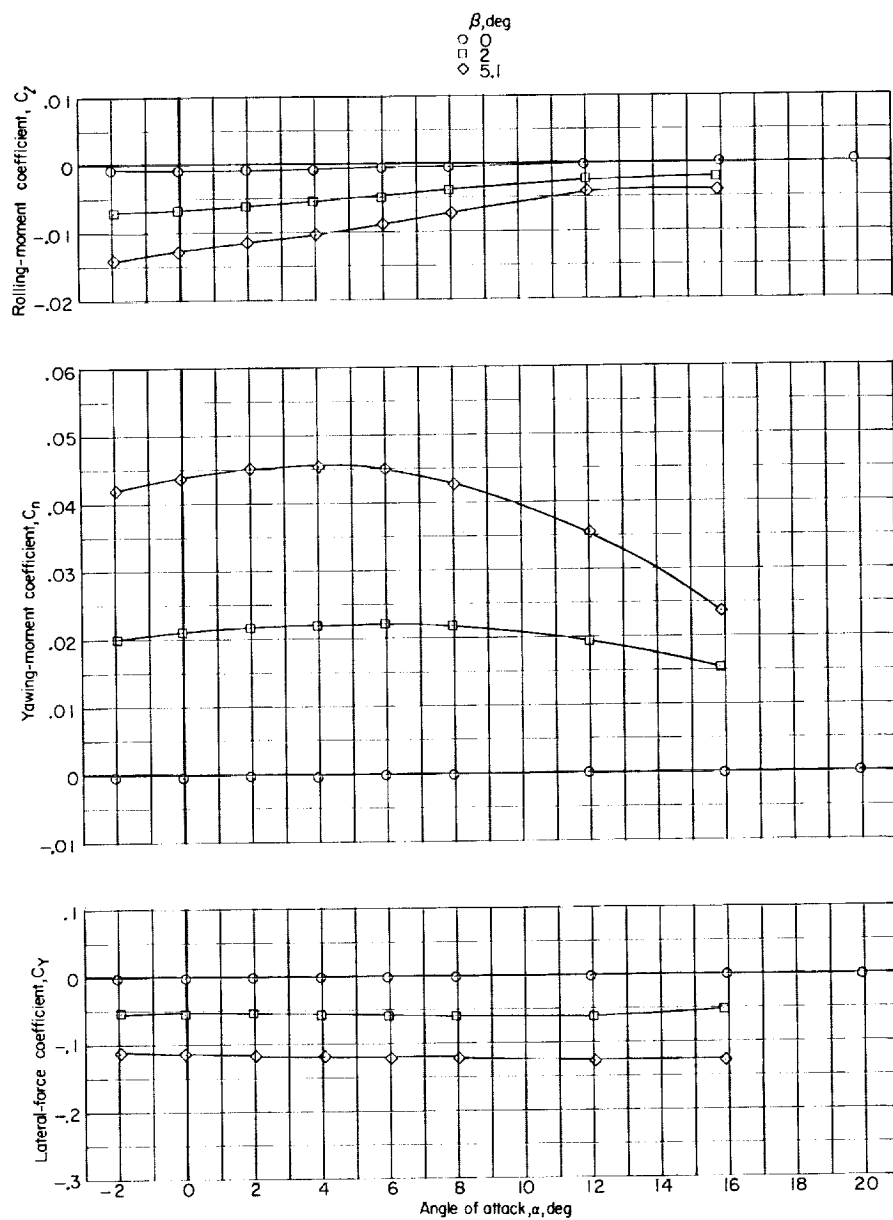
Figure 11.- Concluded.



(a) Longitudinal characteristics.

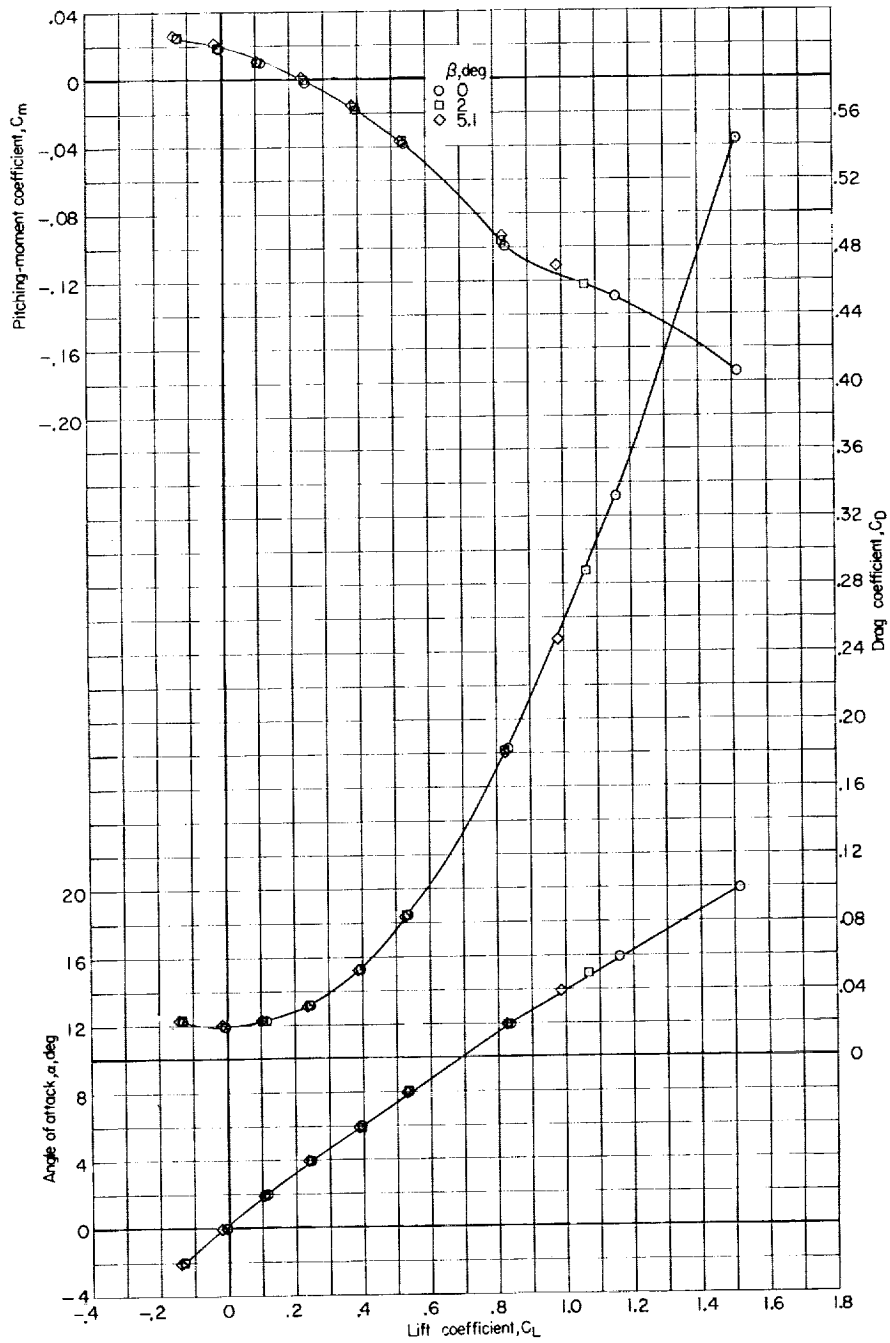
Figure 12.- Longitudinal and lateral-directional characteristics of the model with the horizontal tail and fuselage side fairings off at various angles of sideslip. $M = 1.43$.

L-376



(b) Lateral-directional characteristics.

Figure 12.- Concluded.

(a) $M = 0.60$.Figure 13.- Longitudinal characteristics of the model with the vertical tails off at various angles of sideslip. $\delta_e = 0^\circ$; $\delta_a = 0^\circ$.

L-376

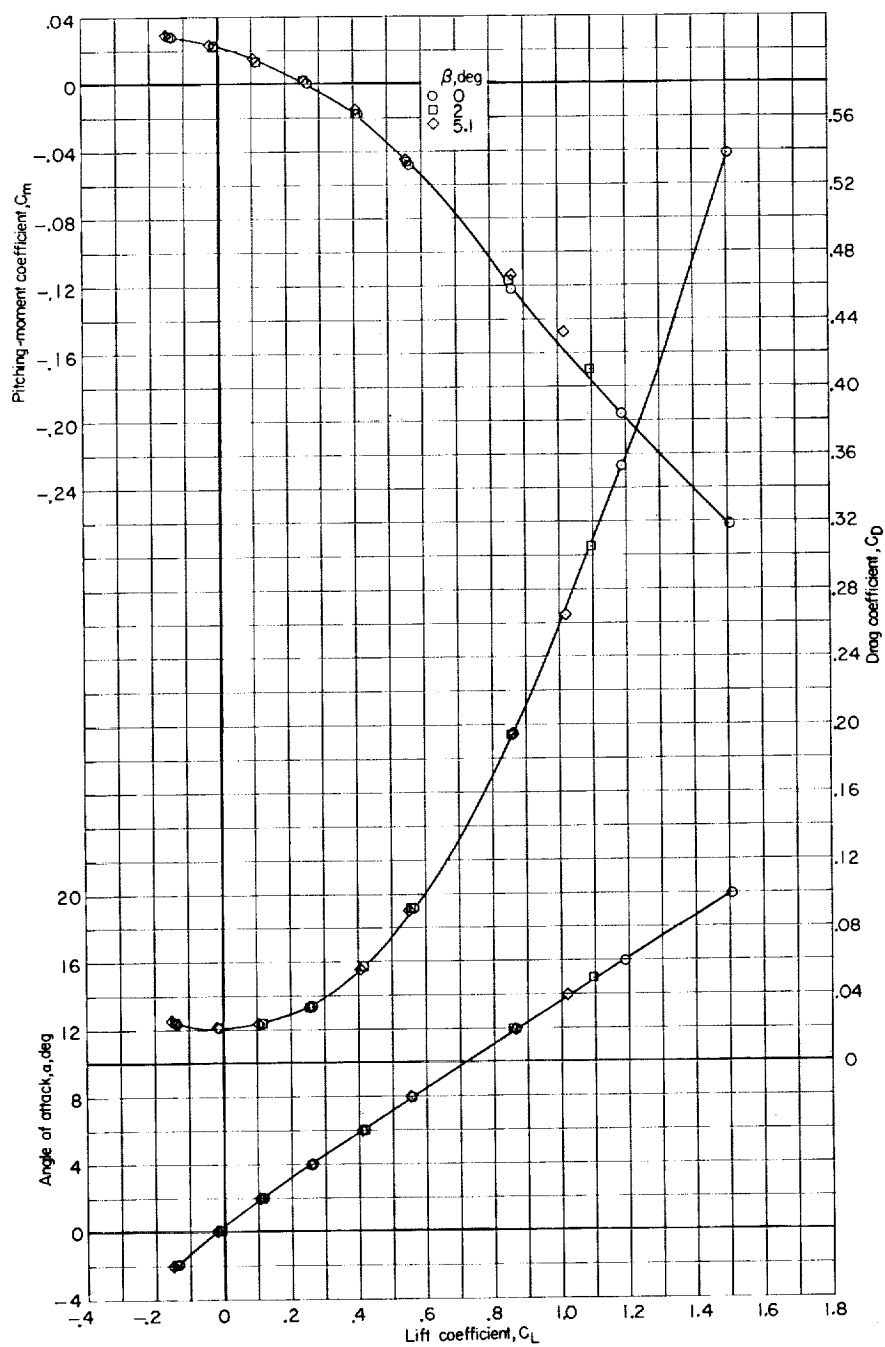
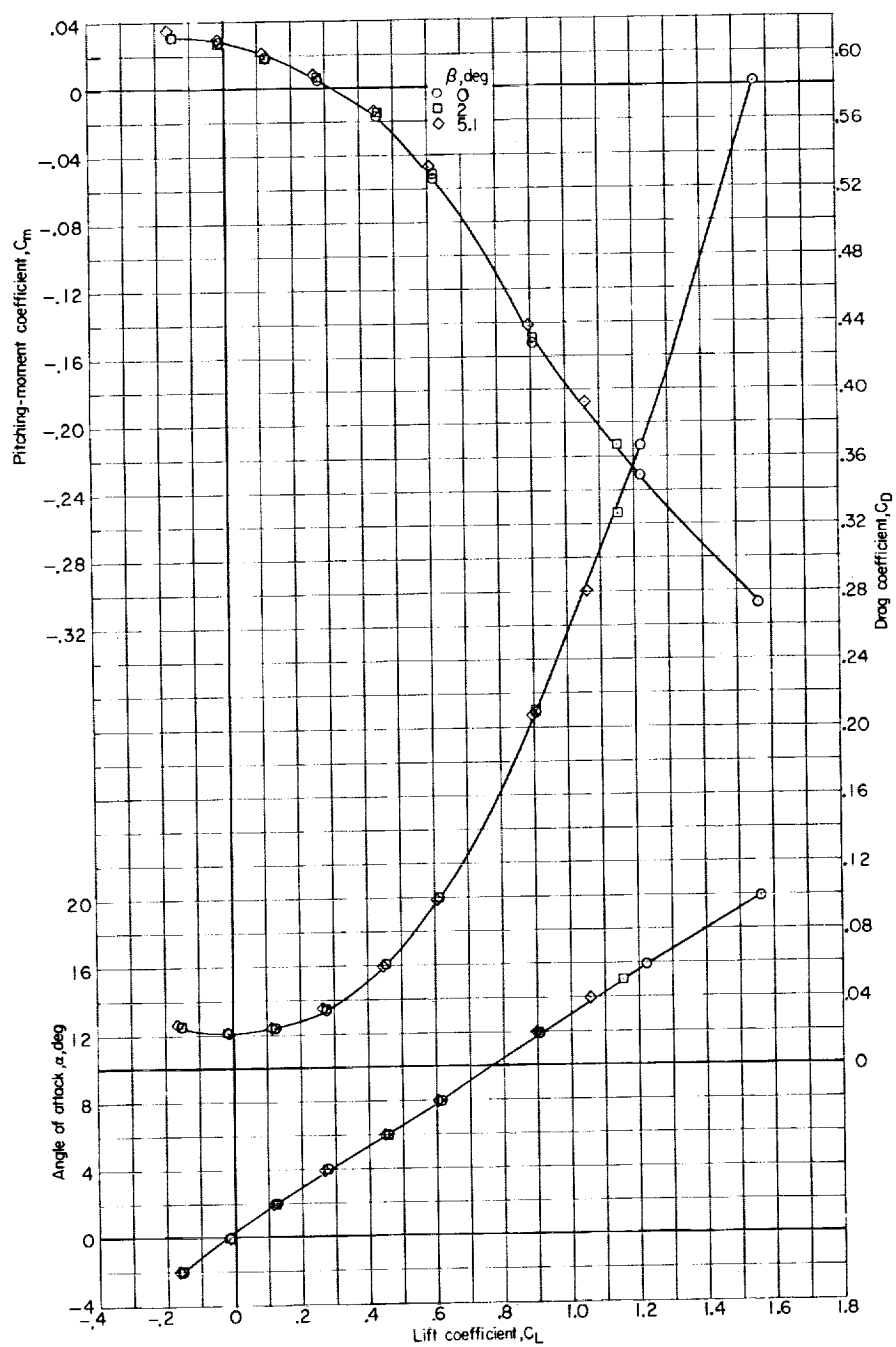
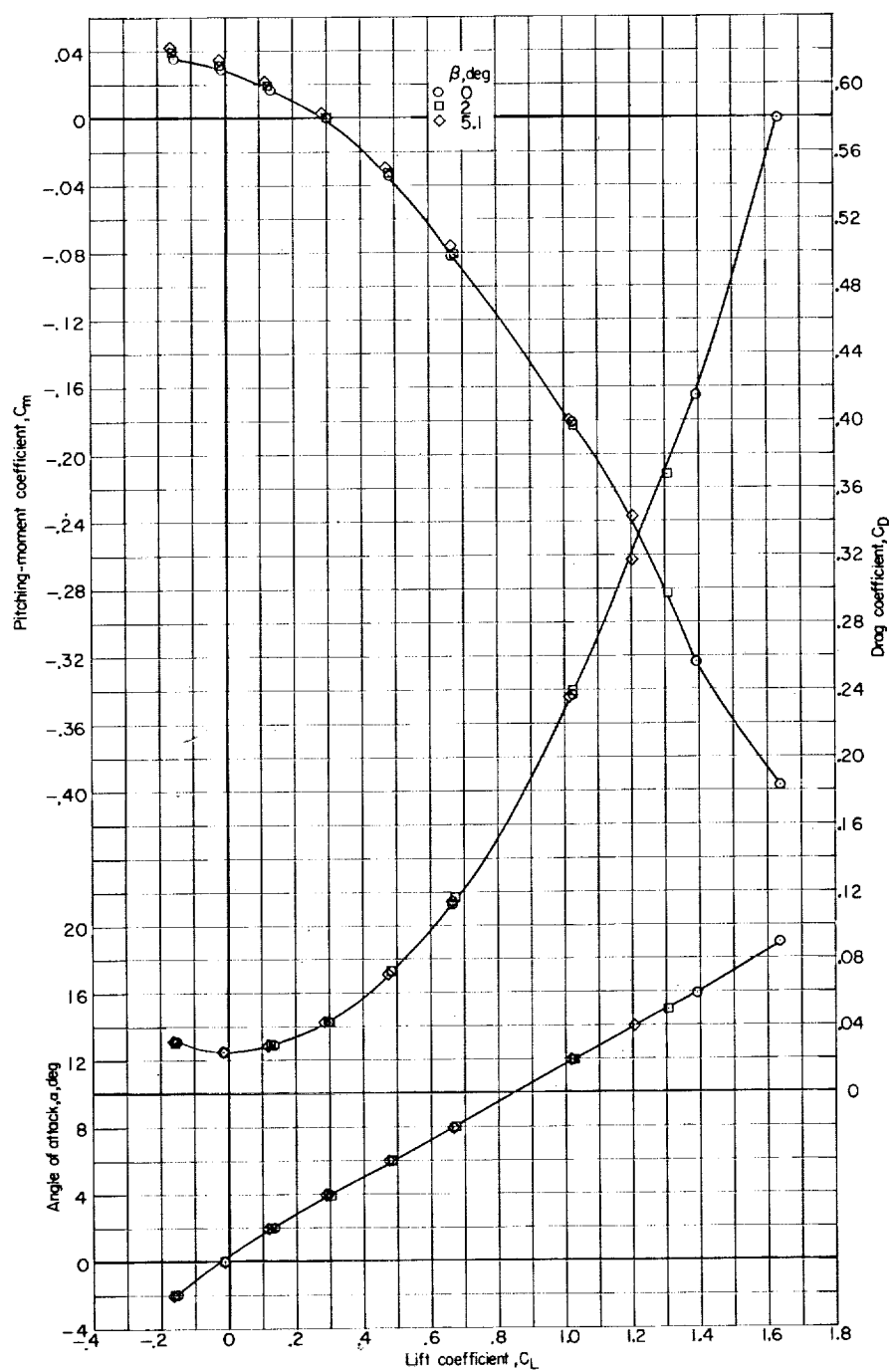
(b) $M = 0.80$.

Figure 13.- Continued.



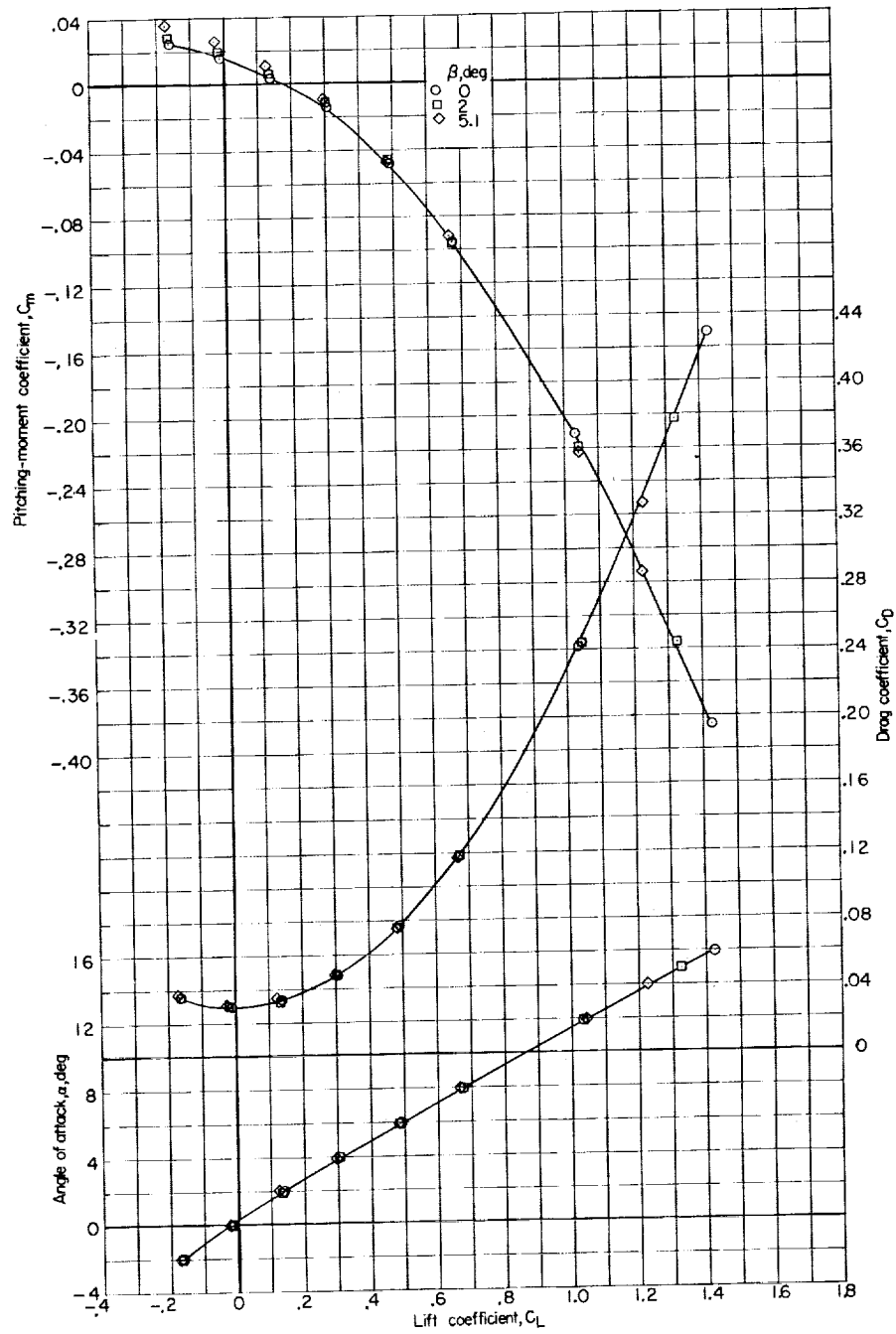
(c) $M = 0.90$.

Figure 13.- Continued.



(d) $M = 0.95$.

Figure 13.- Continued.



(e) $M = 0.975$.

Figure 13.- Continued.

I-376

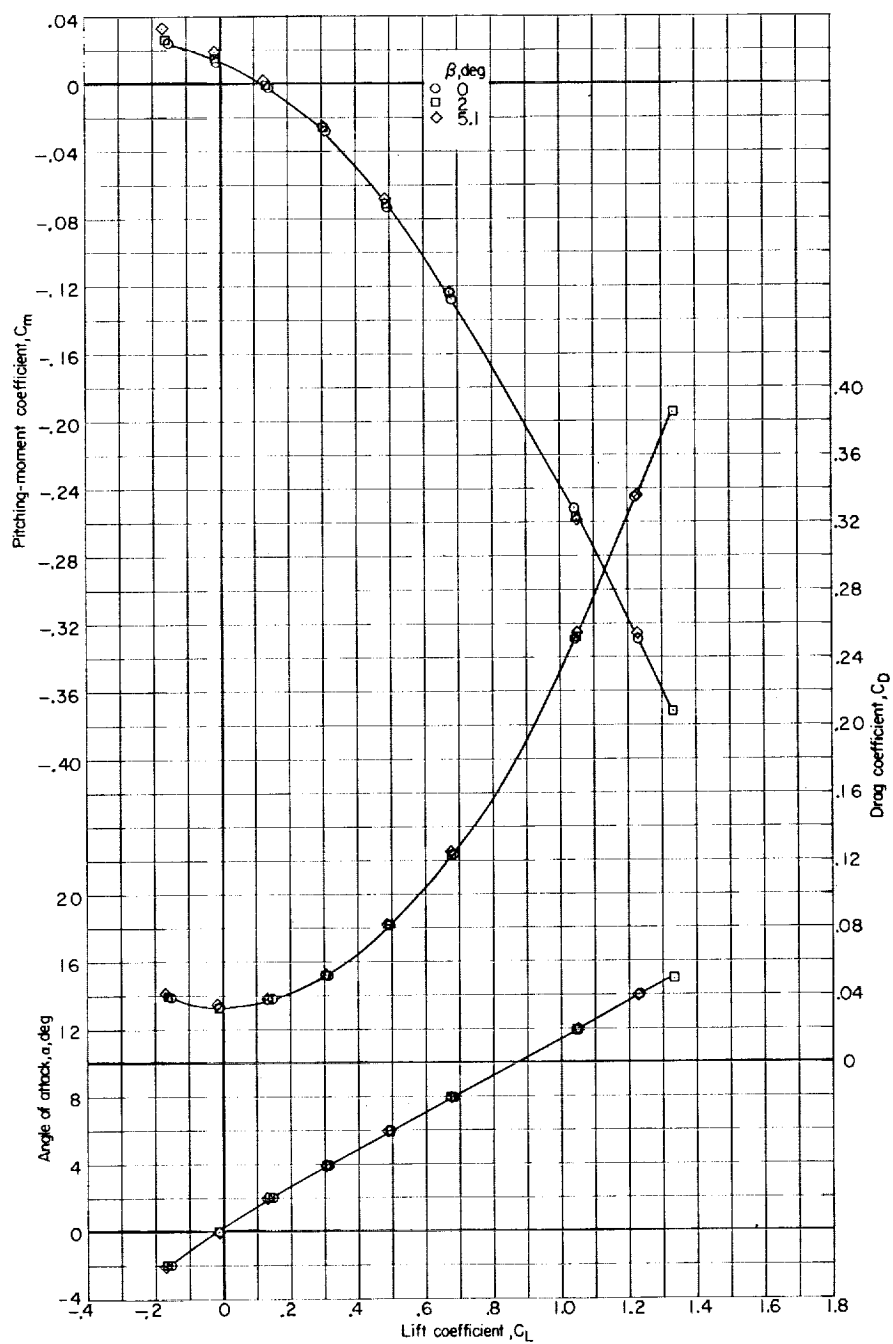
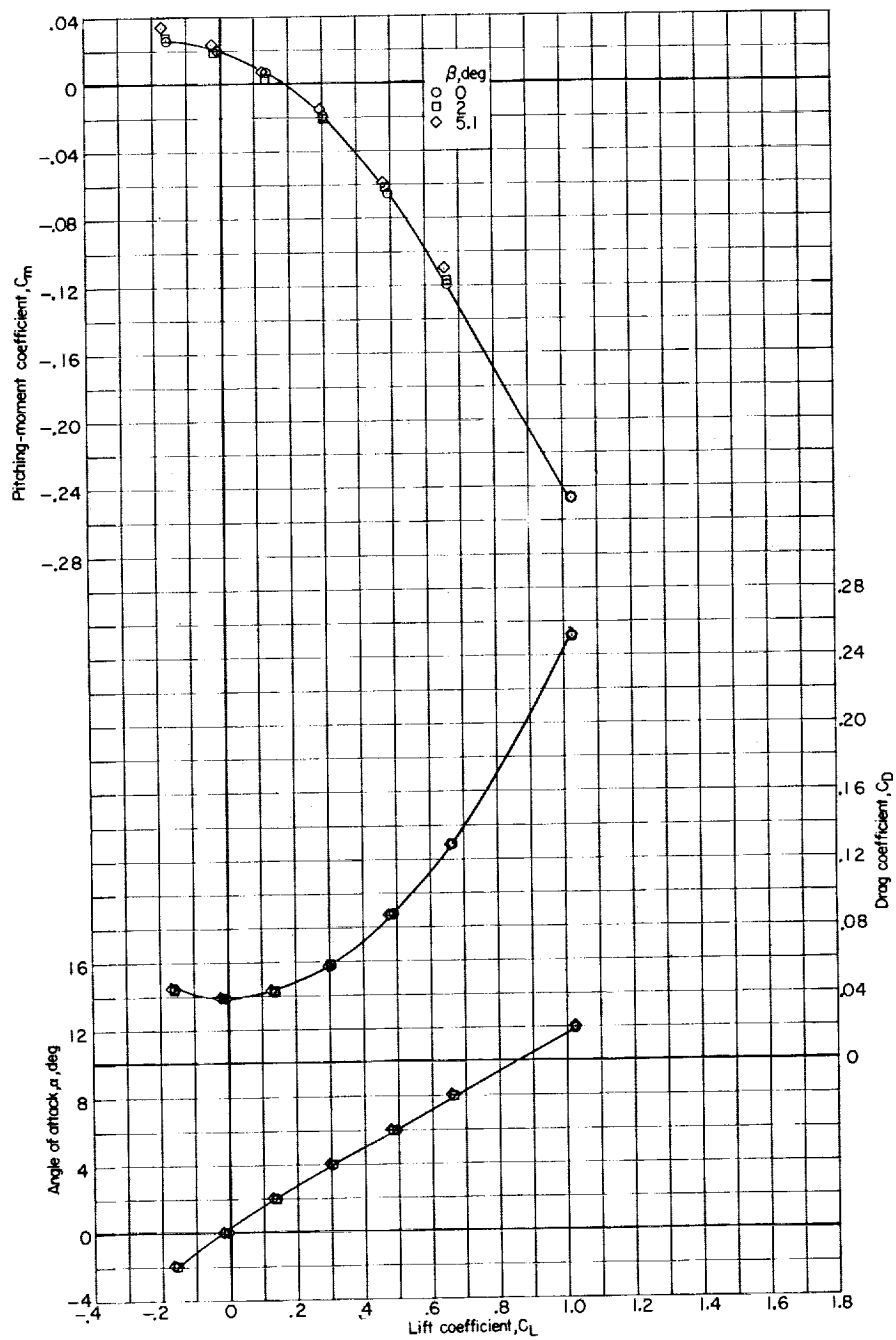
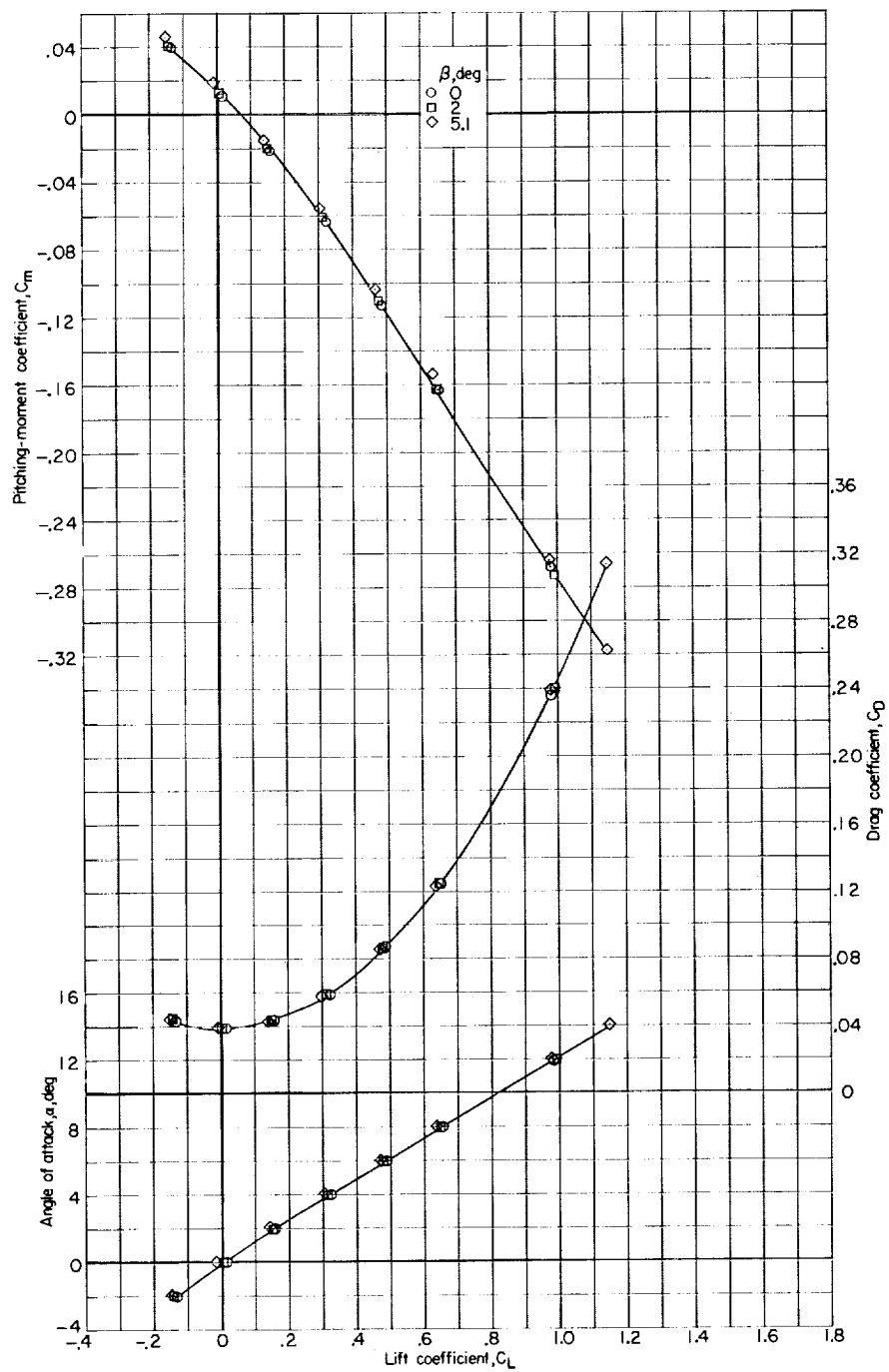
(f) $M = 1.00$.

Figure 13.- Continued.



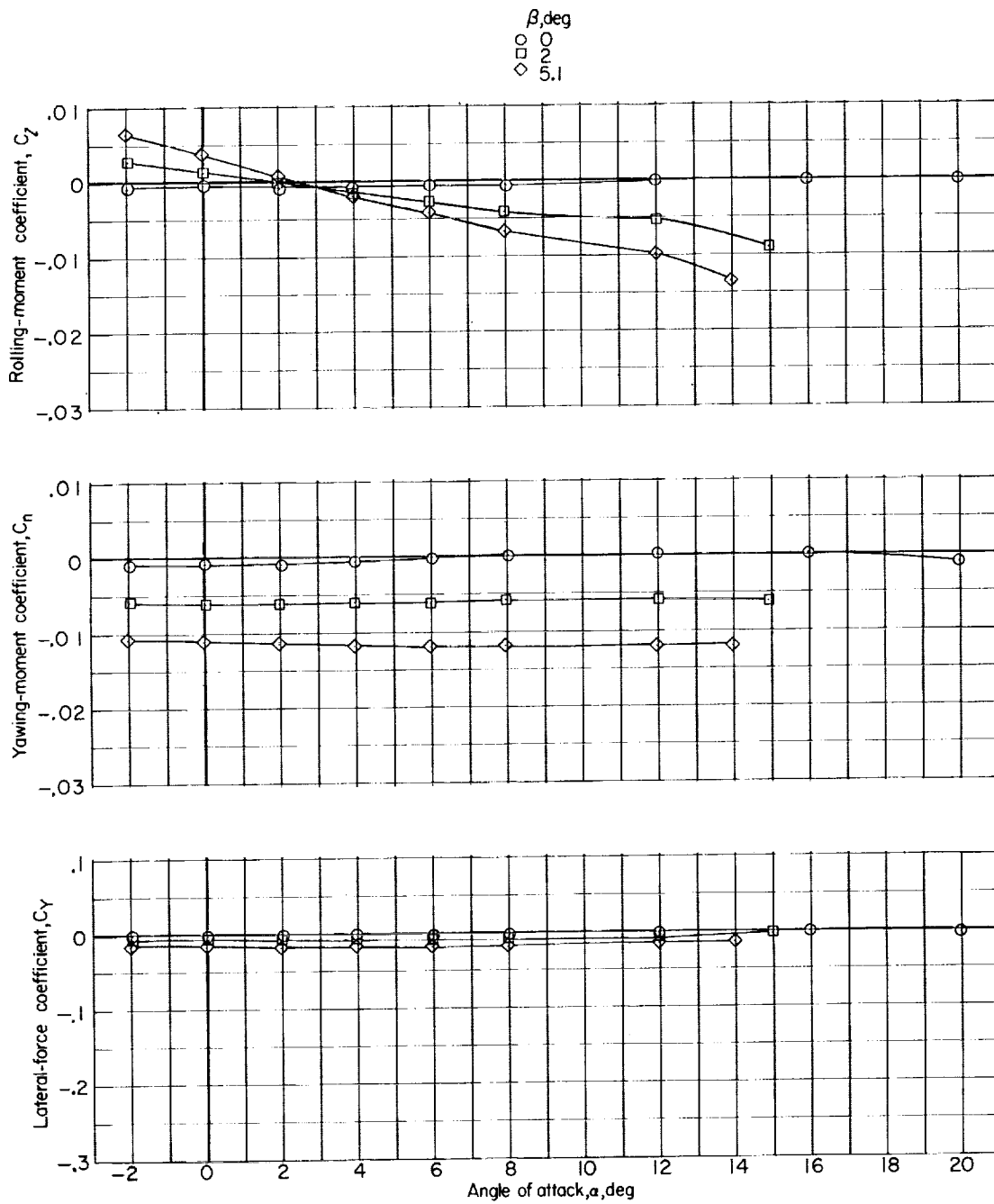
(g) $M = 1.03$.

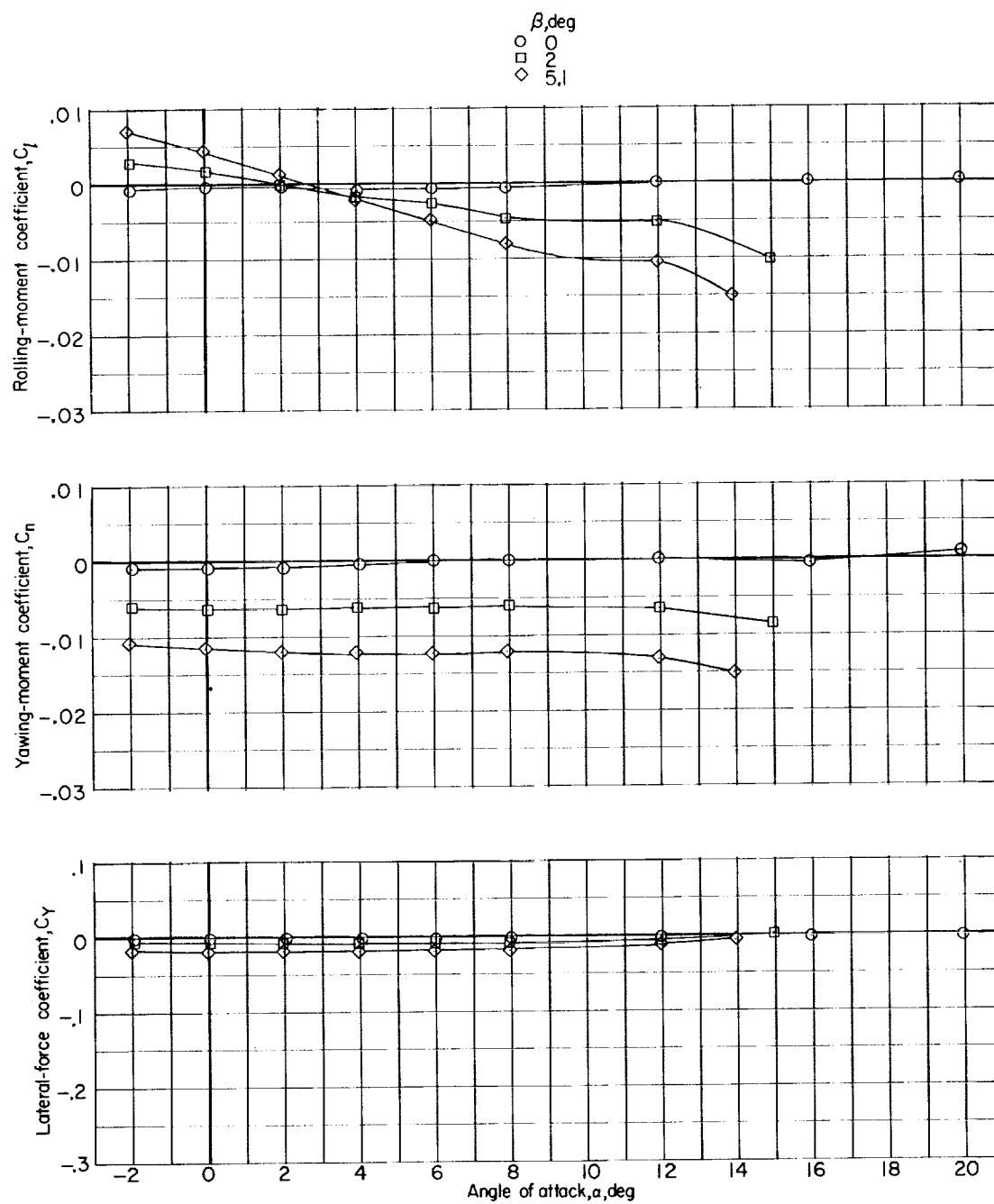
Figure 13.- Continued.



(h) $M = 1.18$.

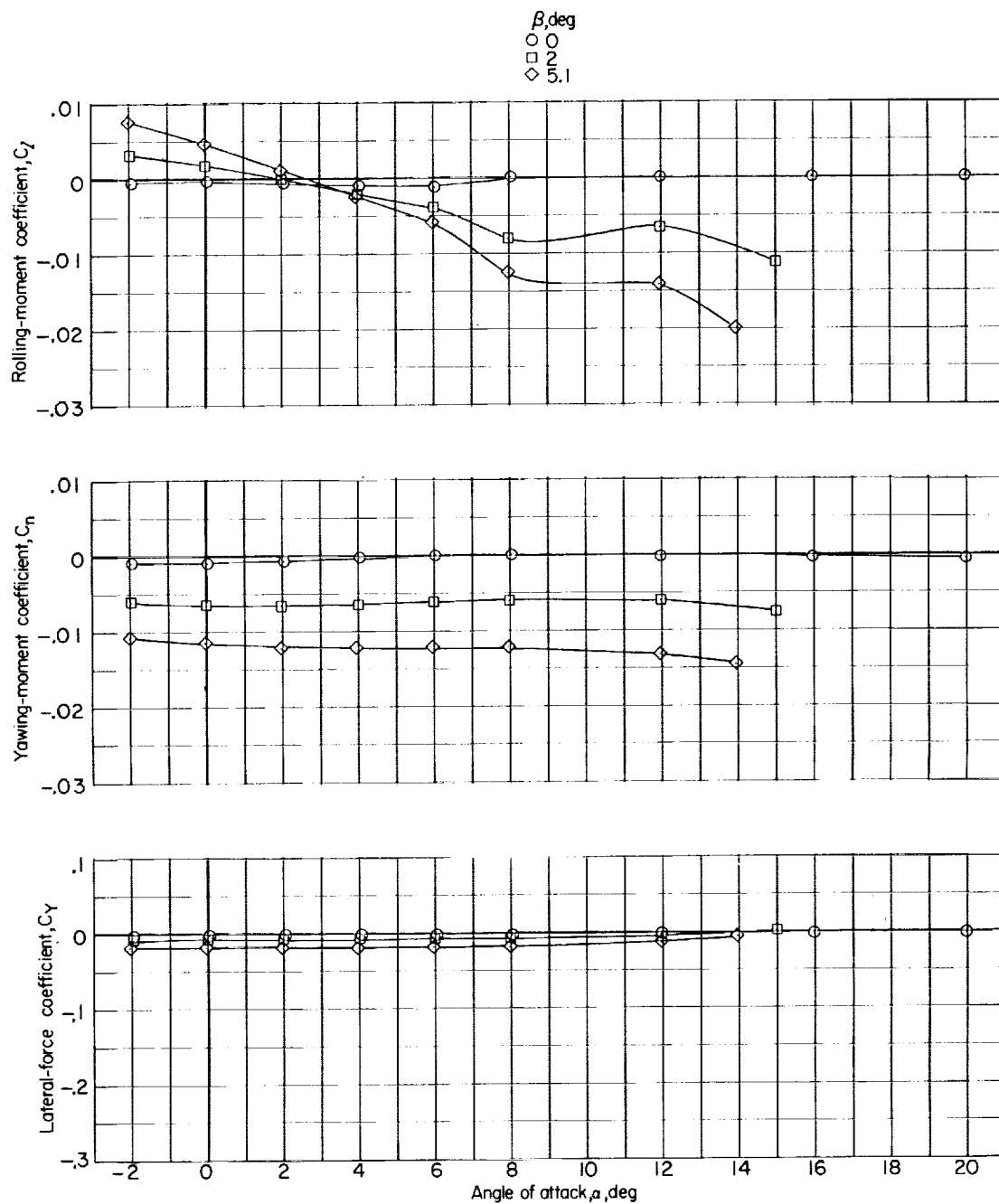
Figure 13.- Concluded.

(a) $M = 0.60$.Figure 14.- Lateral-directional characteristics of the model with the vertical tails off at various angles of sideslip. $\delta_e = 0^\circ$; $\delta_a = 0^\circ$.



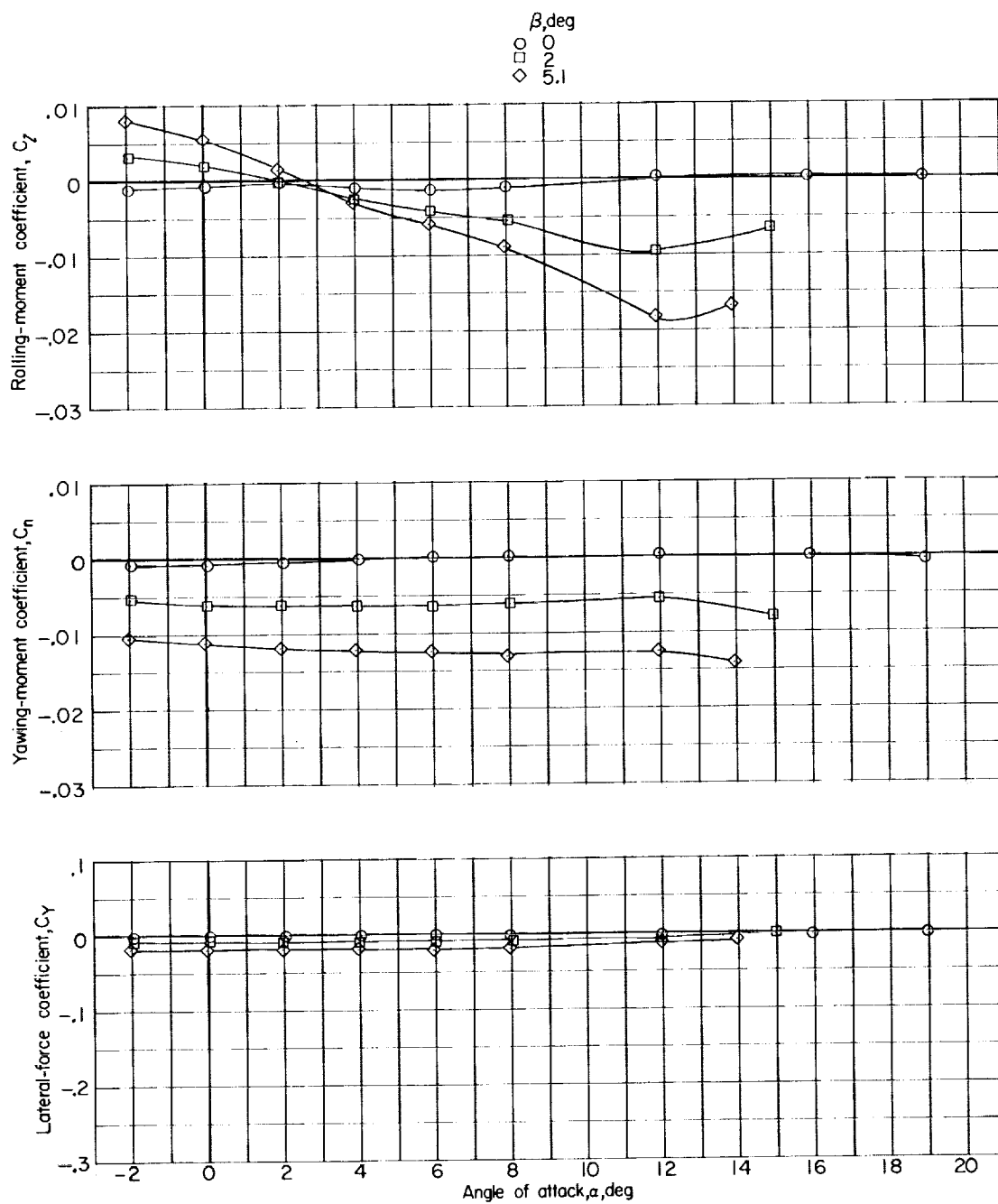
(b) $M = 0.80$.

Figure 14.- Continued.



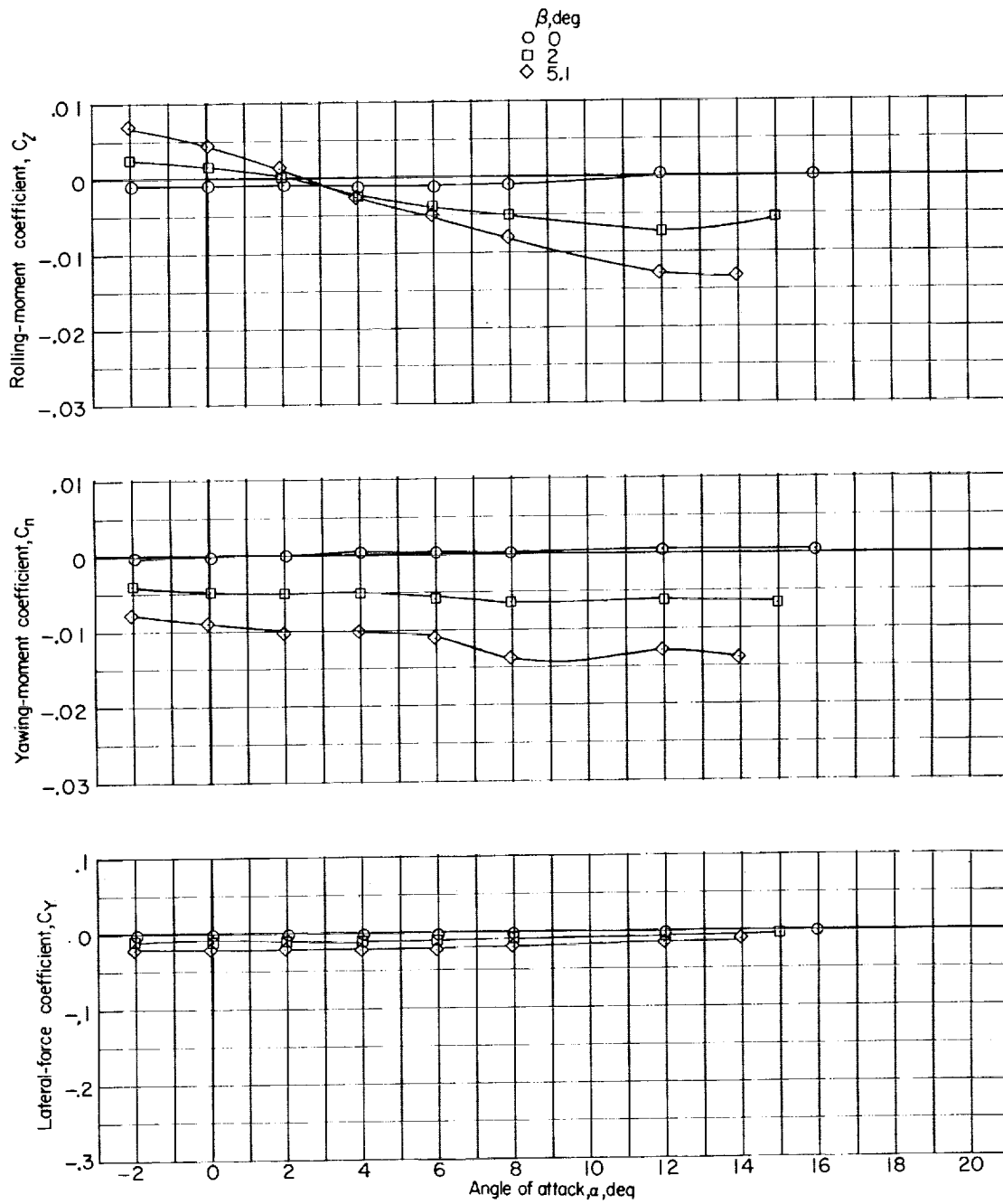
(c) $M = 0.90$.

Figure 14.- Continued.



(d) $M = 0.95$.

Figure 14.- Continued.



(e) $M = 0.975$.

Figure 14.- Continued.

L-376

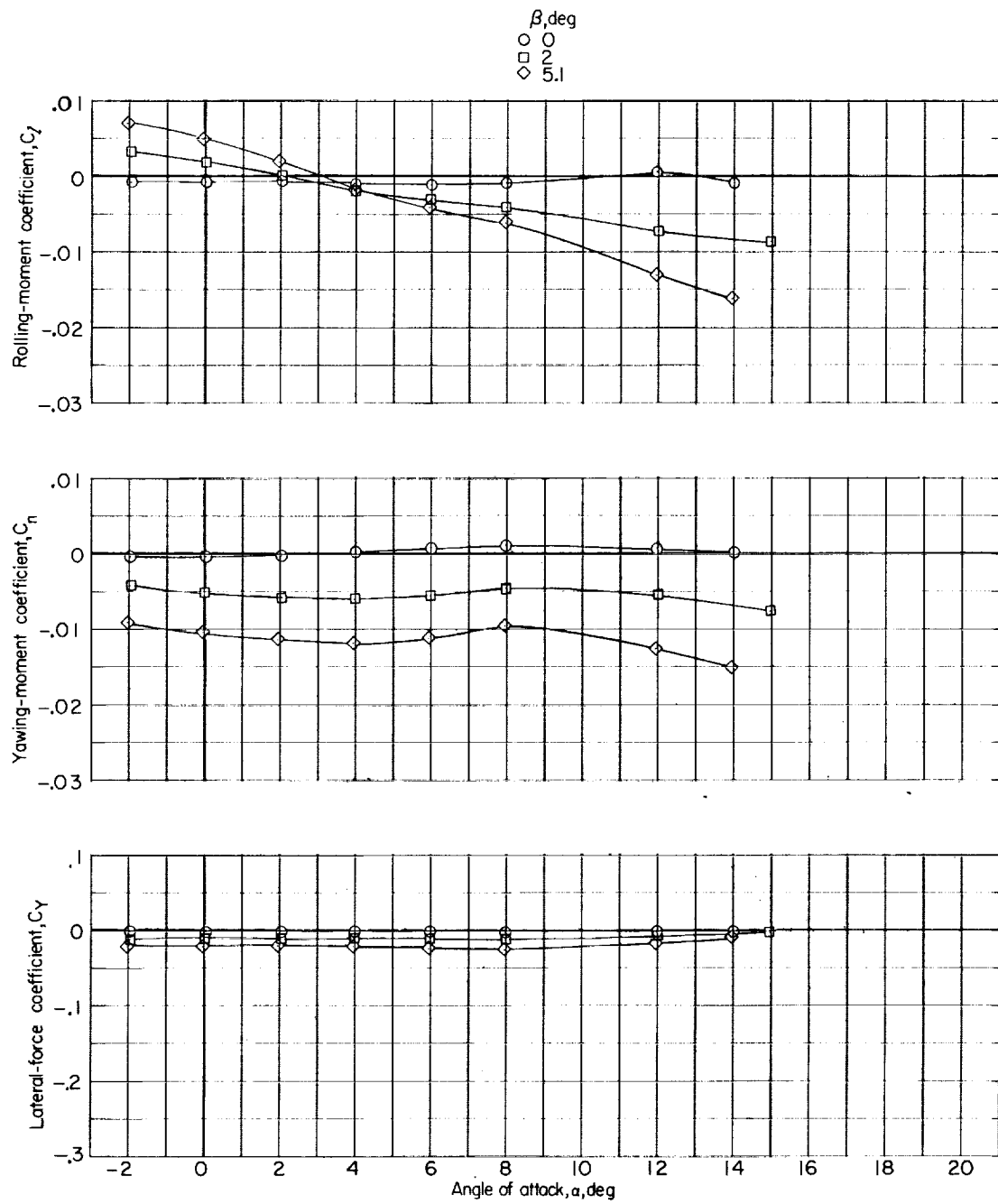
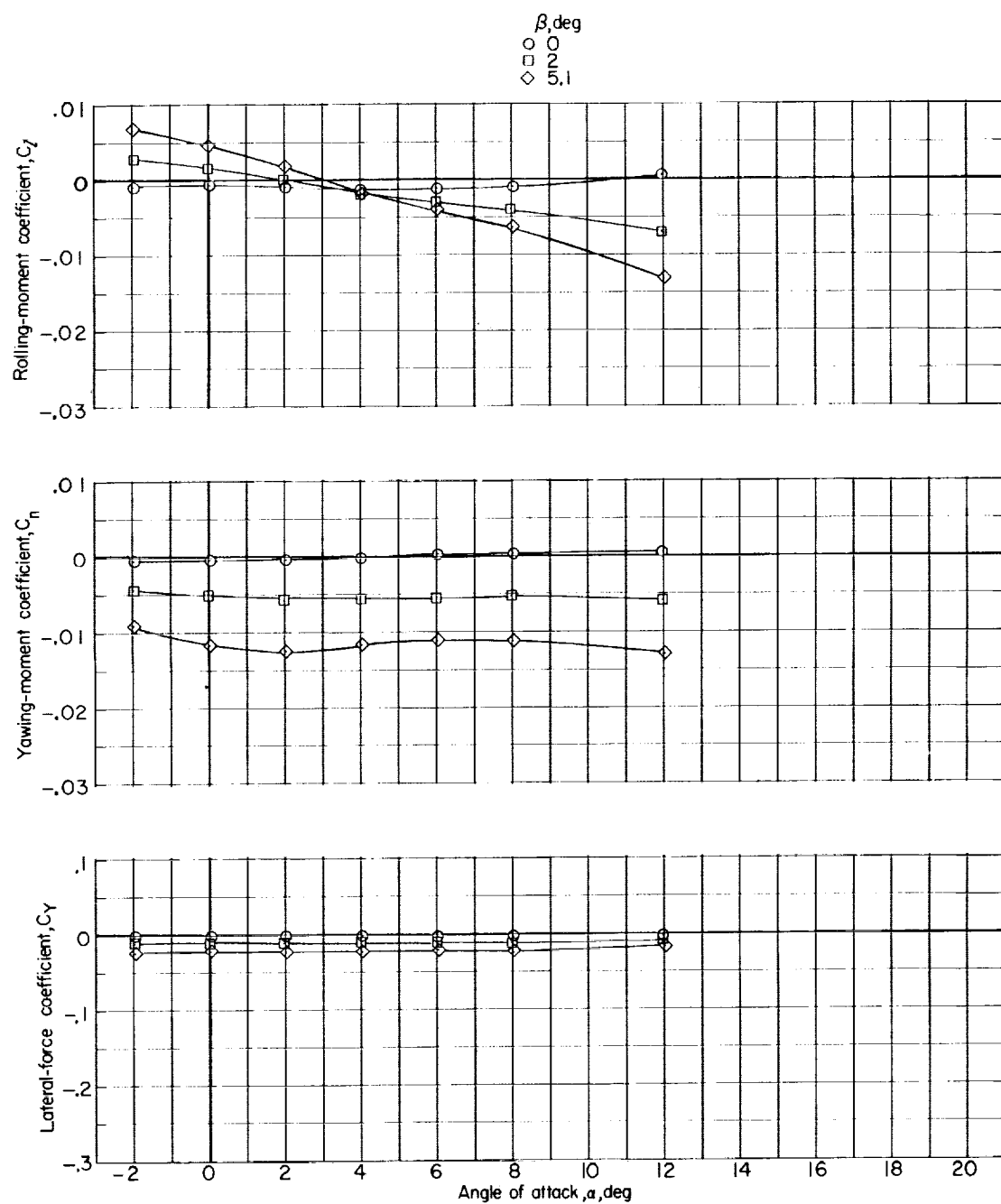
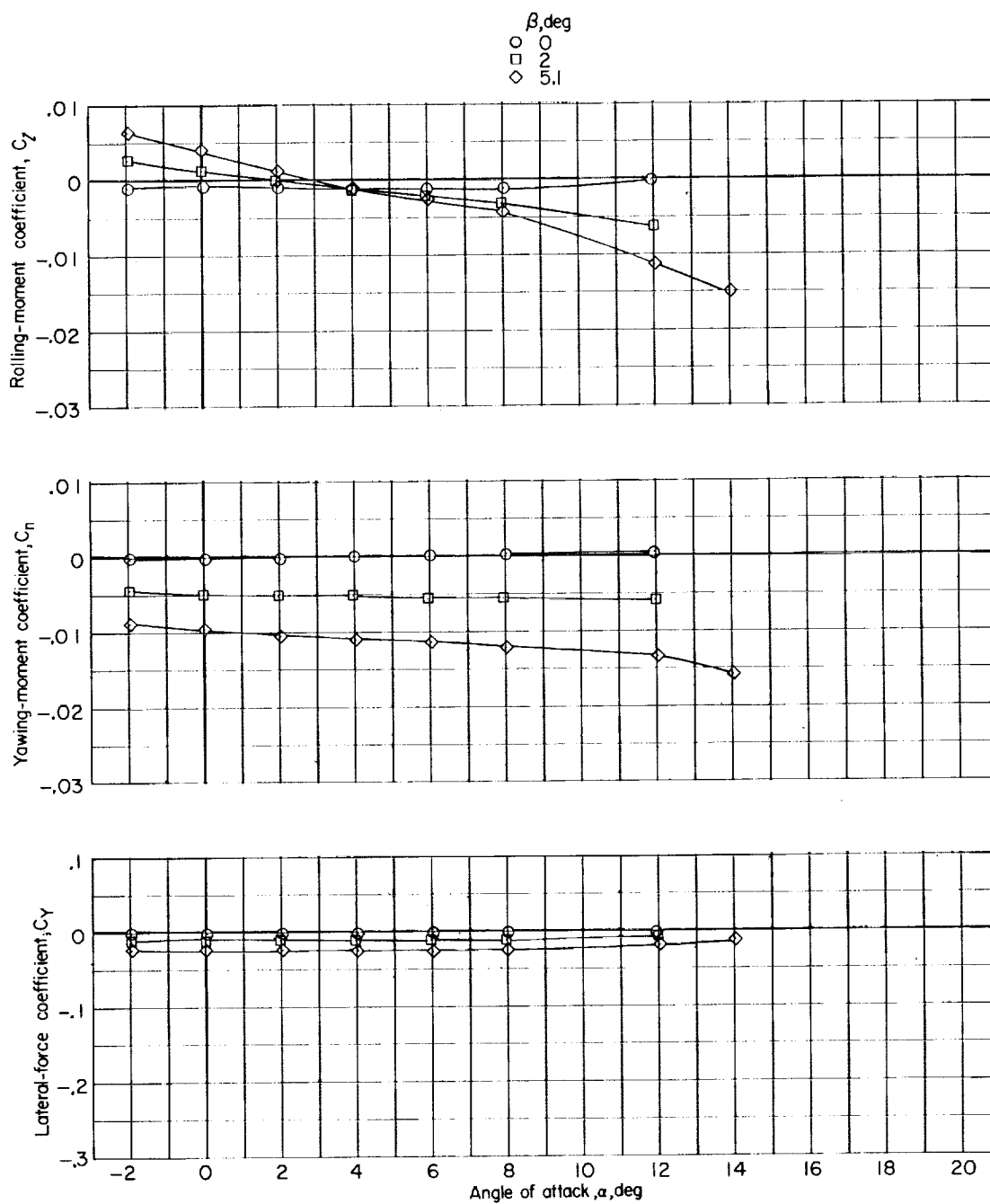
(f) $M = 1.00$.

Figure 14.- Continued.



(g) $M = 1.03$.

Figure 14.- Continued.



(h) $M = 1.18$.

Figure 14.- Concluded.

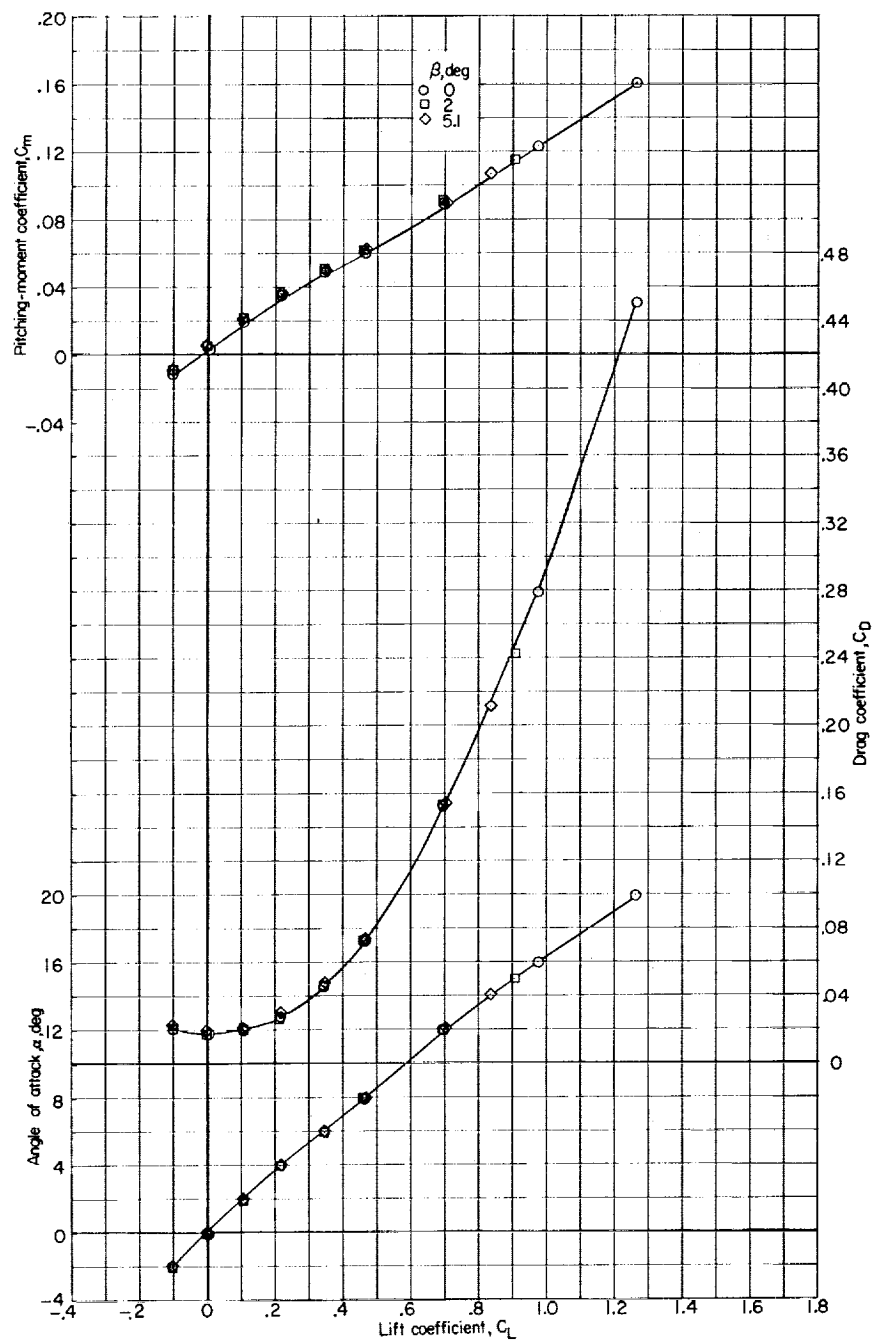
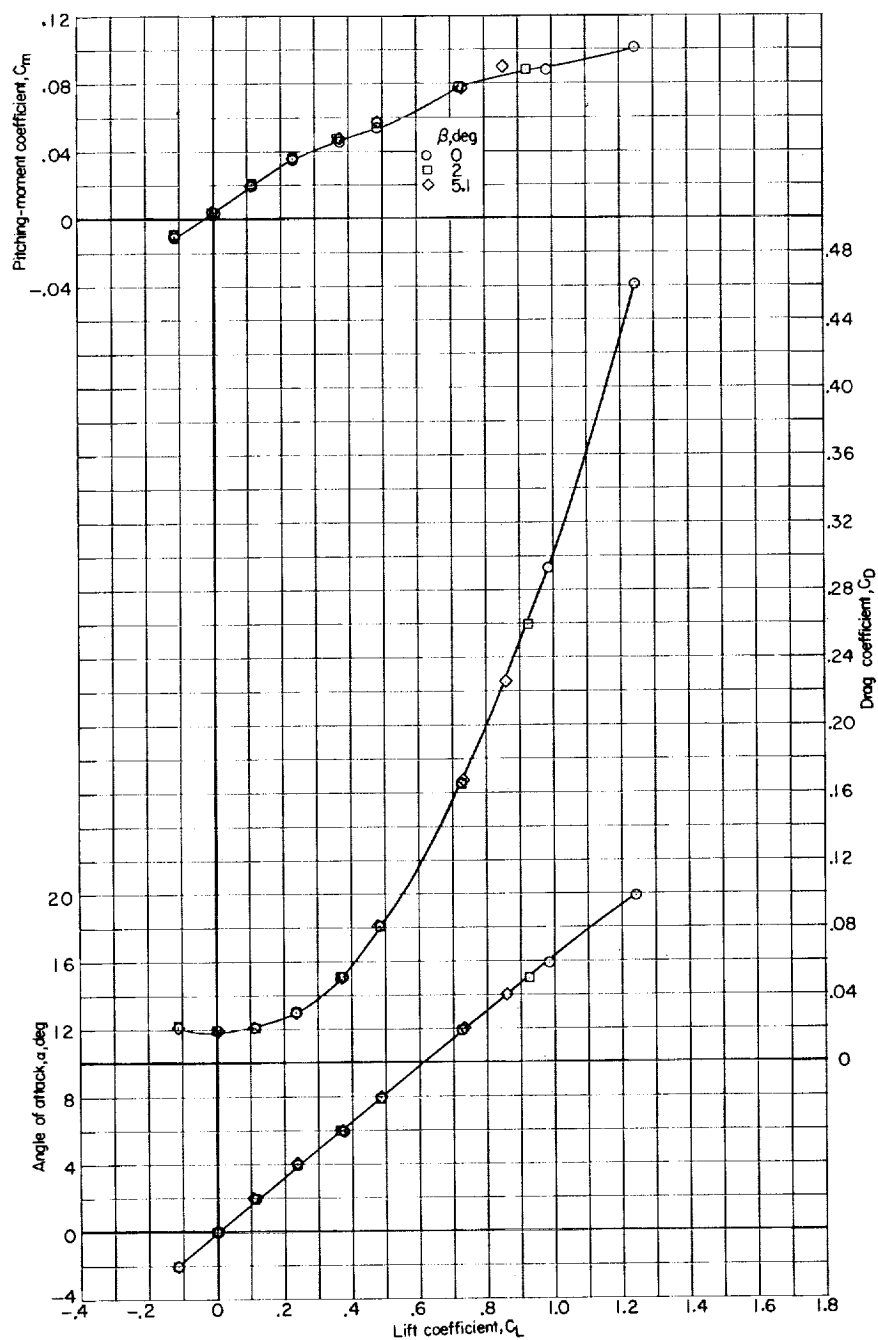
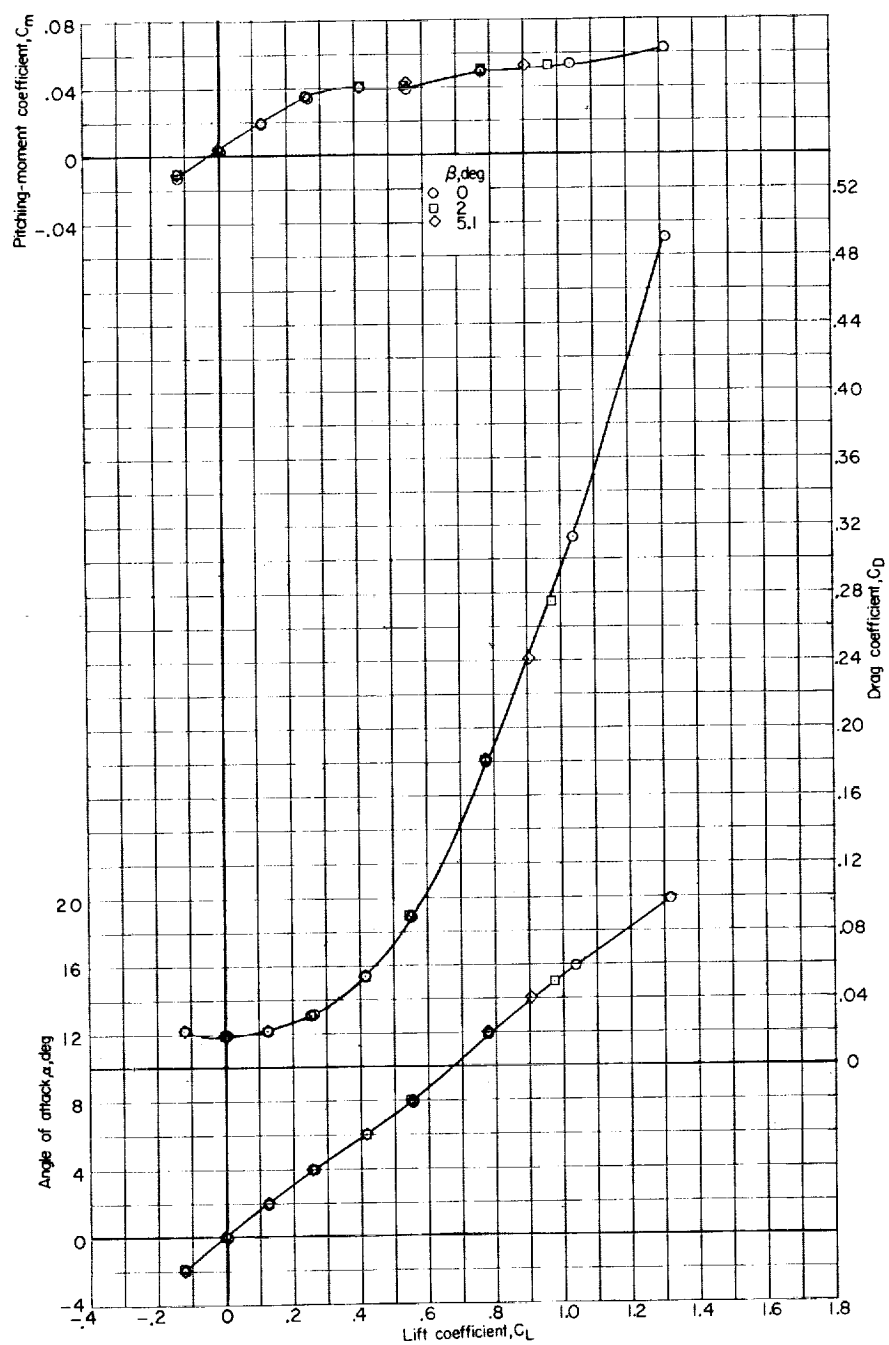
(a) $M = 0.60$.

Figure 15.- Longitudinal characteristics of the model with the horizontal and vertical tails off at various angles of sideslip.



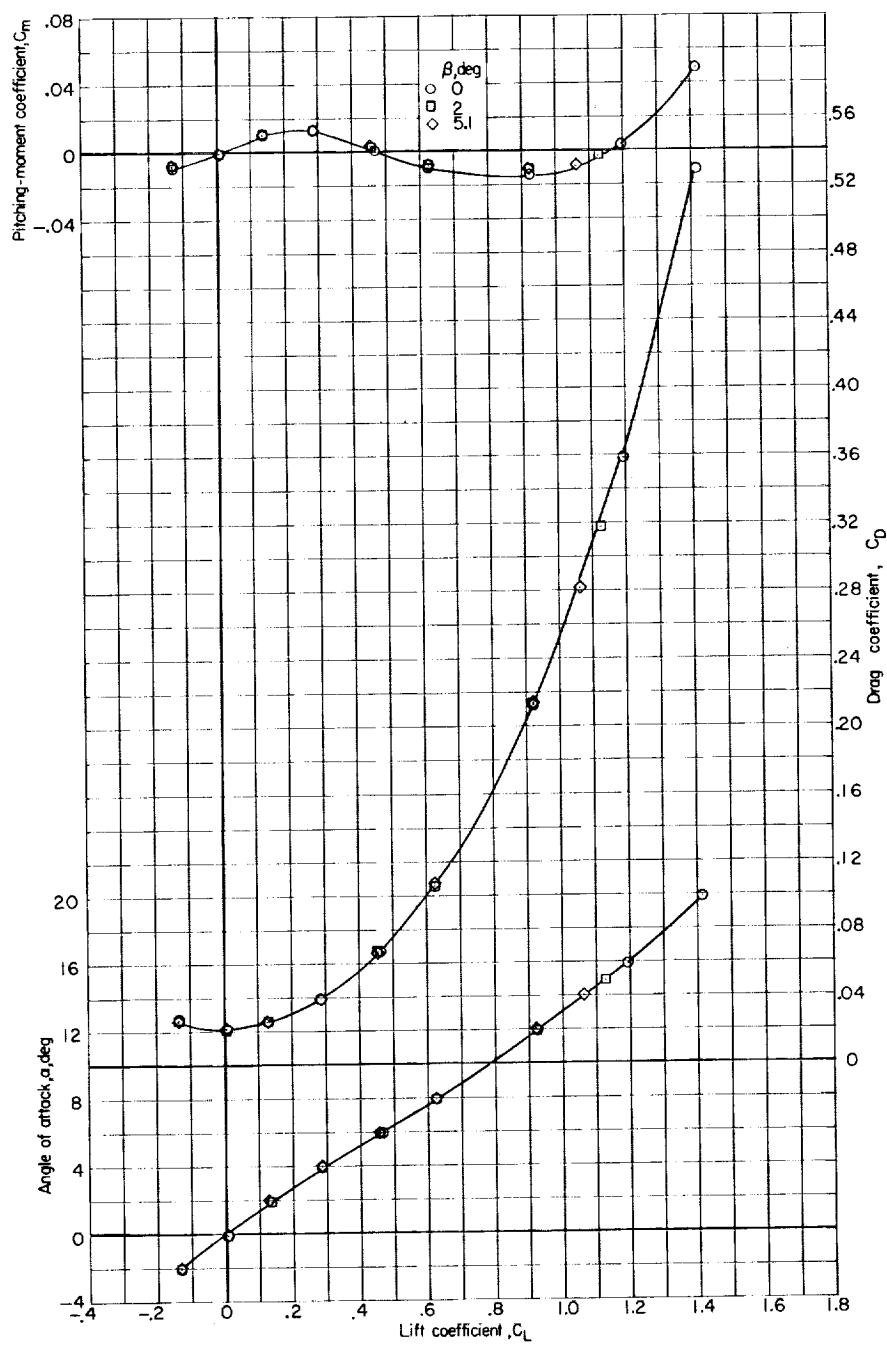
(b) $M = 0.80$.

Figure 15.- Continued.



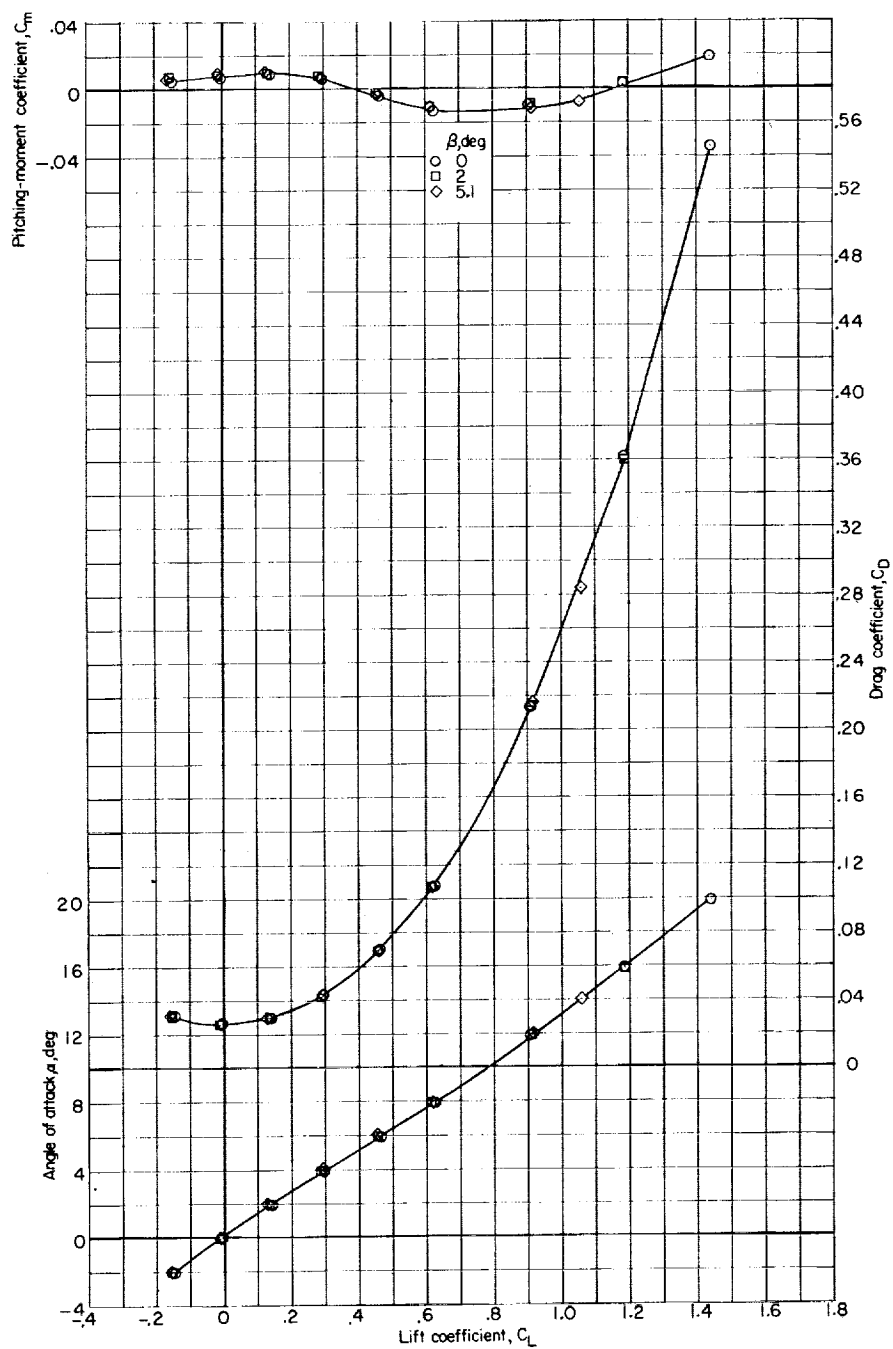
(c) $M = 0.90$.

Figure 15.- Continued.



(d) $M = 0.95$.

Figure 15.- Continued.



(e) $M = 0.975$.

Figure 15.- Continued.

L-376

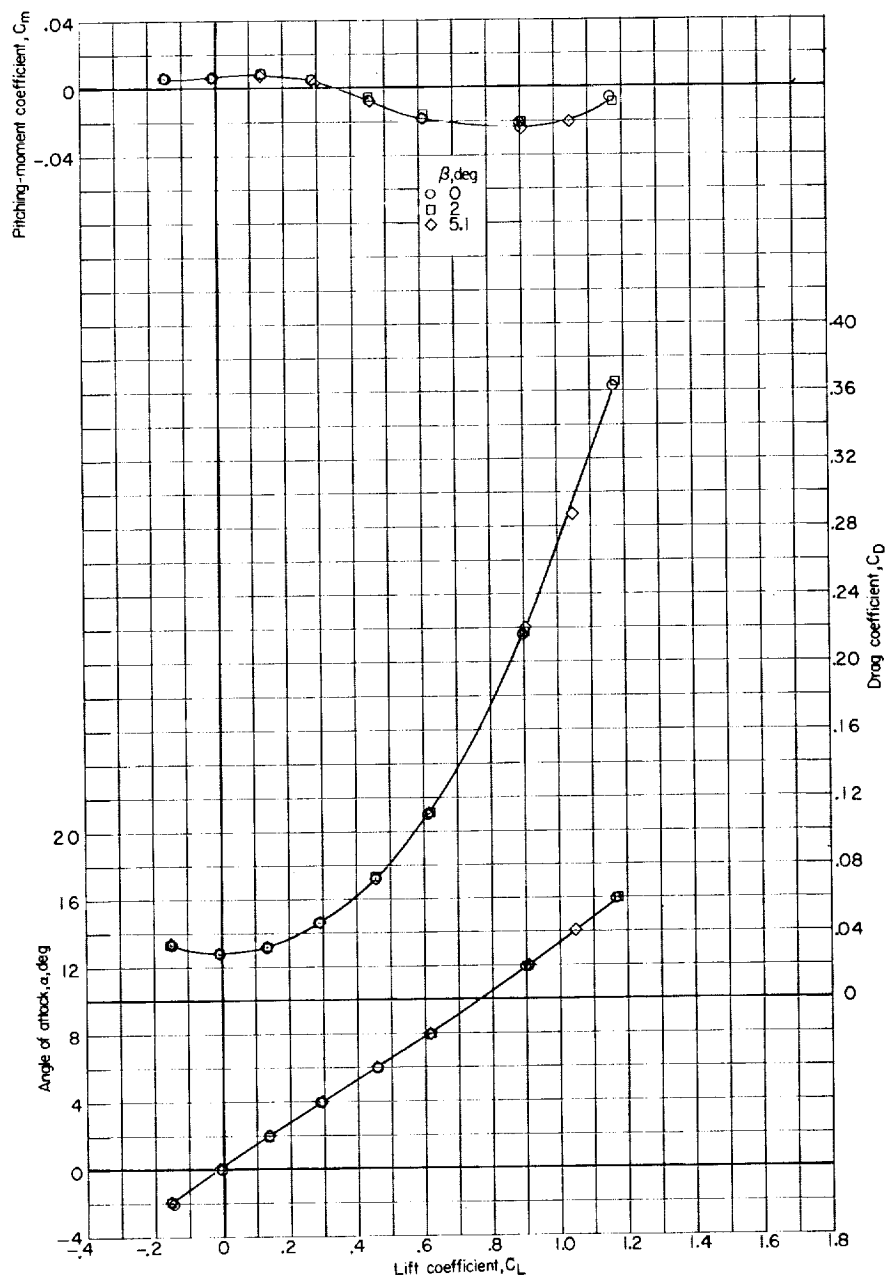
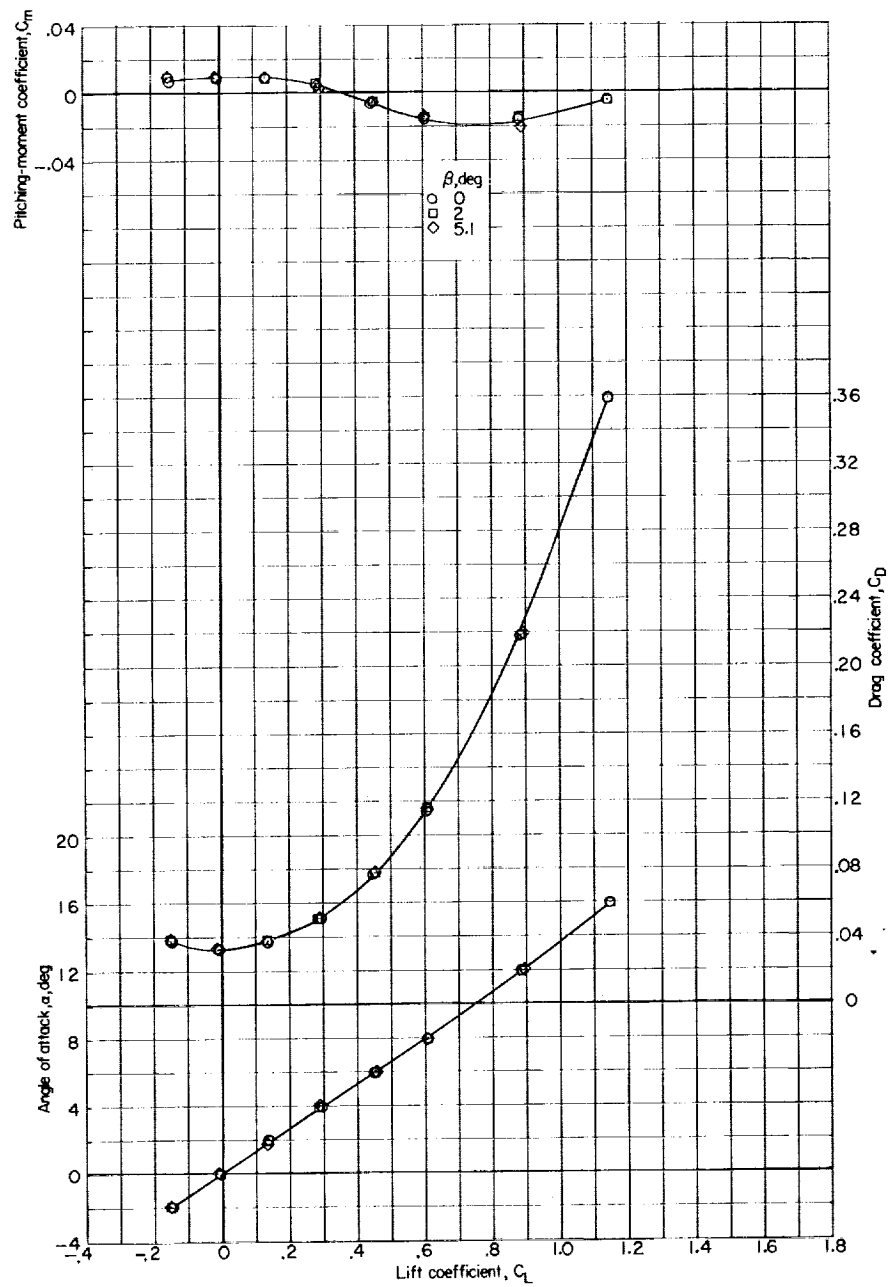
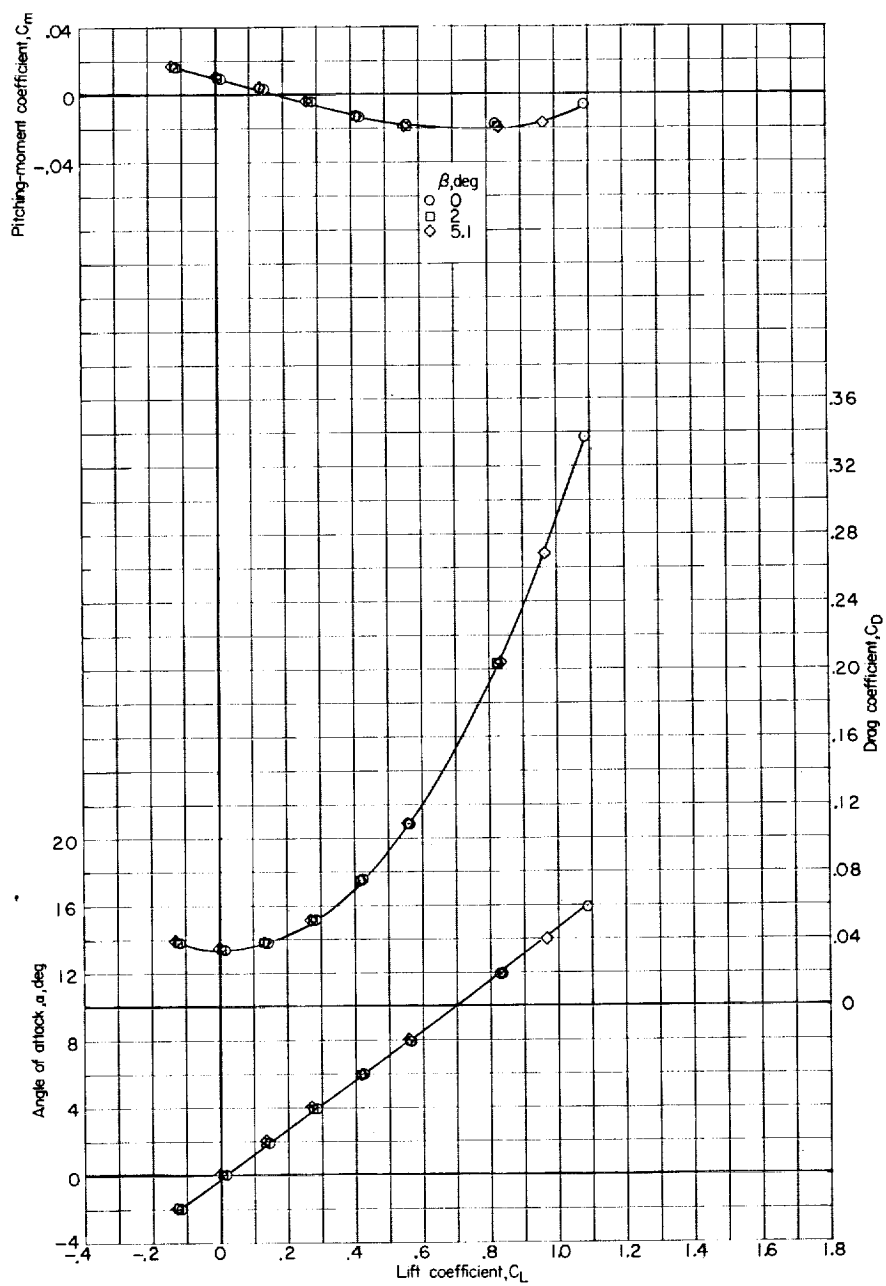
(f) $M = 1.00$.

Figure 15.- Continued.



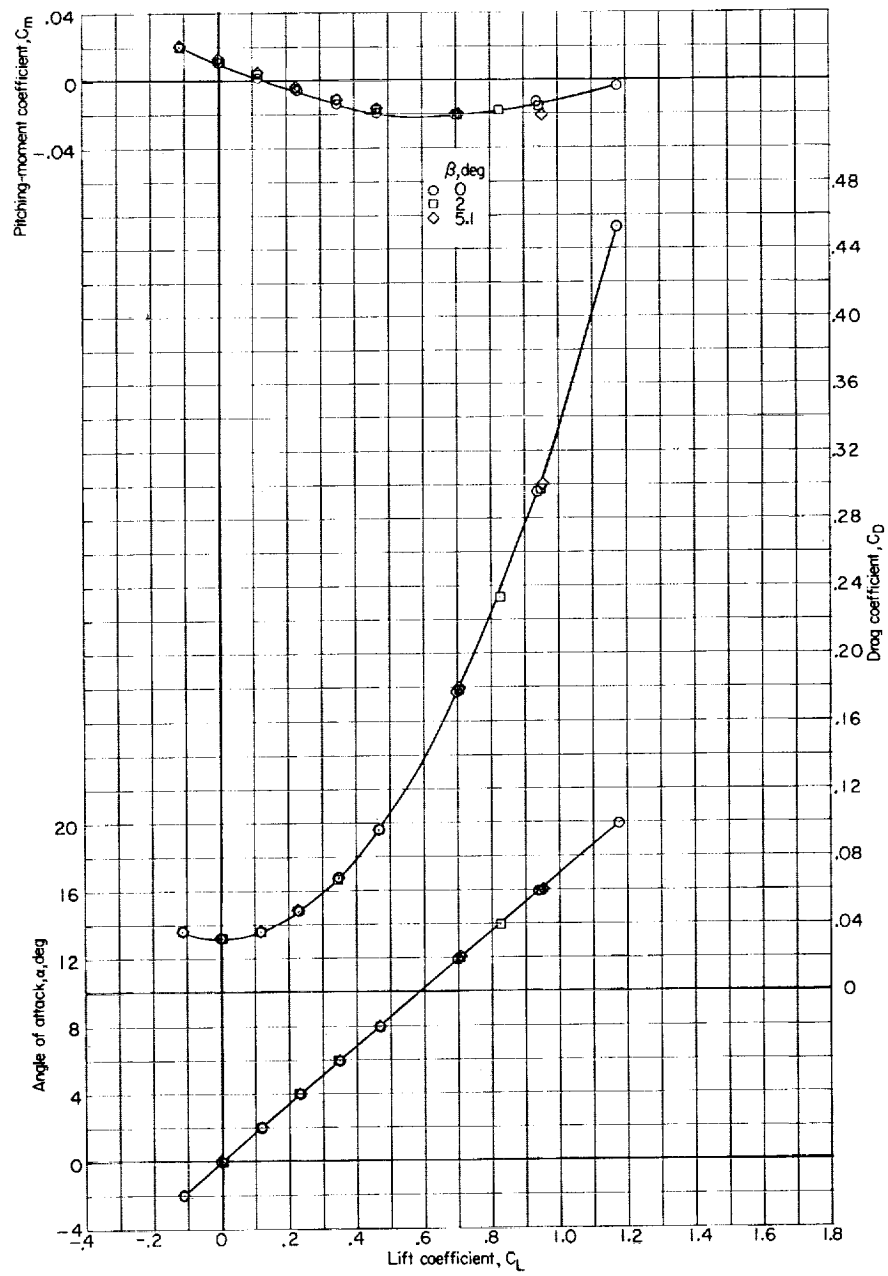
(g) $M = 1.03$.

Figure 15.- Continued.



(h) $M = 1.18$.

Figure 15.- Continued.



(1) $M = 1.43$.

Figure 15.- Concluded.

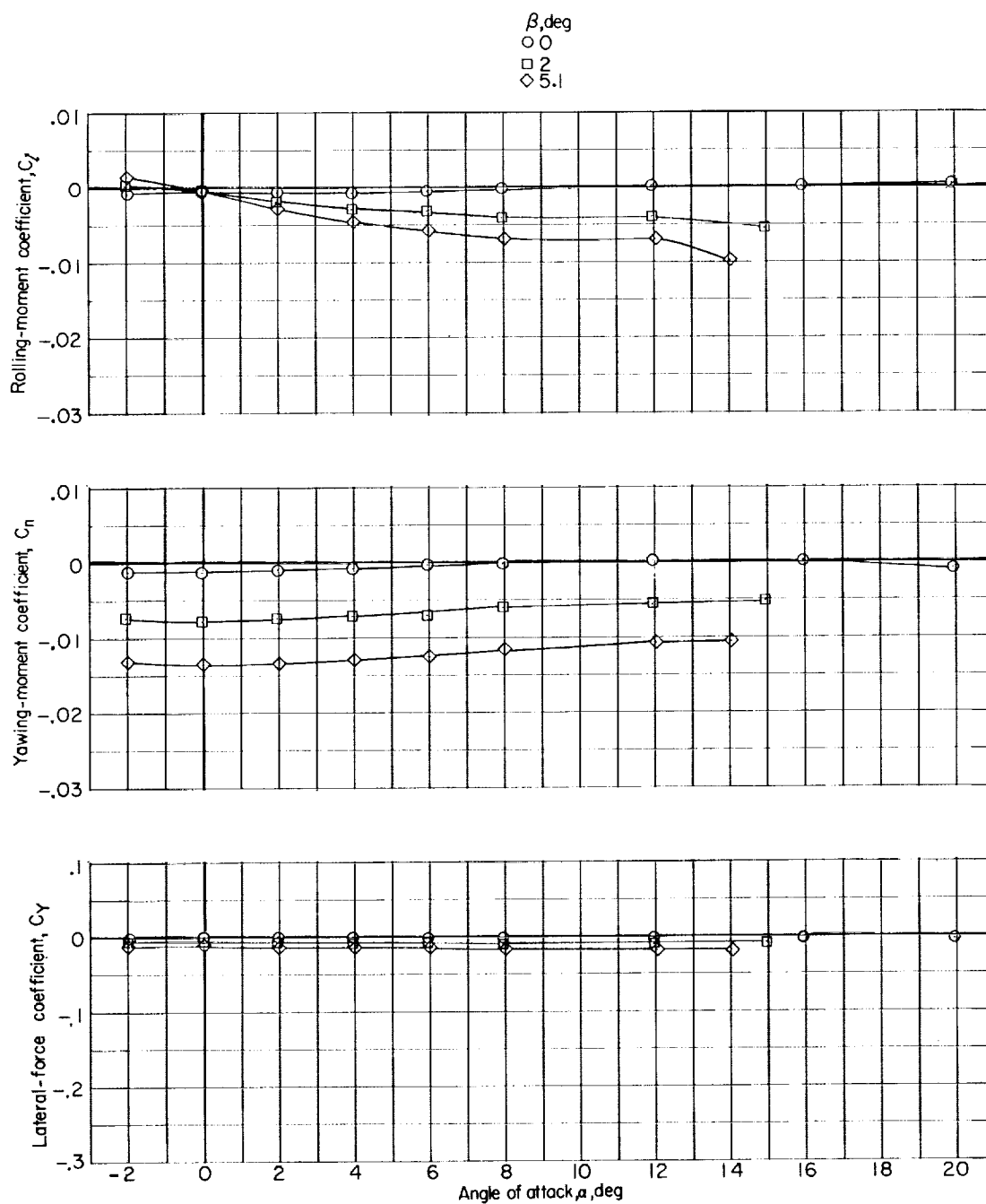
(a) $M = 0.60$.

Figure 16.- Lateral-directional characteristics of the model with the horizontal and vertical tails off at various angles of sideslip.

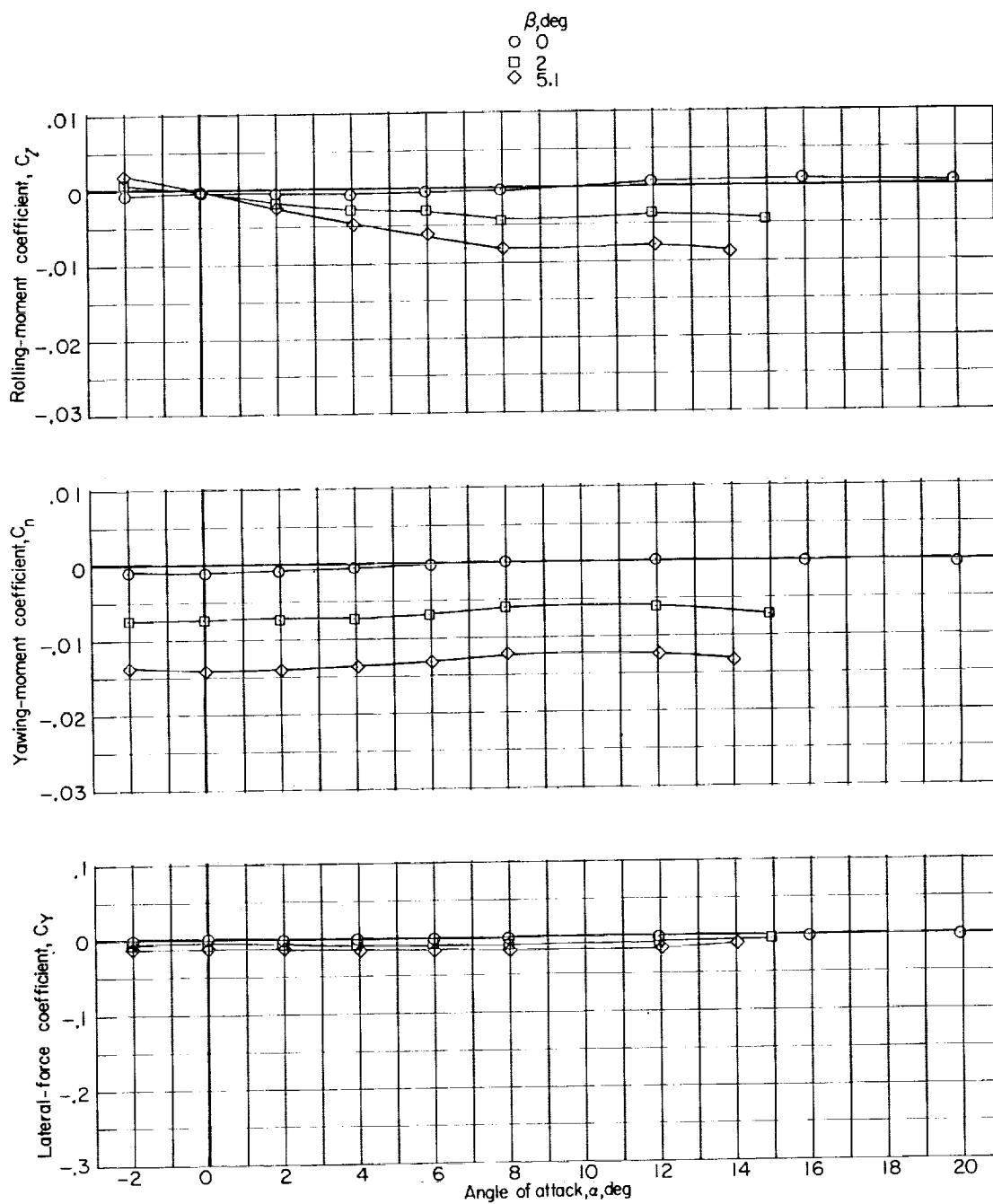
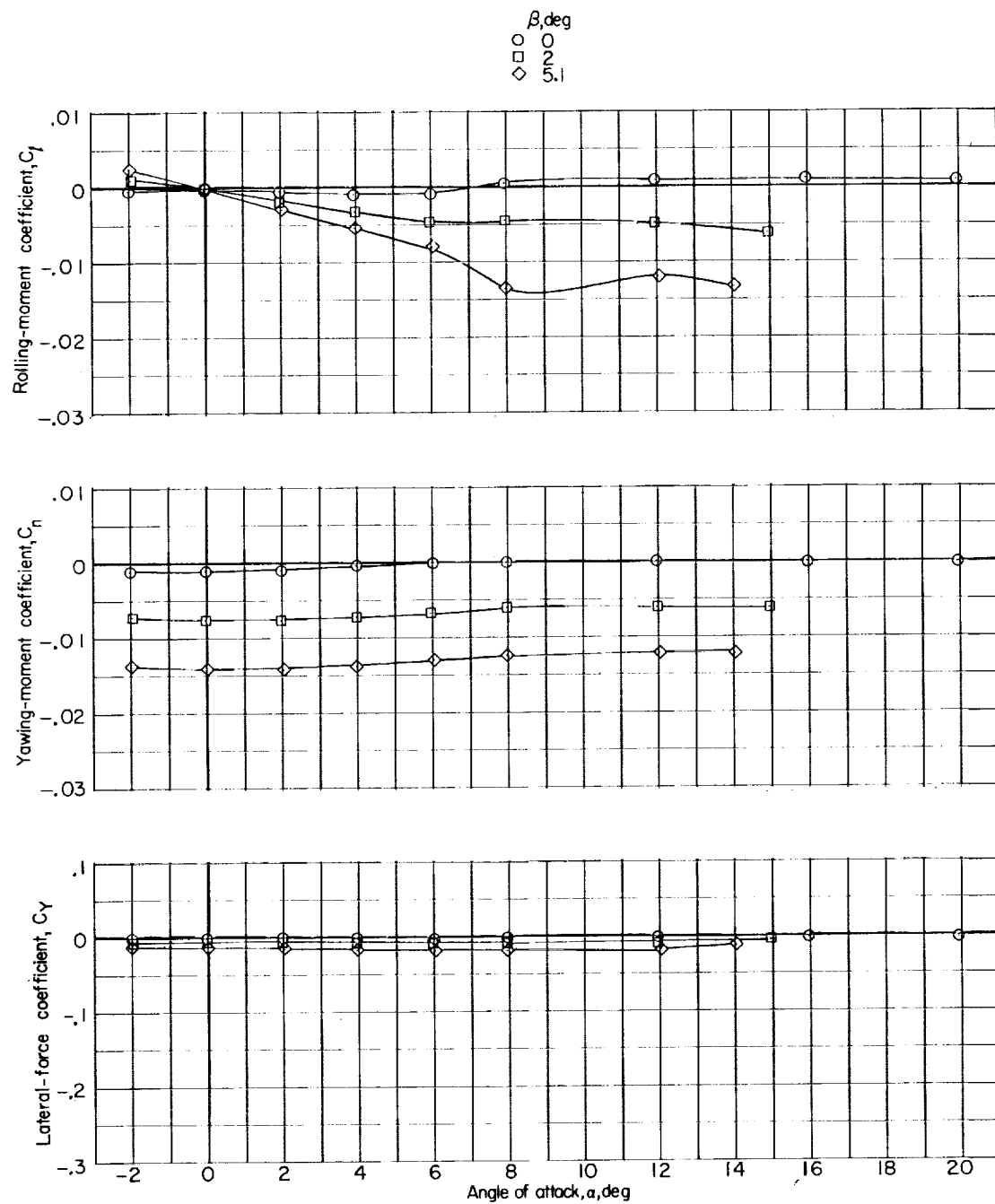
(b) $M = 0.80$.

Figure 16.- Continued.



(c) $M = 0.90$.

Figure 16.- Continued.

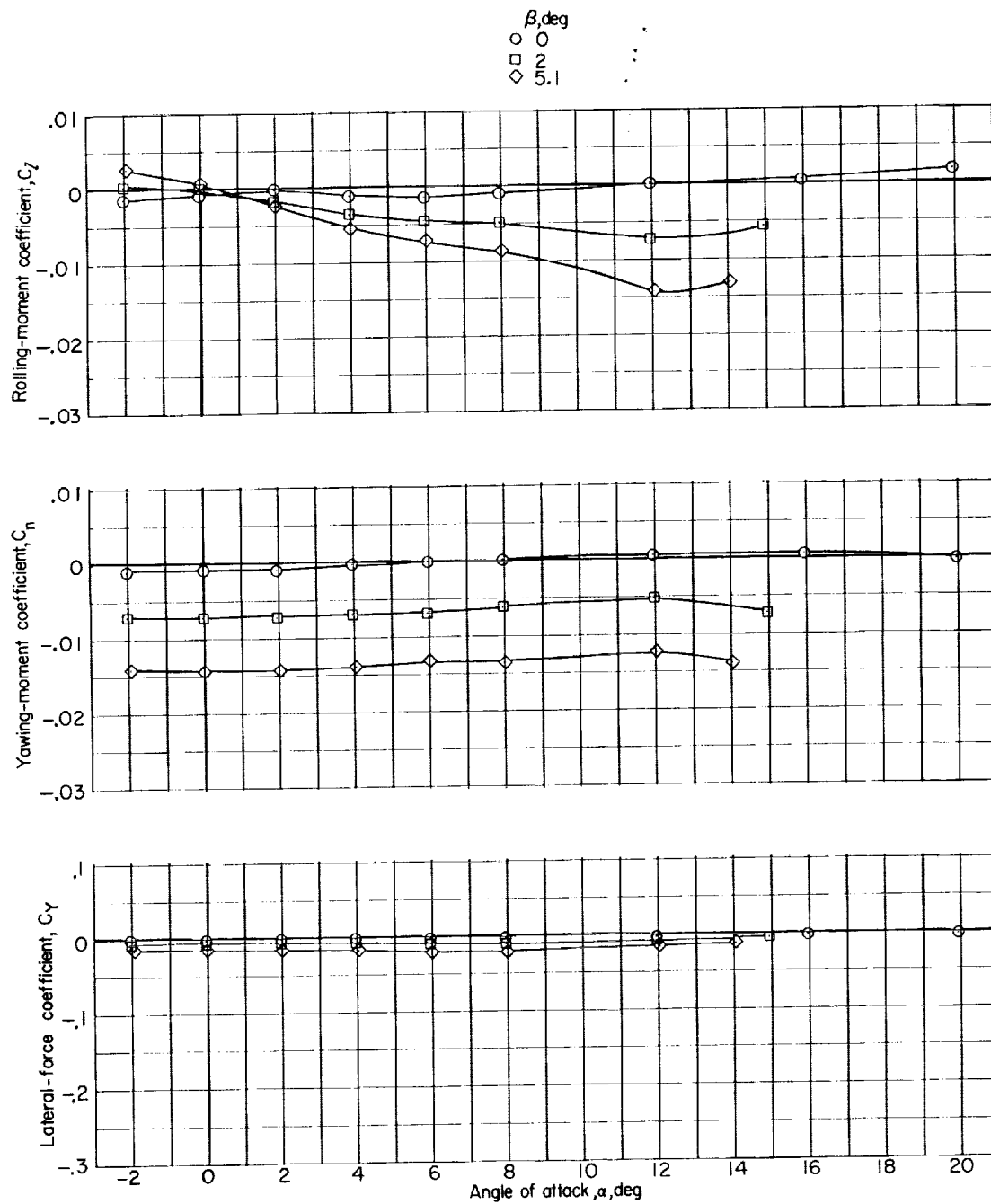
(d) $M = 0.95$.

Figure 16.- Continued.

L-376

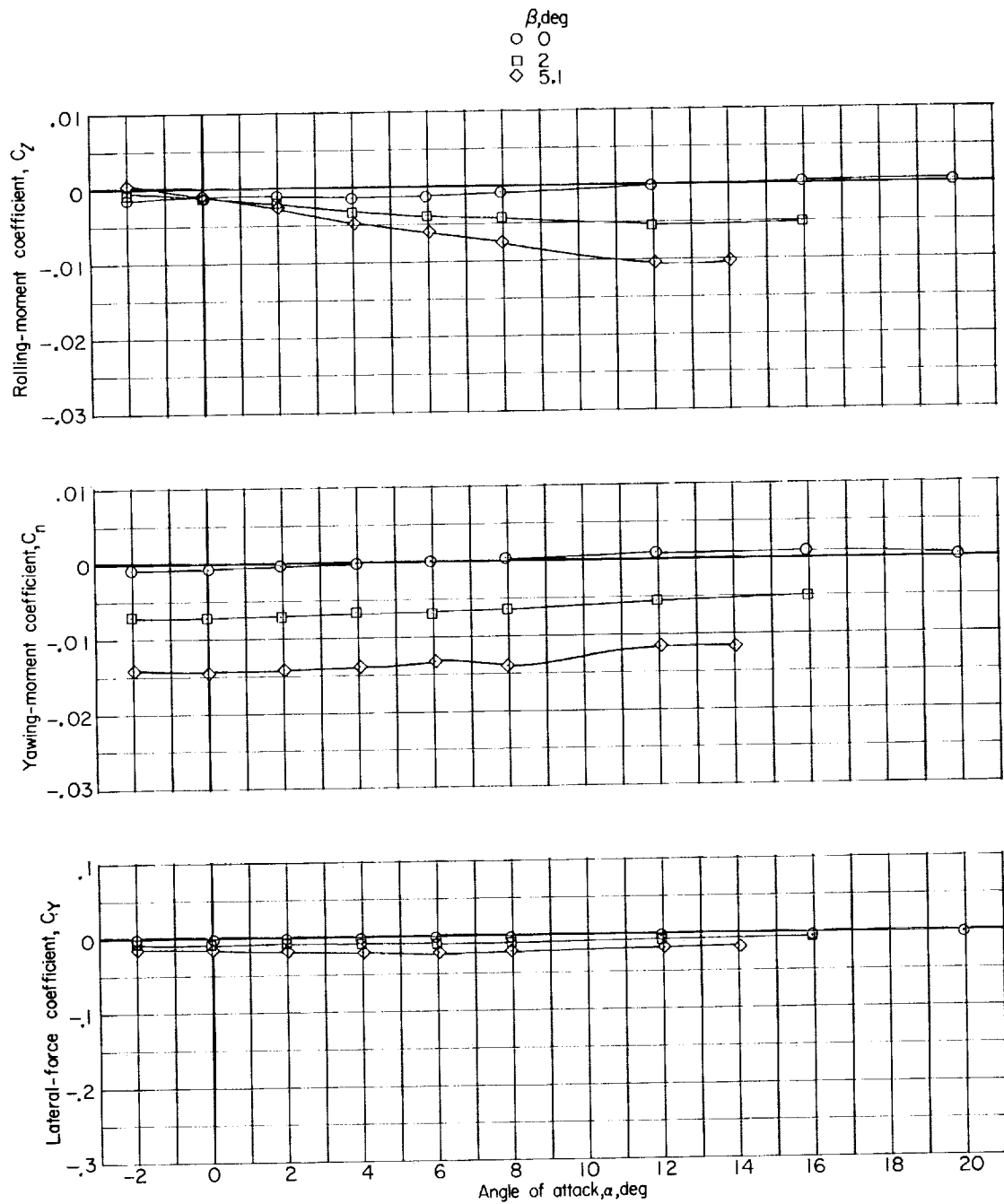
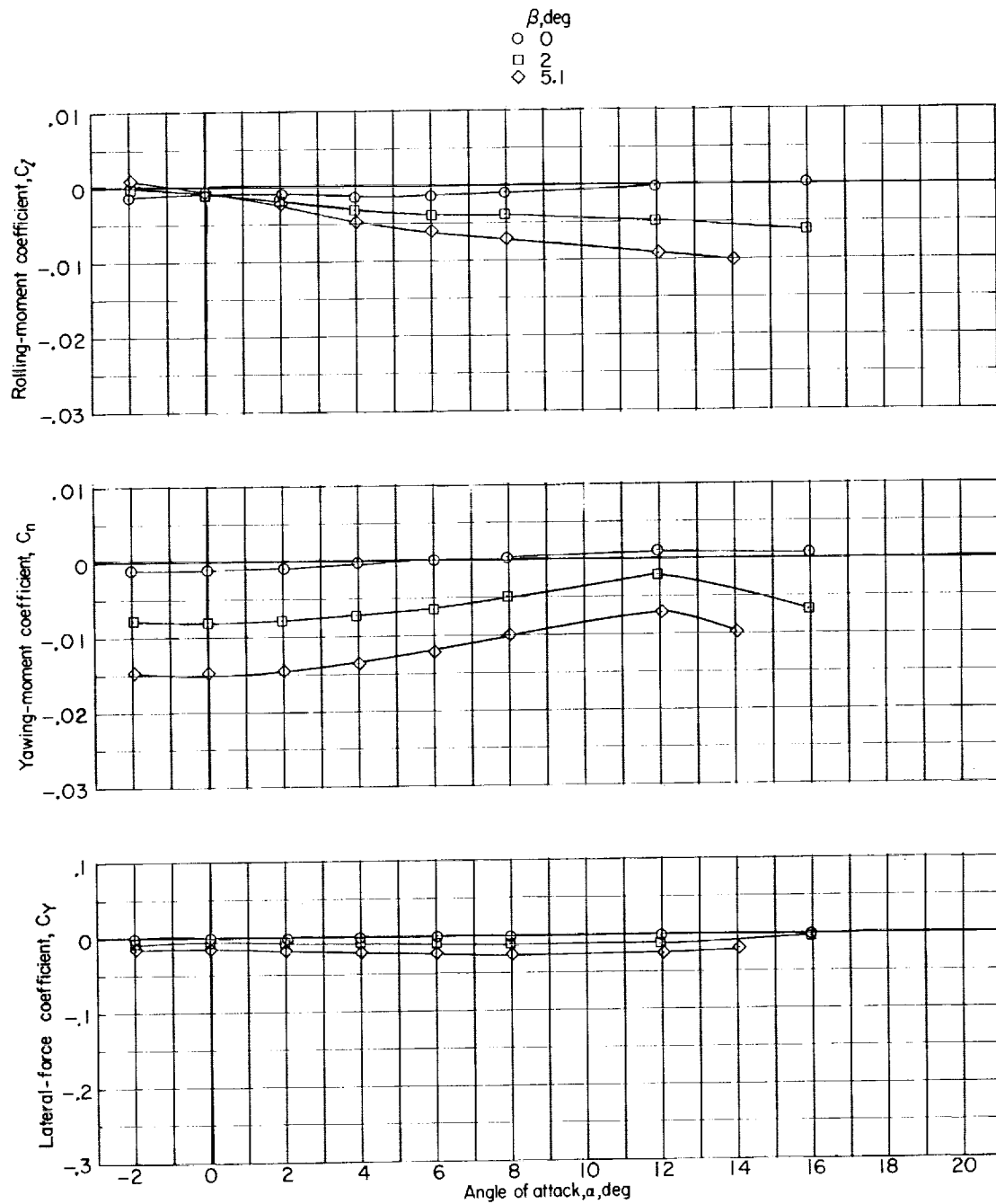
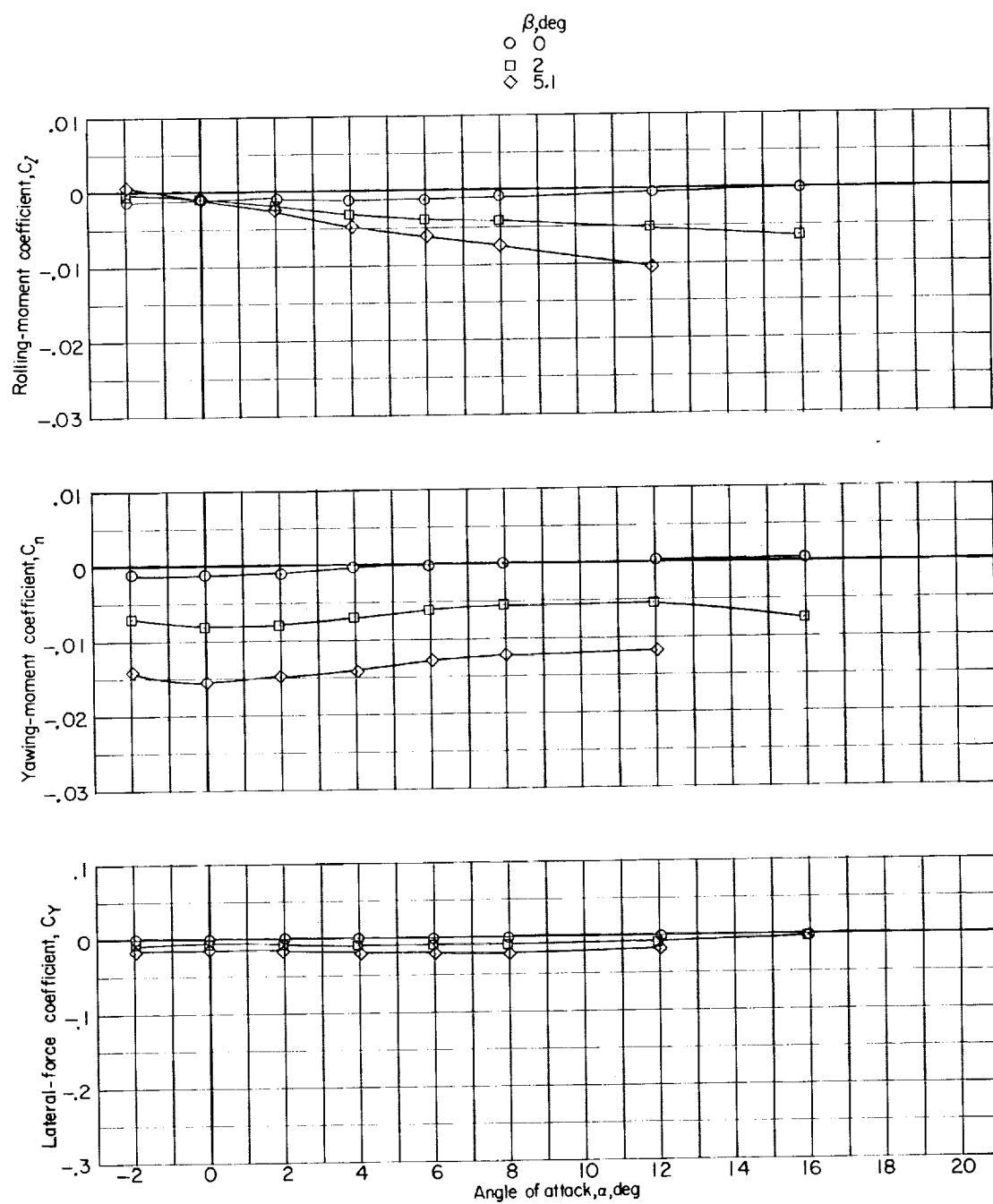
(e) $M = 0.975$.

Figure 16.- Continued.



(f) $M = 1.00$.

Figure 16.- Continued.



(g) $M = 1.03$.

Figure 16.- Continued.

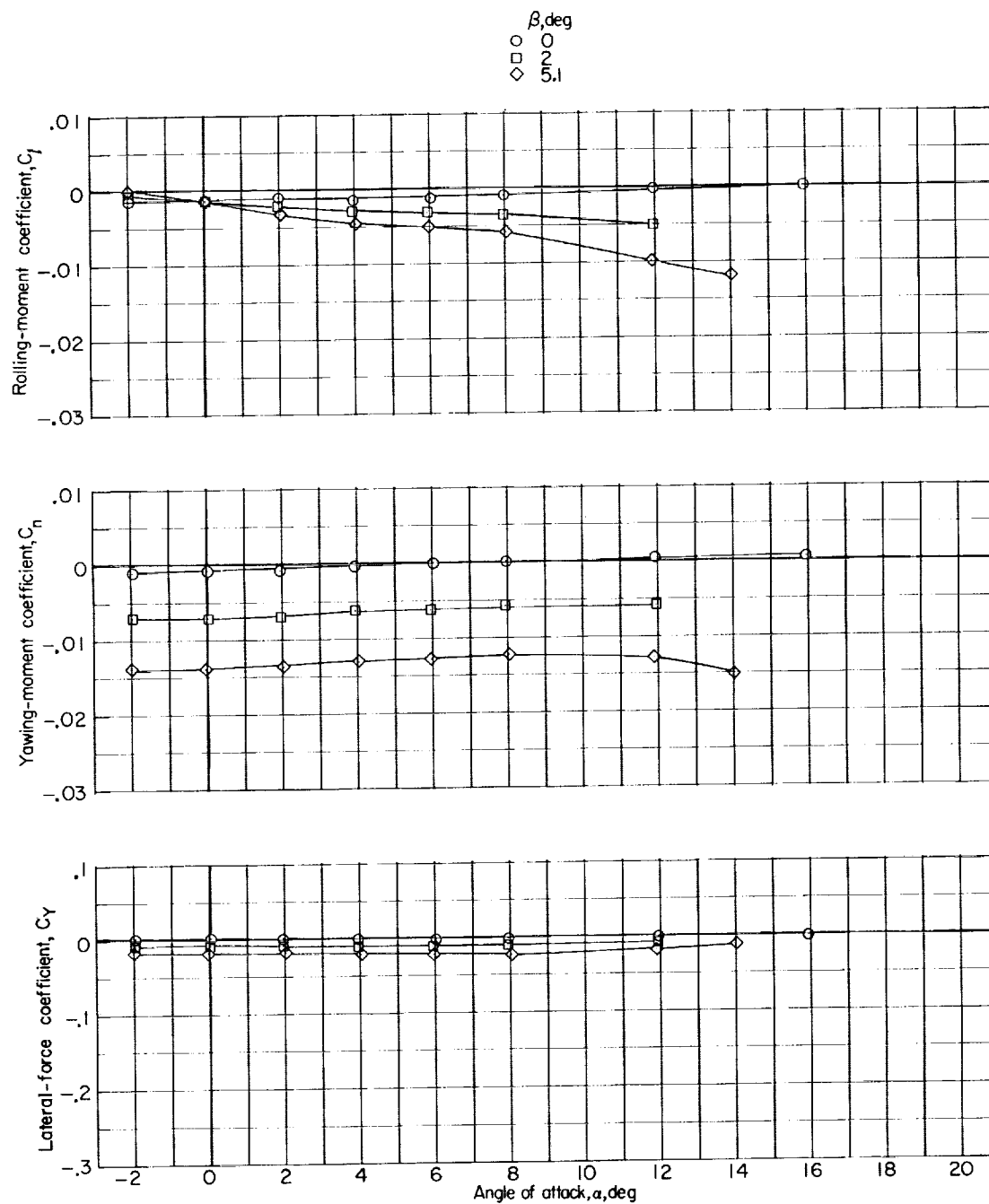
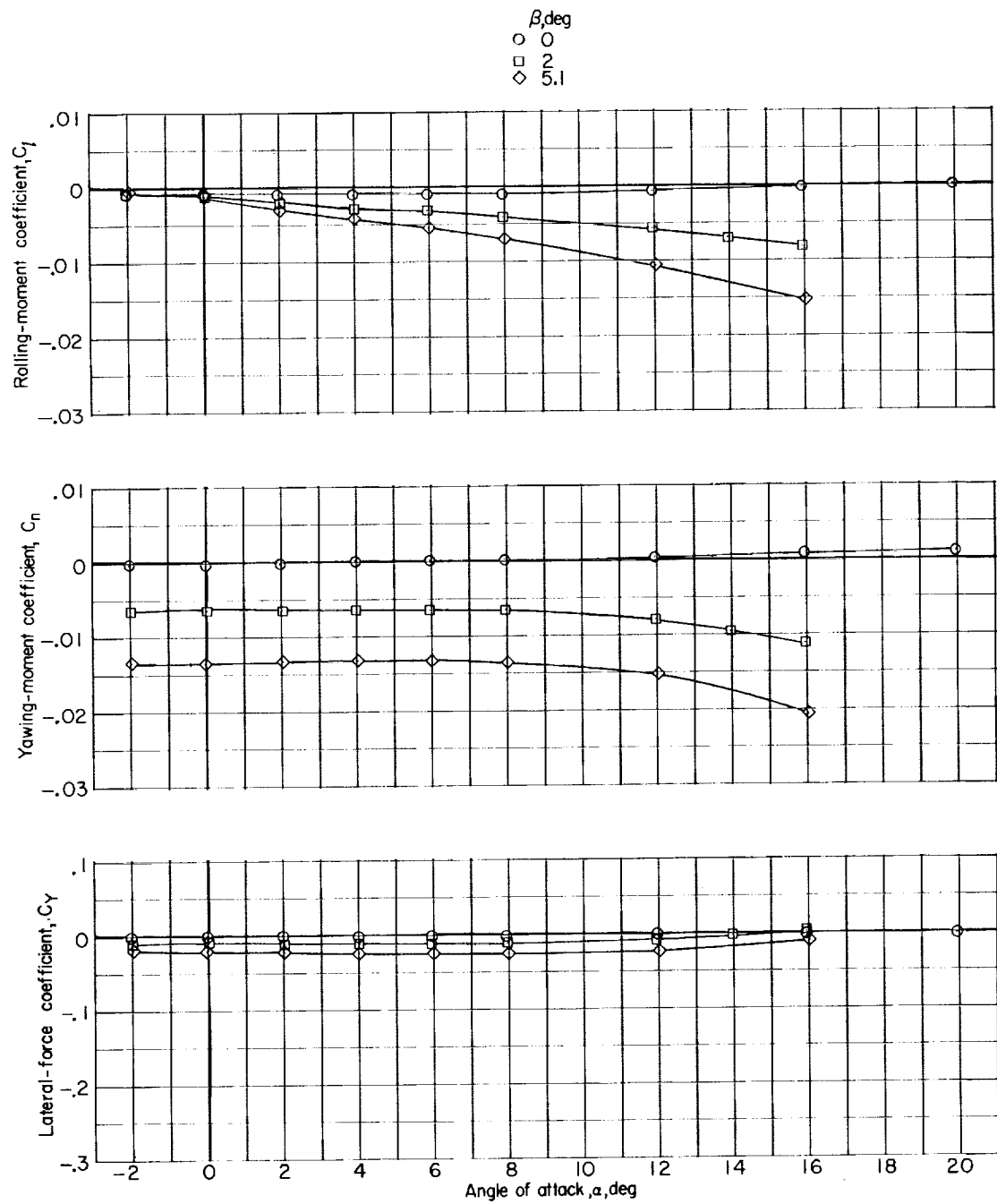
(h) $M = 1.18$.

Figure 16.- Continued.



(1) $M = 1.43$.

Figure 16.- Concluded.

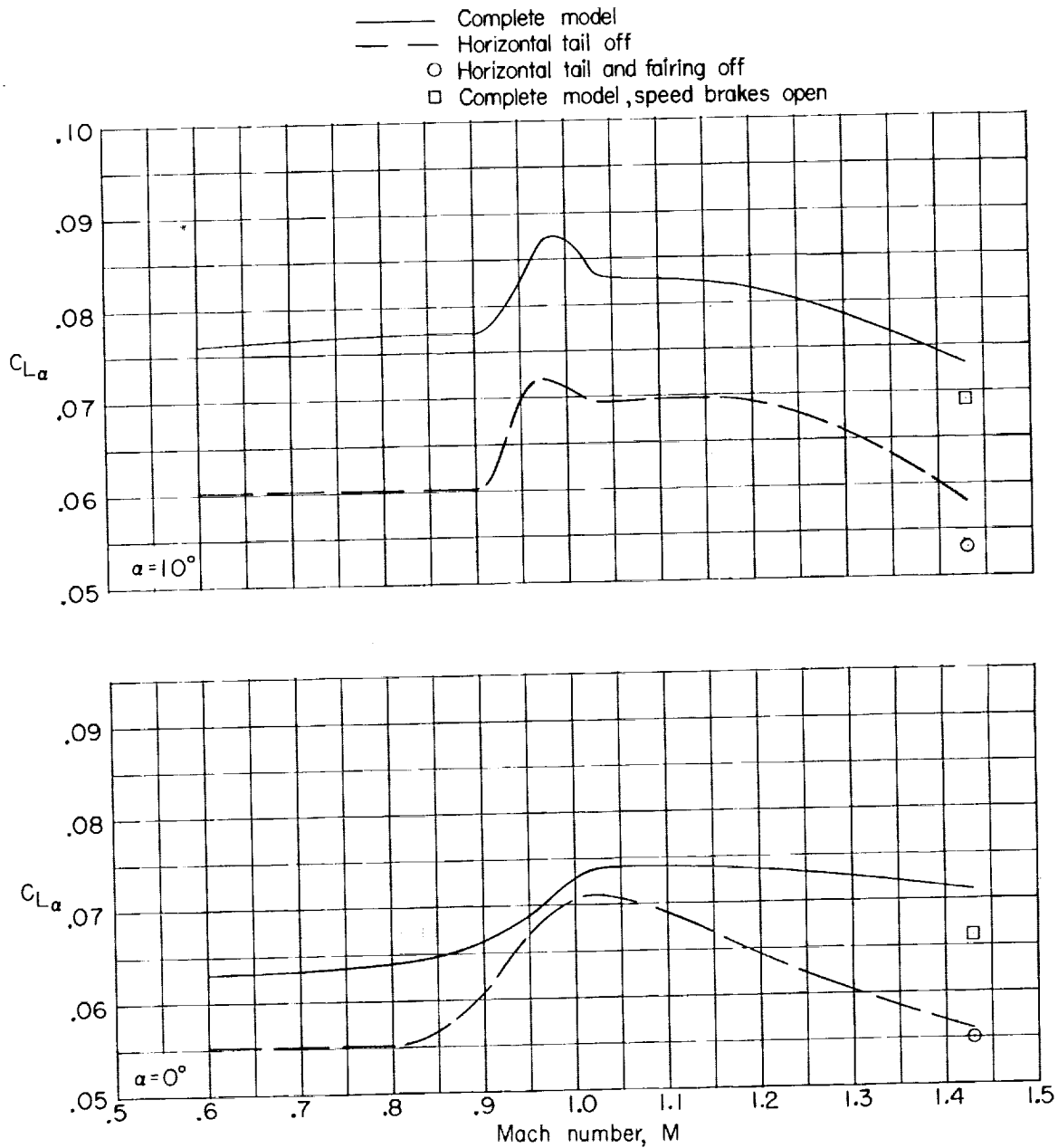


Figure 17.- Variation with Mach number of lift-curve slopes for two angles of attack at zero sideslip. Surfaces undeflected unless otherwise noted.

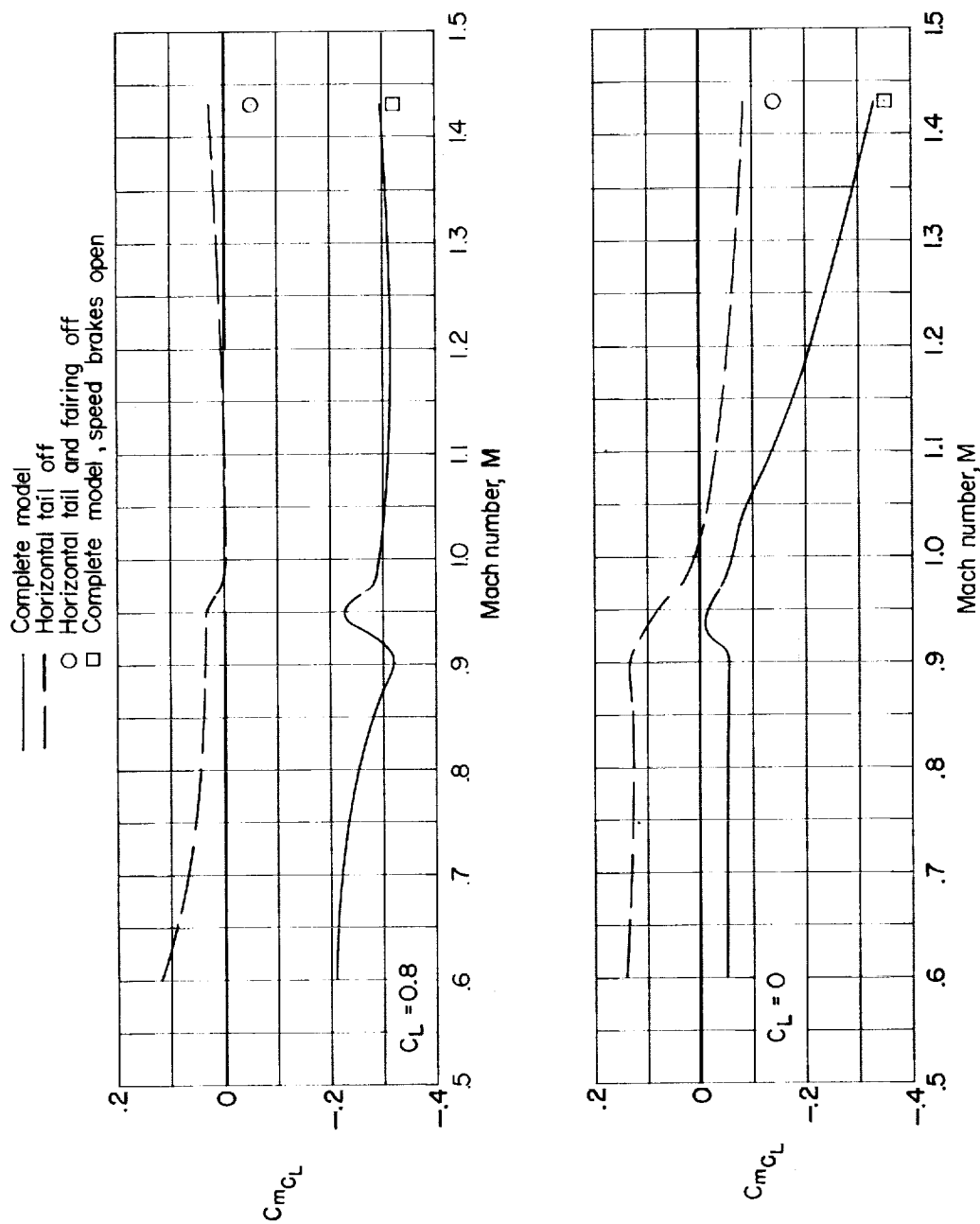


Figure 18.- Variation with Mach number of the static longitudinal stability parameter for two lift coefficients at zero sideslip. Surfaces undeflected unless otherwise noted.

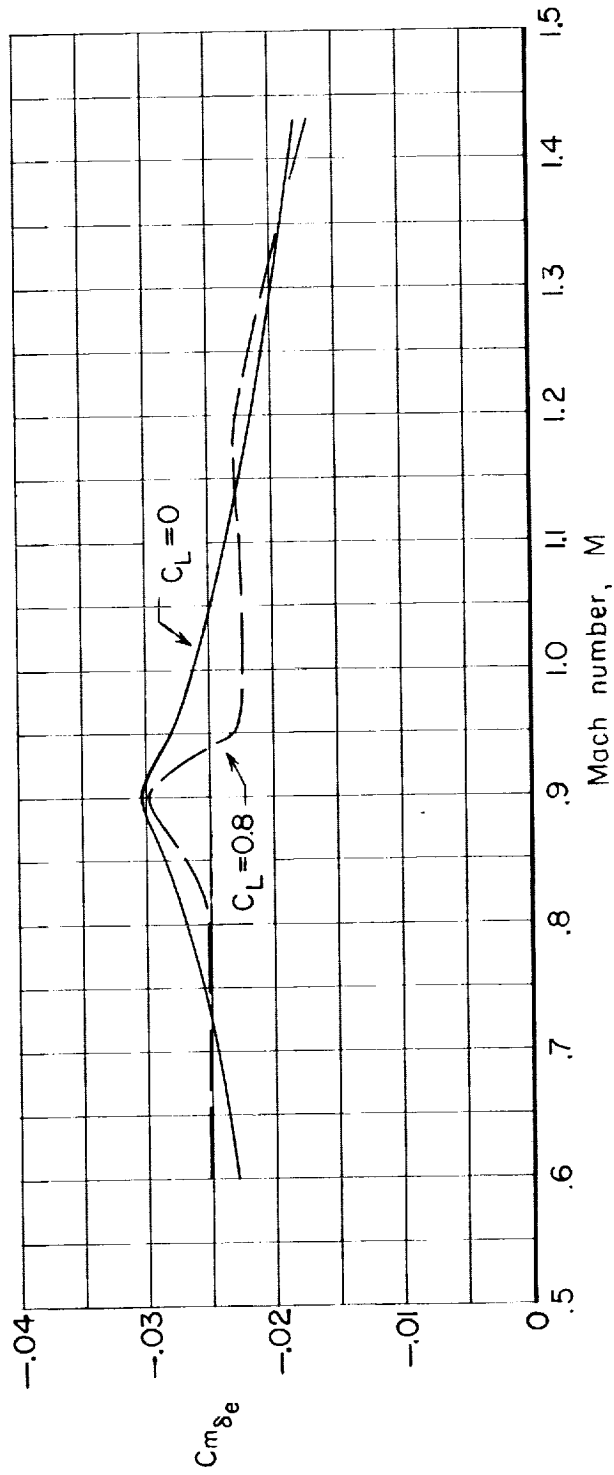
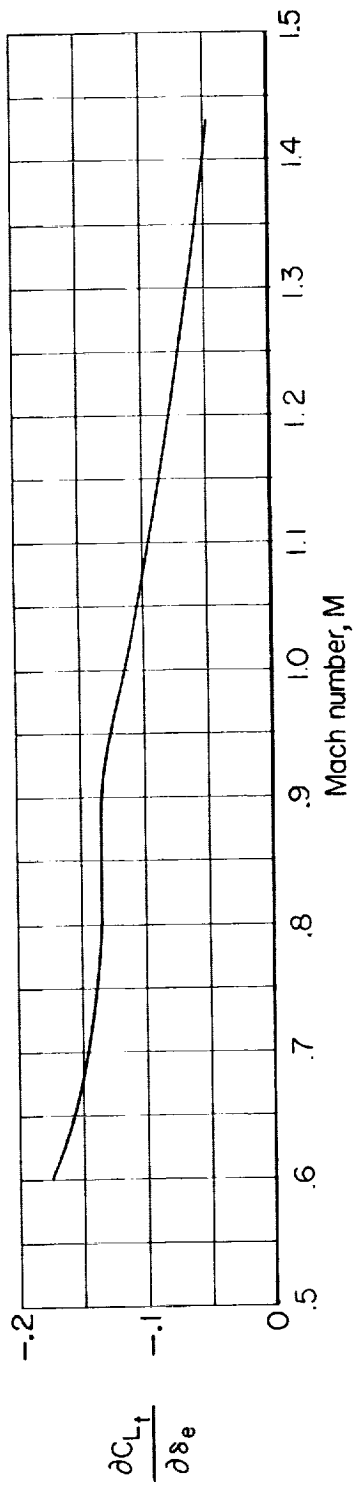


Figure 19.- Variation with Mach number of the longitudinal control parameters for the complete configuration with speed brakes closed at zero sideslip.

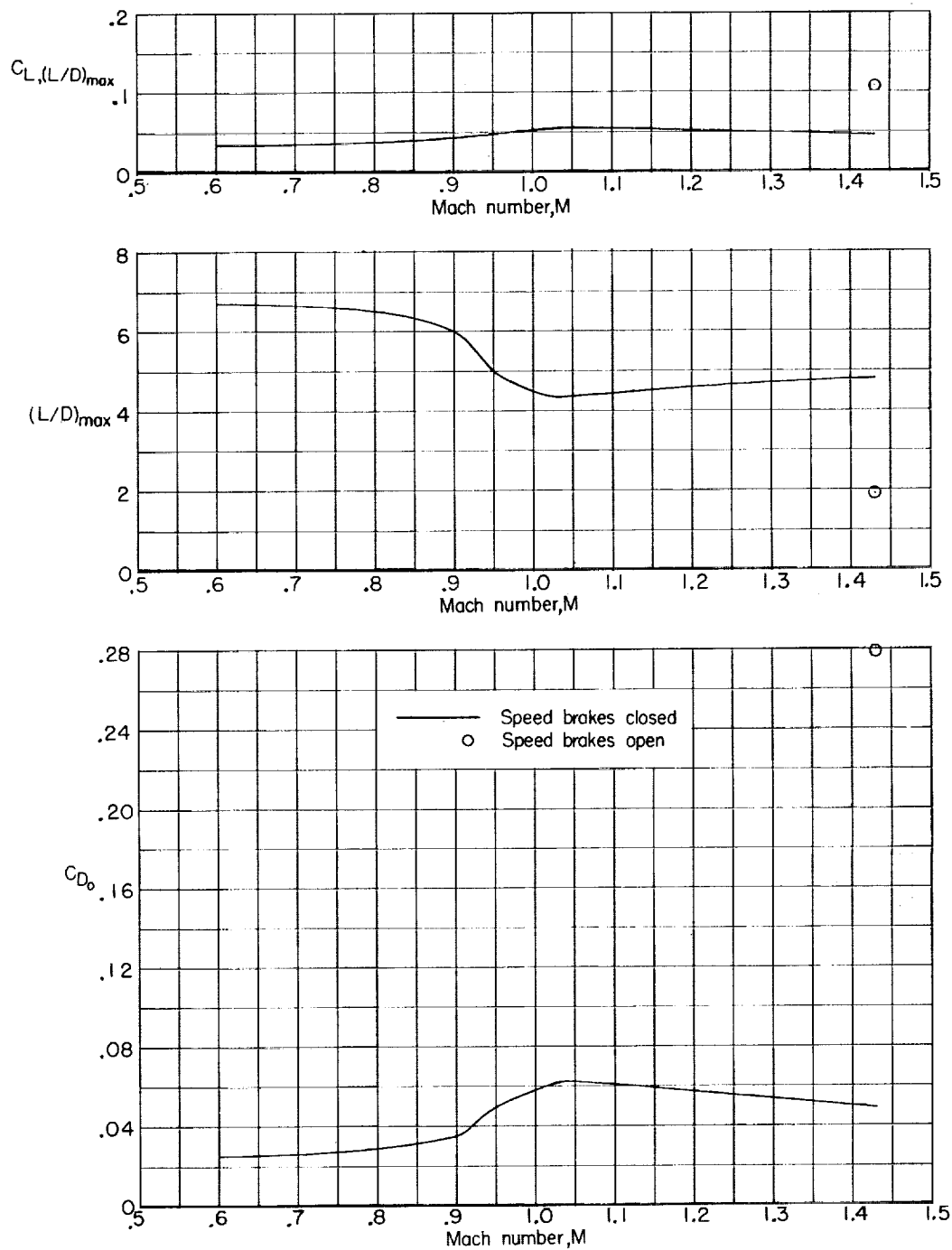


Figure 20.- Variation with Mach number of drag and maximum lift-drag ratio parameters for the complete configuration with the horizontal tail undeflected at zero sideslip.

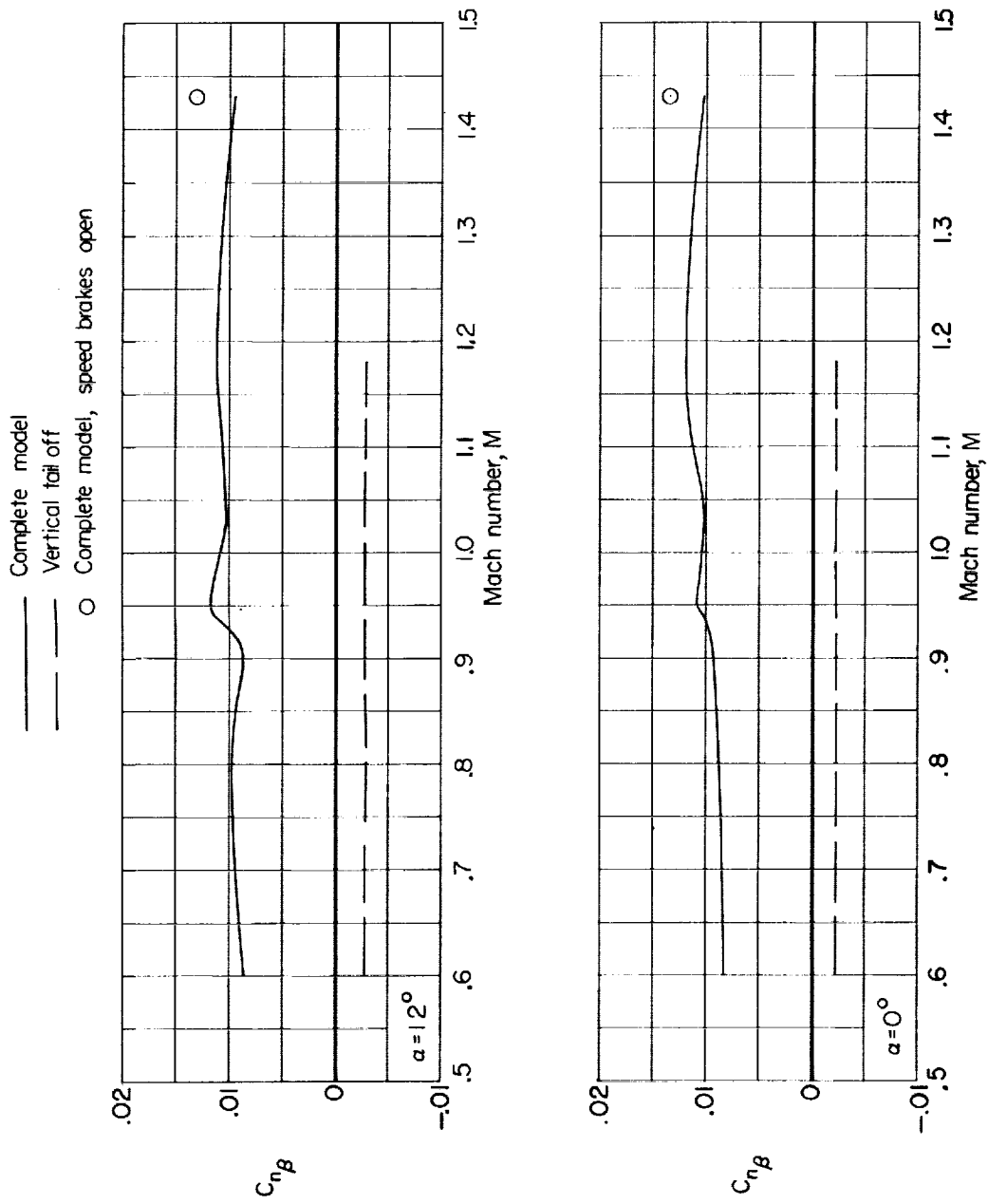


Figure 21.- Variation with Mach number of the static directional stability parameter for two angles of attack. Surfaces undeflected unless otherwise noted.

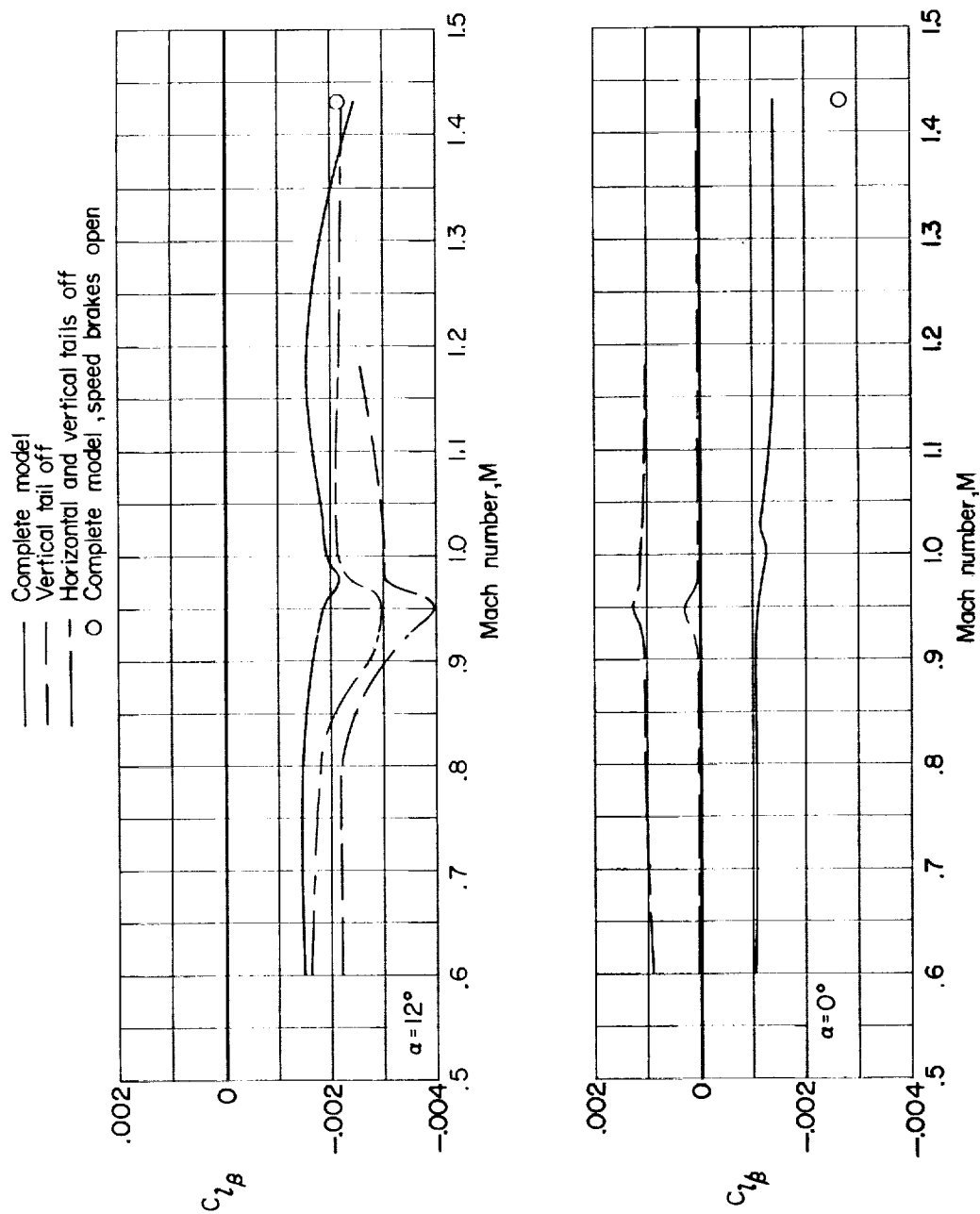


Figure 22.- Variation with Mach number of the effective dihedral parameter for two angles of attack. Surfaces undeflected unless otherwise noted.

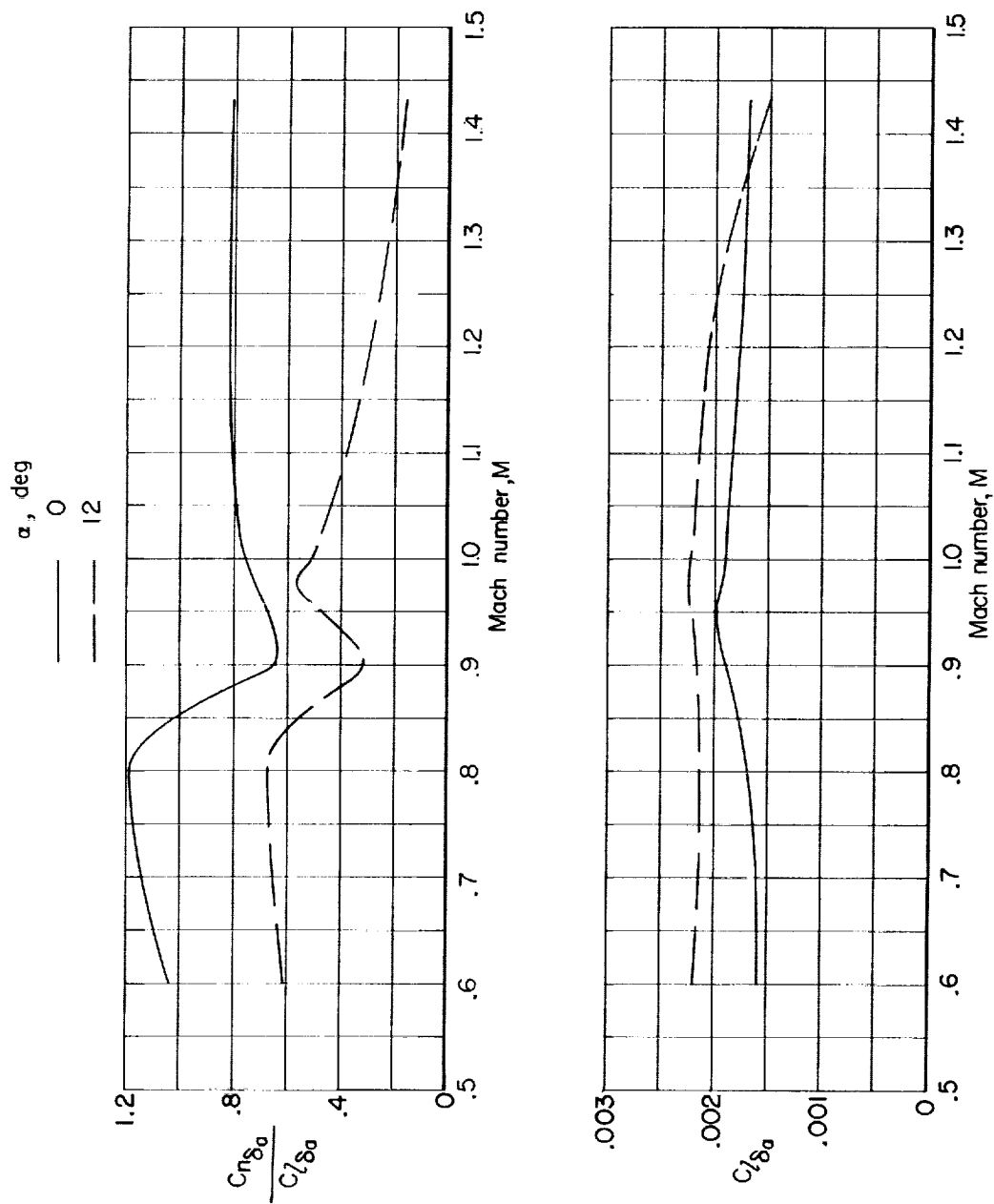


Figure 23.- Variation with Mach number of the lateral control parameters for two angles of attack at zero sideslip. $\delta_e = -3^\circ$, speed brakes closed.